# Robotics For In Vivo Whole Cell Patch Clamping

A Dissertation
Presented to
The Academic Faculty

By

Suhasa Bangalore Kodandaramaiah

In Partial Fulfillment

Of the Requirements for the Degree

Doctor of Philosophy in Mechanical Engineering

Georgia Institute of Technology

May, 2013

# Robotics For In Vivo Whole Cell Patch Clamping

**Approved by:**


**Craig R Forest**, Advisor

Woodruff School of Mechanical Engineering

*Georgia Institute Of Technology*

**Andres Garcia**

Woodruff School of Mechanical Engineering

*Georgia Institute Of Technology*

**Cheng Zhu**

School of Biomedical Engineering

*Georgia Institute Of Technology*

**Garrett Stanley**

School of Biomedical Engineering

*Georgia Institute Of Technology*

**Edward S Boyden**

Media Arts and Sciences

*Massachusetts Institute of Technology*


Date Approved: 12th December 2012

To my dearest nana…

# Acknowledgements

This thesis would not have been possible without the support and help of my friends, family and my colleagues. First and foremost, I would like to thank Ed and Craig. Working on this inter-disciplinary project across two different universities gave me the unique opportunity and privilege of being mentored by not just one, but by two advisors. Both Craig and Ed were instrumental in not only providing me with the necessary guidance, but also supported my travel to and from Boston throughout my PhD. Their contrasting mentoring styles made for a unique and highly enriching graduate school experience. I would like to thank my thesis reading committee, Prof. Andres Garcia, Prof. Garrett Stanley and Prof. Cheng Zhu, who's insightful comments and guidance was instrumental in the successful completion of this thesis.

I would like to thank a number of members of the Forest Laboratory as well as the Boyden Laboratory. In particular I would like to thank Melissa Li, Christopher Phaneuf and Nikita Pak who were constant source of ideas, and sounding boards during my initial days in Atlanta. Greg Holst, was of enormous help in with electronic circuits design and fabrication when I started working on the multipatcher projects as was Ash Turza (Boyden Laboratory). A number of undergraduate research assistants helped out at various stages of my thesis work. I would like to thank Mike Dergance, who helped with

fabrication of the first multipatcher prototypes in the Fall semester of 2009. Matt Emerick, Jamison Go and Saifullah Malik helped with the design and fabrication of the more advanced prototypes later in Summer 2010.

Coming from a mechanical engineering background, far removed from neuroscience, I had to negotiate a particularly steep learning curve when I first started work in Ed's lab. Of tremendous help during those early days were Mike Henninger, Dr. Brian Chow and Nathan Klapoetke. Mike guided me through my first baby steps of setting up an electrophysiology rig, explaining the basics of de-noising it and supervised me until I got good at performing animal surgeries. Brain Chow and Nathan Klapoetke, taught me the basics of patch clamping *in vitro*. The earliest experiments with the multipatcher were done with express help from Mike Henninger and Giovanni Talei Franzesi. Helping me along the way were several other members of the Boyden lab. I would like to thank Dr. Mike Baratta who taught how to perform trans-cardial perfusions in mice, Dr. Annabelle Singer who taught me how to carry out immunohistochemical staining protocols, Dr. Yongku Cho who trained me on using the confocal microscope, and Patrick Monahan who taught me how to perform lentivirus injection surgeries. I had the opportunity to work closely with Dr. Steve Bates and Dr. Ian Wickersham, who will be taking forward some of the single cell phenotyping work. Working in the basement of the windowless old media lab building meant you often did not meet many people during the course of a day other than those ran experiments down in 044. I have often times had lengthy and fruitful discussion about electrophysiology with Giovanni Talei Franzesi and

Leah Acker, my co-denizens of the 044. Giovanni aka Nic, and Annabelle were also integral to some of the first awake patch clamp recordings attempted in Summer of 2012.

I would like to thank a number of people whom I worked closely with on a number of related projects during my time in Ed's laboratory: Patrick Monahan, Dr. Masaaki Ogawa, Dr. Fumiaki Yoshida, Dr. Daniel Schmidt and Amy S Chong. I spent the summer of 2012 working in the laboratory of Dr. Xue Han, who graciously hosted me and made sure I had all the necessary means for a particularly productive few months. I would to thank all members of the Han laboratory, especially Tyler Xuan Gu and Dr. Jaimin Zhao. I would like to thank my collaborators Dr. Hongkui Zeng (Allen Brain Institute), Dr. Hae Yoon and Dr. Derek Buhl (Tonegawa Laboratory at MIT) and Dr Alex Chubykin (Mark Bear's lab at MIT), Dr. Dannis Brouwer (University of Twente), Ronald Aarts (University of Twente) and Mareike Krijnen (University of Twente).

I would like to dedicate this thesis to nana (my father) who's unconditional love, support and sacrifice brought me where I am today. My elder brother Ullasa, has always been a source of constant inspiration, whom I have always looked up to for advice and counsel as any younger brother would.

Finally and most importantly, I would like to thank my loving wife Jyotsna. Graduate school with its numerous challenges can be a tough ride for most people I would not have made it through but for Jyotsna's infinite love, patience, support and understanding.

# TABLE OF CONTENTS

# LIST OF TABLES

# LIST OF FIGURES

# LIST OF ABBREVIATIONS

**ACSF:** artificial cerebrospinal fluid

**R(Z):** pipette resistance at depth Z in the brain, in microns (with the z-axis pointing downward, e.g. larger values of Z indicate deeper targets)

**Zu:** upper depth limit of the region targeted by the regional pipette localization stage

**Zl**: lower depth limit of the region targeted by the regional pipette localization stage

**R(ZNeuron):** pipette resistance at the depth at which the neuron is being recorded

**Rt**: pipette resistance threshold for neuron detection

**$Z_{0i}$:** Depths at which the multipatcher starts actuating the pipettes, i.e. outside the brain. *I* denotes the channel number

**$R_{Z0i}$:** Pipette resistances at depth $Z_{0i}$

**$Z_{Ui}$:** Upper depth at which pipettes i=1,2… n start neuron hunting

**R($Zi_{Neuron}$):** resistance of pipette in channel *i* at the depth at which the neuron is being recorded.

# SUMMARY

Whole-cell patch clamp electrophysiology of neurons *in vivo* enables the recording of electrical events in cells with great precision, and supports a wide diversity of morphological and molecular analysis experiments important for the understanding of single-cell and network functions in the intact brain. However, high levels of skill are required in order to perform *in vivo* patching, and the process is time-consuming and painstaking. Robotic systems for *in vivo* patching would not only empower a great number of neuroscientists to perform such experiments, but would also open up fundamentally new kinds of experiments enabled by the resultant high throughput and scalability. We discovered that *in vivo* blind whole cell patch clamp electrophysiology could be implemented as a straightforward algorithm and developed an automated robotic system that was capable of performing this algorithm. We validated the performance of the robot in both the cortex and hippocampus of anesthetized mice. The robot achieves yields, cell recording qualities, and operational speeds that are comparable to, or exceed, those of experienced human investigators. Building upon this framework, we developed a multichannel version of "autopatcher" robot capable establishing whole cell patch clamp recordings from pairs and triplets of neurons in the cortex simultaneously. These algorithms can be generalized to control arbitrarily large number of electrodes and the high yield, throughput and automation of complex set of tasks results in a practical solution for conducting patch clamp recordings in potentially dozens of interconnected neurons *in vivo*.

# CHAPTER 1

# INTRODUCTION

The vertebrate brain is a complex organ consisting of billions of neurons[1], each of which is interconnected with thousands of other neurons through synapses[2]. Each neuron receives information via synaptic transmission, computes an electrical signal within it, and transmits information to downstream neurons. They express different sets of genes[3], have myriad morphologies, and undergo intrinsic molecular changes in different ways during cognitive tasks such as learning. One of the fundamental challenges for neuroscientists has been the inability to link the knowledge we have on cellular level phenomena, such as synaptic transmission, often gained by *in vitro* experimental preparations; to characterizations of the higher order system properties like learning and memory. To gain a mechanistic understanding of how cellular level activities of neuronal networks give rise to these higher level cognitive abilities, and how they go awry in brain disorders, one would have to observe networks of neurons processing electrical signals in the living mammalian brain, while at the same time extract their genetic and morphological information of each individual neuron.

## 1.1 Patch Clamping

One technique that is uniquely able to do this is the whole cell patch clamping technique. First developed by Erwin Neher and Bert Sakmann's groups in the early 1980's[4], patch clamping involves the use of a glass pipette with a tip size comparable to the size of the recorded neuron (~1 μm), filled with a conduction saline solution. The pipette is carefully manipulated until it makes physical contact with the cell being targeted, at which point application of a slight suction pulls in 'patch' of the membrane into the tip of the glass electrode, resulting in the formation of a high resistance seal between the glass tip and the cell membrane. This high resistance seal also called a 'gigaseal' or 'gigaohm seal' because the resistance of the seal is greater than a gigaohm, enables the electrical isolation of the patch of the membrane. All current measured by the pipette pass through the 'patched' membrane with very little external noise being picked up as a result of the high resistance. In this seminal work, Hamill *et al* demonstrated several versions of this technique such as the outside out patch, the inside out patch, cell attached patch and whole cell patch recording techniques, each of which are uniquely suited for a number of single cell, and single ion channel experiments. In the whole cell patch clamp version of this technique, which will be the primary focus of this thesis, the patch of membrane trapped in the tip is ruptured either by application of a brief pulses of suction, or by application of a voltage pulse and this allows access to the intracellular space of the cell. In this case, the current measured by the pipette is the net summation of the all the currents flowing through the various ion channels of the particular cell.

While initially developed to study the electrophysiology of cultured cells *in vitro*, the whole cell patch clamp technique was further adapted for intracellular recording of single neurons in brain slice preparations[5]. This extension enabled studies of single brain

cells in quasi-intact brain circuits has led to several key insights into the synaptic organization of the brain[6-11]. Further, access to the intracellular space of the recorded neuron offers additional capabilities that are not possible with other extracellular and intracellular recording strategies (such as sharp electrodes). The intracellular pipette solution in the pipette can contain neurobiotin or biocytin to stain the cell via diffusion during whole cell patching and this can be used to determine the morphology of the neuron after the whole cell recording[12, 13]. Furthermore, by accessing the intracellular cystosol and harvesting it, it is possible to characterize the single cell gene expression profile of the recorded cell[3, 14-18] allowing a comprehensive characterization of the cell being recorded from.

### 1.2 Patch clamping of single neurons *in vivo*

More recently, Margrie *et al* demonstrated the ability to conduct whole cell patch clamping recordings of neurons in the intact rodent brain[19]. A key change in the existing patch clamp protocols in slices was the introduction of the patch pipette into the brain at a high positive pressure, so as to prevent the tip from fouling. This work demonstrated that it was possible to obtain high quality whole cell recordings from single cells that were remarkably stable despite the movement of brain tissue due to heartbeat and breathing perturbations. Whole cell recordings obtained under anesthesia, remained viable, even after the animal was removed from the effect of the anesthetic. Further, the low series resistance of whole cell recordings allowed voltage clamp recordings[20-22], unlike the

traditional *in vivo* intracellular recordings done using sharp microelectrodes[23]. The same group later on demonstrated that it was possible combine this technique with a two photon imaging system, to obtained recordings from specific cell types that was genetically tagged with a flourescent molecule such as GFP[24]. As an alternate version of this technique, Kitamura *et al*[25], developed the *in vivo* shadow patching technique, wherein the patch electrode was used to perfuse the extracellular space surrounding the neuron of interest with a fluorescent dye, thus enabling the neuron to be visualized as a negative image ('shadow') and identified on the basis of its somatodendritic structure. The same electrode was then placed on the neuron under visual control using a two-photon microscope to allow formation of a gigaseal. Several groups have since used such optically targeted patch clamp recordings to study the characteristics identified cell types and the causal role played by them in cortical signal processing[26-32]. It must however be noted that due to the limitations of the two photon optics, such targeted methods can be employed only to record from optically accessible layers of the brain (300-400 μm); targeting deeper structure would require more invasive techniques such as careful aspiration of the cortex to image for example the hippocampus[33].

The increased stability of whole cell recordings as compared sharp microelectrode recording enables the recordings of neurons in awake head fixed mice. Albert Lee *et al* demonstrated a head borne version of the *in vivo* patch clamping system, wherein, whole cell recordings were obtained when the animal was under anesthesia, and subsequently anchored to the skull prior to administration of an anesthetic antidote[34-37]. The recordings remained stable even after the animal was woken up and moved freely in a behavior arena.

### 1.3 Electrophysiology of neuronal ensembles the intact brain

Traditionally, extracellular recording techniques have been used for probing of how neurons work together within and between brain regions to generate neural synchrony, population codes, and other manifestations of how neural networks operate by coordination of their circuit elements (e.g., [38-45]). Critical insight has been gained even in the absence of the ability to resolve the sub-threshold synaptic and intrinsic conductances within neurons. In contrast, simultaneous patch clamping among sets of neurons *in vivo* can not only resolve supra-threshold spiking activity, but also enables assessment of additional core measures of neural dynamics, including patterns of intrinsic channel conductance dynamics, and gap junction-mediated neural network activity. Further, the ability to isolate mRNA from individual cells for molecular analysis, the ability to fill cells with dyes for assessment of morphology and connectivity, and the ability to dialyze in pharmacological agents, also enable relatively comprehensive characterization of each neuron within a network. Although microcircuit connectivity has been probed in slices using parallel patch clamp with 2-12 electrodes (e.g., [6, 46-48]), this strategy has been impractical to conduct in the intact brain, given the difficulties of patch clamping. The existing literature on simultaneous whole cell patch clamping *in vivo* in two neurons, give us important insights into how sub threshold membrane potential dynamics manifest across neuronal networks in different brain states[27, 29, 31]. By combining the capabilities of measuring cell connectivity, as well as gene expression patterns to large numbers of cells

*in vivo*, it will be possible to link cellular phenomena such as synaptic plasticity to systems properties such as learning and memory.

### 1.4 Limitations and Challenges of *in vivo* patch clamping

Despite being the gold standard of electrophysiology, patch clamping *in vivo* as a reproducible technique for large-scale studies, both at the single cell level, as well as being utilized for studying ensembles of neurons has not progressed very much over the last 10 years. One of the fundamental challenges has been that *in vivo* patch clamping has is something of an artform to perform requiring a considerable degree of skill and mastery. The success rates of *in vivo* patch clamping experiments as reported in existing literature are low (~20%). The complexity of the tasks involved has precluded studies requiring the simultaneous recordings of multiple neurons.

One strategy that can be employed to overcome the low throughput and difficulty of the process, and enable scalability is to automate the process of *in vivo* patch clamping. Many pioneering technologies have been proposed that automate the patching of cultured cells *in vitro*[49], often by sucking a freely floating cell down onto a microscale pore, or by otherwise bringing a planar substrate into contact with a cultured cell. These technologies, however, are not usable in intact tissues such as in the living brain. Other technologies proposed for intracellular recording (e.g., static arrays of microfabricated nanowire or other nanoscale probe[50]) have similarly been utilized on cultured cells, but

are currently difficult to make and utilize, have significantly lower signal quality than that yielded by patch clamping, have not been successfully deployed *in vivo*, and are not capable of transcriptomic harvesting, dye filling, and other tasks critical for linking electrophysiological phenotype with other cell phenotypes. In contrast, the intrinsically fluidic aspect of patch clamping supports, in the intact brain, the tip cleanliness required for good intracellular recordings; additionally, the ability to move the patch pipette enables higher yields of cells than obtainable with static probes, as well as the ability to target neurons visualized in two-photon microscopy.

Once the *in vivo* patch clamping process has been automated, robotic systems can be developed that employ these automation algorithms to control multiple devices at the same time, enabling a degree or have multiple electrodes in a single device targeting many cells simultaneously at the same time. Furthermore, these robotic systems will have be designed from the ground up, with the specific function of patch clamping *in vivo,* as traditional planar microelectrode array devices[51, 52] used for *in vitro* patch clamping applications cannot be used in the complex three dimensional structure of the brain.

### 1.5 Thesis Outline

In chapter 2 of this thesis, we describe in detail how we discovered an algorithm for automating whole cell patch clamping. We report on the development of an automated robotic system that was capable of performing this algorithm. We validated the performance of the robot in both the cortex and hippocampus of anesthetized mice. The robot achieves yields, cell recording qualities, and operational speeds that are

comparable to, or exceed, those of experienced human investigators. In Chapter 3 we demonstrate how such an autopatching robot can be combined with optogenetic stimulation hardware, to optically perturb recorded neurons, to identify specific cell types in the brain. Building upon this framework, we developed a multichannel version of "autopatcher" robot capable establishing whole cell patch clamp recordings from pairs and triplets of neurons in the cortex simultaneously. These algorithms can be generalized to control arbitrarily large number of electrodes and the high yield, throughput and automation of complex set of tasks results in a practical solution for conducting patch clamp recordings in potentially dozens of interconnected neurons *in vivo*. We report on these finding in Chapter 4 of this thesis.

# CHAPTER 2

# AUTOMATED WHOLE CELL PATCH CLAMPING OF NEURONS *IN VIVO*

## 2.1. Introduction

Whole-cell patch clamp electrophysiology, in which a glass pipette electrode is used to gain electrical and molecular access to the inside of a cell[4], is a gold standard technique for the high-fidelity recording of electrical activity in neurons embedded within intact tissue, such as in brain slices[53-57], or *in vivo*[20, 26, 31, 36, 58-62]. *In vivo* patching of cells in intact brain presents several capabilities that make it of great use: the recordings present extremely high signal-to-noise ratios and thus can be used to reveal subthreshold responses such as synaptic or ion channel events. Current can be delivered into a pipette to drive or silence the cell being recorded, or to support the characterization of specific receptors or channels in the cell. This technique also allows for infusion of chemicals such as cell-filling dyes that enable anatomical visualization, as well as the extraction of cell contents for transcriptomic analysis[14, 16, 63]. However, whole-cell patch clamping of cells in intact tissue is laborious, being something of an art to perform, especially *in vivo*. Although protocols exist for performing whole-cell patch clamp recording in such conditions[20, 21, 24, 60, 64-68], much practice is required by individual investigators to master the technique, since each step in the process of looking for a neuron and establishing the

recording requires intuition as well as fast judgment and action. This has limited adoption to a small number of labs, and also prevents systematic or scalable *in vivo* patch clamping experiments from being possible.

Ideally, an algorithm could be developed which could be executed by a robotic system in order to enable automated whole-cell patch clamp neural recording *in vivo*. Such an "autopatching" robot would greatly increase throughput, opening up this technology to a greater user base within neuroscience. Additionally, the scalability and parallelizability enabled by an automated *in vivo* patching system would support novel kinds of experiment – such as the use of such an autopatcher to systematically profile many individual cells for electrophysiological and molecular characterization in a brain disorder model, or the ability to perform novel kinds of pharmaceutical assessments that examine the impact of drugs on many individual cells in the context of the intact brain. It would also open up the ability to perform systematic single-cell analyses in intact tissue in other areas of bioengineering, biotechnology, and medicine, where the low throughput of, and high skill required for, patch clamping cells within intact tissues have remained barriers to adoption.

In order to derive an algorithm for automatic patch clamping, we assessed each of the actions and decisions that humans perform during the process of patch clamping cells in intact tissue. We focused on blind whole-cell patch clamp recording *in vivo*, because of its relative inexpensiveness, its usefulness in a diversity of brain regions (and not just in surface structures visualizable by optical microscopy), and its widespread utility in

performing unbiased neural recordings in a diversity of species. We discovered that a simple robot comprising a programmable linear motor, and a bank of pneumatic valves, was capable of identifying candidate cells to record from, and establishing quality recordings of neurons *in vivo*, when programmed to monitor the pipette for precise sequences of changes in electrical resistance, and to actuate the motors and valves rapidly upon recognition of these changes. The precision measurement and actuation of this autopatching robot is essential for performance of the algorithm described here, as it requires quantitative measurement and analysis, as well as fast reaction times.

We demonstrate the utility of the autopatcher in obtaining recordings in both the cortex and hippocampus of the anesthetized mouse brain. The autopatcher was capable of achieving high yields of both whole-cell patch and gigaseal cell-attached patch recordings (~30% of overall attempts, even in deep tissue, resulted in successful recordings), exceeding yields of many trained human investigators. Acquisition of high-quality recordings proceeded rapidly (taking just 3-7 minutes each), neuron recordings could be held for an hour or longer, and recording qualities were comparable to those of trained humans (e.g., access resistances in the tens of MΩ). Being a robot, its performance did not decrease over time due to declines in attention or energy. Because the robot is automated, an individual can monitor multiple rigs at once, making the number of cells recordable by a single unskilled human investigator perhaps 100 per day or greater, and thus opening up the possibility of systematic electrical and molecular analyses of single cells in intact tissue. The autopatcher is easy to implement on existing patch clamp rigs, requiring just one inexpensive motor and a signal acquisition board, as

well as a few pneumatic control valves, making it a practical solution for labs interested in automating their existing rigs, or in newly adopting the use of patch clamp technology for intact tissue analysis at the single cell level.

## 2.2 An autopatching robot: components, overview of algorithm, and success rate

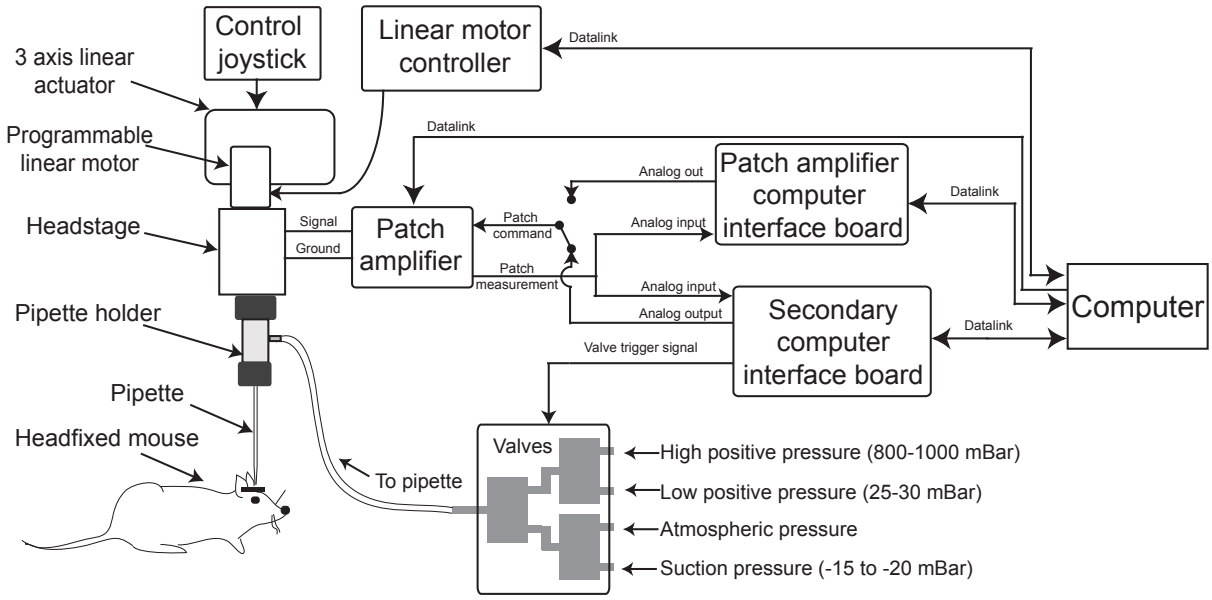


**Figure 2.2.1: The autopatcher: a digitally controlled *in vivo* patch clamp setup:** Schematic of the robotic system we implemented both to explore the parameterization of the *in vivo* patch process, and to perform the autopatching algorithm (**Fig. 2.3.1**). In essence, the system consists of a conventional *in vivo* patch setup (i.e., pipette, headstage, 3 axis linear actuator, patch amplifier plus computer interface board, and computer), equipped with three additional simple modules: a programmable linear motor (to move the pipette up and down in a temporally precise fashion), a controllable bank of pneumatic valves for pressure control, and a secondary computer interface board to enable closed-loop control of the motor based upon sequences of pipette resistance measurements.

Our robot shares many core components with those of conventional *in vivo* patch clamp systems as shown schematically in **Fig 2.2.1**. The recording probe is a glass micropipette pulled to a fine tip, and filled with conductive saline solution, into which a silver chloride wire is inserted that electrically connects the conductive solution to an amplifying headstage. This headstage is held in place and moved by a three axis linear actuator; the headstage communicates electrically with an amplifier and computer interface board that both records the neural signals and delivers neural control signals to the headstage. In addition to these conventional components, our robot also contains an additional linear motor for precision advancement and retraction of pipettes, as well as additional computer interface boards for monitoring the pipette electrical signals and for controlling the linear motor, and a bank of valves to control the pressure applied to the inside of the pipette. A photograph of the linear actuators, and the programmable linear motors used for pipette actuation is shown below in **Fig. 2.2.2**.

The process of the robot performing whole-cell patch clamp neural recording *in vivo* is outlined in **Fig. 2.2.2**. First, high pressure is applied to the pipette to prevent pipette blockage as it enters the brain, and the pipette electrical resistance is evaluated (e.g., between 3-9 MΩ is typical). If the pipette is of acceptable resistance, it is automatically lowered to a pre-specified target region within the brain (the stage here labeled "regional pipette localization"), followed by a second critical examination of the pipette resistance for quality control. This check is followed by an iterative process of lowering the pipette by small increments, while looking for a pipette resistance change indicative of proximity to a neuron suitable for recording (the "neuron hunting" stage).

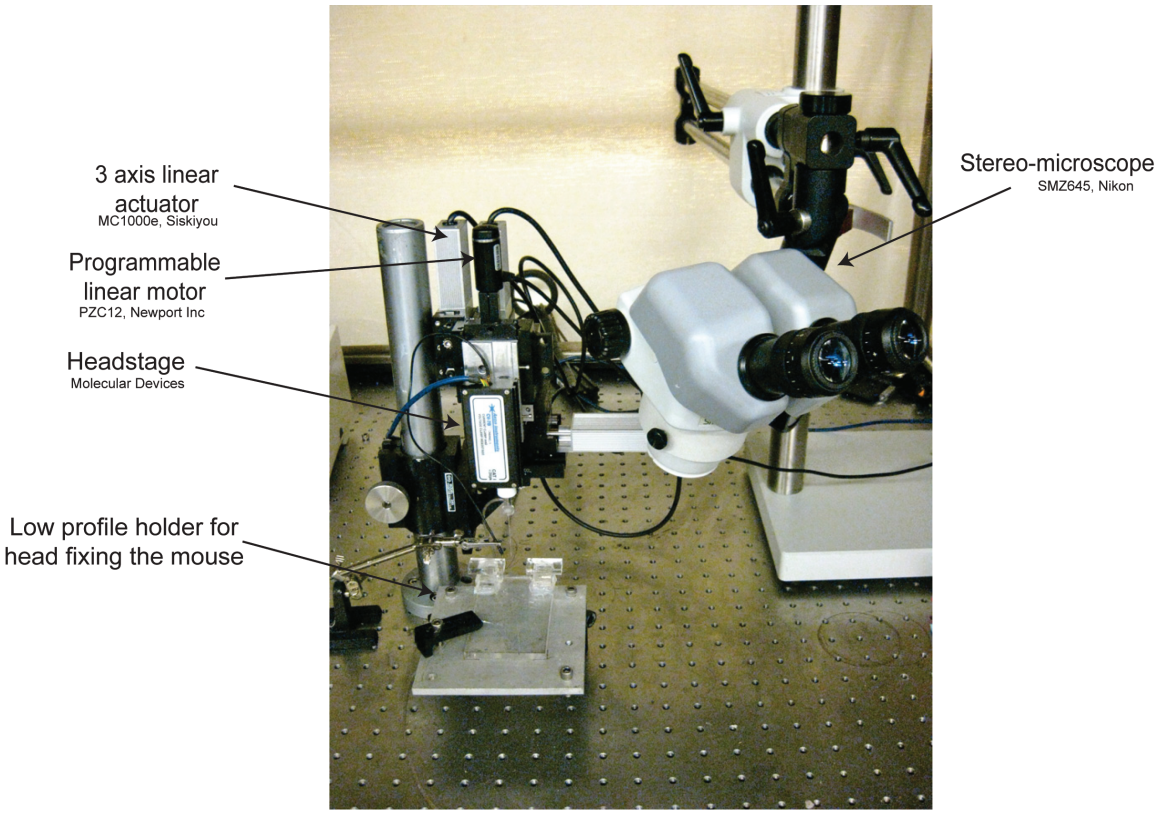


**Figure 2.2.2: Photograph of automated patch clamping system**, focusing on the linear motor attached to the 3 axis linear actuator, and also showing the low-profile holder for head-fixing the mouse.

During this phase, the robot looks for a specific sequence of resistance changes that indicates that a neuron is proximal, attempting to avoid false positives that would waste time and decrease cell yield. After detecting this signature, the robot halts movement, and begins to actuate suction and pipette voltage changes so as to form a high-quality seal connecting the pipette electrically to the outside of the cell membrane (the "gigaseal formation" stage), thus resulting in a gigaseal cell-attached recording.

If whole-cell access is additionally desired, the robot then performs controlled application of suction as well as brief electrical pulses to break into the cell (the "break-in" stage). Throughout the process, the robot applies a voltage square wave to the pipette (10 Hz, 10

mV alternating with 0 mV relative to pipette holding voltage), and the current is measured, in order to calculate the resistance of the pipette at a given depth or stage of the process. Throughout the entire process of robot operation, this pipette resistance is the chief indicator of pipette quality, cell presence, seal quality, and recording quality, and the algorithm attempts to make decisions – such as whether to advance to the next stage, or to restart a stage, or to halt the process – entirely on the temporal trajectory taken by the pipette resistance during the experiment. The performance of the robot is enabled by two critical abilities of the robot: its ability to monitor the pipette resistance quantitatively over time, and its ability to execute actions in a temporally precise fashion upon the measured pipette resistance reaching quantitative milestones.

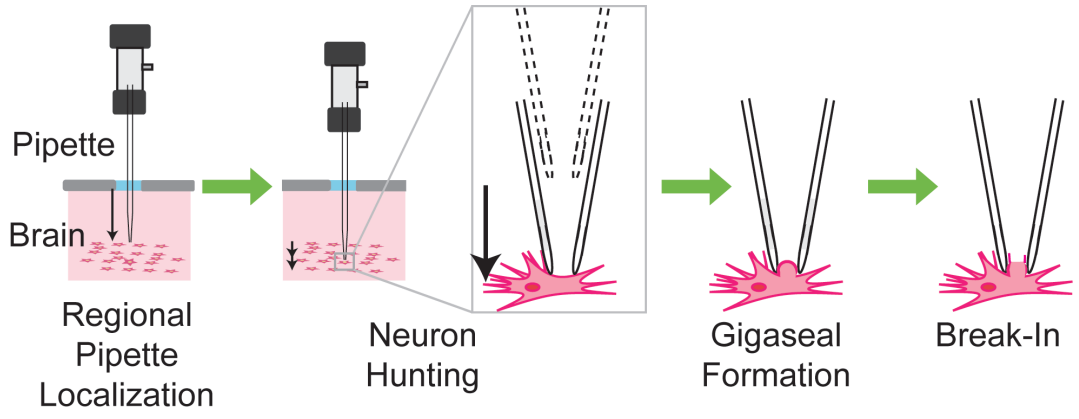


**Figure 2.2.3: Algorithmic breakdown of the *in vivo* patch clamping process:** The four stages of the *in vivo* patch process which we iteratively optimized: "regional pipette localization," in which the pipette is lowered to a target zone in the brain; "neuron hunting," in which the pipette is advanced until a neuron is detected via a change in pipette resistance; "gigaseal formation," in which a gigaseal cell-attached patch state is achieved; "break-in," in which the whole cell configuration is achieved. For each stage, we systematically explored the parameters governing success of the stage, as well as the success of the overall procedure, discovering a number of stereotyped strategies appropriate for robotic execution, as well as precise numerical milestones governing within-stage and between-stage decisions (including quantitative measures of pipette quality, cell presence, and seal quality derived from the pipette resistance).

In the next section, we describe the algorithm performed by the robot (**Fig. 2.3.1 and 2.3.2**) in detail, as well as how we discovered, implemented, and tested this algorithm. But first, we summarize the performance of the robot (**Table 2.2.1**). When validated on a final robot validation test set of neural targets within the cortex and hippocampus of anesthetized mice, the robot (**Fig. 2.2.1**), running the algorithm (**Fig. 2.3.1**), obtained successful whole-cell patch clamp recordings 29.1% of the time (defined as the holding of a cell with under 500 pA of holding current for at least 5 minutes; n = 23 out of 79 attempts starting with pipette loading into the pipette holder), and successful gigaseal cell-attached patch clamp recording 30.8% of the time (defined as obtaining of a stable seal higher than 1 GΩ in resistance; n = 24 out of 78 attempts). These success rates are similar to, or exceed, those reported by trained investigators for blind whole-cell patch clamping *in vivo*[25, 37, 60].

**Table 2.2.1:** Yields and durations of each of the four stages, when executed by the robot of **Fig. 2.2.1 and 2.2.2**, running the autopatching algorithm in the living mouse brain, aiming for targets in cortex and hippocampus (fully automated successful attempts defined as < 500 pA of current when held at –65 mV, for at least 5 minutes; *n* = 24 out of 73 attempts, successful gigaseal cell-attached patch clamp recording defined as a stable seal of > 1 GΩ resistance; *n* = 27 out of 75 attempts).

| | **Regional Pipette Localization** | **Neuron Hunting** | **Gigaseal Formation** | **Break-In** |
|---|---|---|---|---|
| **%age yield, whole cell patch** | 81% | 93% | 51% | 82% |
| **%age yield, gigaseal cell-attached** | 80% | 93% | 41% | N.A |
| **Duration of stage (mean ± s.d.)** | 10 s | 2.2 ± 1.7 min | 2.6 ± 1.0 min | 1-10 s |

Focusing on the robot's performance after the "regional pipette localization" stage (i.e., leaving out losses due to pipette blockage during the descent to depth), the autopatcher was successful at whole-cell patch clamping 41.8% of the time (n = 23 out of 55 attempts starting with the "neuron hunting" stage), and at gigaseal cell-attached patch clamping 40.7% of the time (n = 24 out of 59 attempts). From the beginning of the neuron-hunting phase, to acquisition of successful whole-cell or gigaseal cell-attached recordings, took 5 $\pm$ 2 minutes for the robot to perform (n = 47 successful recordings; discussed in detail in **Fig. 2.4.2** and accompanying text), similar to, or better than, the rate reported by trained investigators. The quality of the neural recordings was high, with pipette access resistances and cell leaks comparable to those of past work performed by skilled humans (discussed in detail in **Fig. 5** and accompanying text). Thus, the autopatcher was capable of high yields, comparable to those achieved by trained human *in vivo* patch clamp electrophysiologists, with speeds that can support experimental yields of many dozens of cells per day, in an automated, scalable, and parallelizable fashion.

## 2.3. Derivation of the autopatcher algorithm: principles of whole cell patch clamp *in vivo*

We derived the autopatcher algorithm (**Fig. 2.3.1**) by analyzing and optimizing successively each of the four stages of robot operation (**Fig. 2.2.2**). Importantly, the algorithm derivation described below was performed completely in the cortex, but the testing of the algorithm was performed on both cortical neurons as well as hippocampal neurons. This generalization of the algorithm from cortex to hippocampus implies that the algorithm possesses a certain degree of generalization power, i.e., we did not

unconsciously optimize the algorithm just for one brain region. Nevertheless, it is likely that very specialized neurons in novel brain regions may require tuning of select algorithm parameters, and the ability to perform this optimization using the robot would accelerate this process of customization, allowing for rapid iteration beginning from the parameters derived here. We also tested the autopatcher on brain slices, where it was capable of obtaining good recordings (data not shown).

At the beginning of the algorithm (gray flowchart shapes in the "setup" stage at top of **Fig. 2.3.1**), a pipette is placed in the holder and provided strong positive pressure, and the robot then (stage 1, "regional pipette localization") lowers the pipette at a speed of 200 μm/s[24, 36, 60, 61, 66] to the appropriate depth for neuron hunting. We found that using a high positive pressure (800-1000 mBar), greater than done in the past[9, 11, 15, 16, 25], greatly improved the yield of subsequent stages. Another key finding was that after this first localization stage was complete, many pipettes had slightly increased their resistances over their original values. Pipettes that acquired greater increases in resistance in this first stage had, in later stages of robot operation, more variability in their pipette resistance measurements than pipettes with smaller increases. For example, the variance between successive measurements of pipette resistance across multiple steps taken during the "neuron hunting" stage was 87 $\pm$ 60 kΩ for pipettes that experienced zero increase in resistance acquired during the first localization stage, but was 218 $\pm$ 137 kΩ for pipettes that experienced 500 kΩ increases, significantly more variability (mean $\pm$ std. dev; $p < 0.05$, t-test, n = 7 trials each).

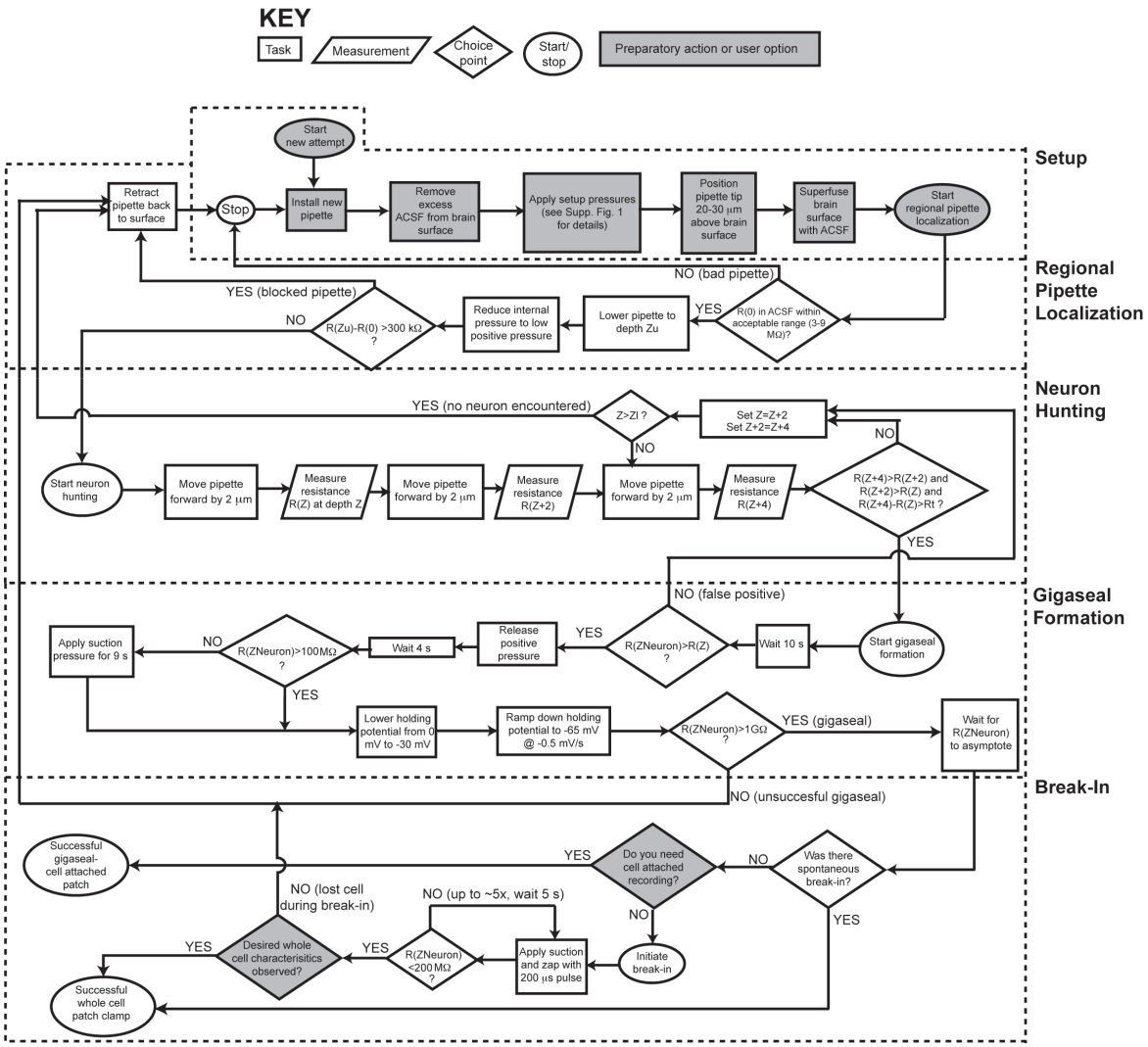


**Figure 2.3.1: Detailed flowchart, showing all steps for the automated *in vivo* patch process, including stereotyped strategies for stage execution, and quantitative milestones governing process flow and decision making.** Dotted lines frame each of the stages of the algorithm; within the dotted line frames, symbols representing tasks, measurements, and choice points are indicated, along with text explicating the individual steps and consequences of decisions (see "**KEY**" for definition of symbols). Abbreviations: ACSF, artificial cerebrospinal fluid; R(Z), pipette resistance at depth Z in the brain, in microns (with the z-axis pointing downward, e.g. larger values of Z indicate deeper targets); Zu, upper depth limit of the region targeted by the regional pipette localization stage; Zl, lower depth limit of the region targeted by the regional pipette localization stage; R(ZNeuron), pipette resistance at the depth at which the neuron is being recorded (which will vary over time, as the later stages of the process, gigasealing and breaking-in, occur); Rt, pipette resistance threshold for neuron detection.

By screening out pipettes that underwent large increases in pipette resistance during the first localization stage, the variability of pipette resistance measures in successive stages of robot operation can be reduced, improving the accuracy of the subsequent stages. We found that by excluding pipettes that increased resistance by more than 300 kΩ in the first localization stage (which would result in a 136 $\pm$ 83 kΩ measurement-to-measurement variance in the neuron hunting stage; n = 123), ~15% of the pipettes would be discarded (24 out of 147 total attempts in the final robot validation test set; **Fig. 1Aii**), but because of the low variability of later pipette resistance measurements, it became possible to detect neurons very precisely, as indicated by well-defined increases in pipette resistance, during the neuron hunting stage (stage 2).

In published neuron hunting protocols, a visually identified increase of 20-50% in pipette resistance was considered to be indicative of the presence of a viable neuron, appropriate for attempting gigaseal and break-in stages[60, 61, 66]. One advantage of a robotic system is that it can analyze sequences of pipette resistance values acquired over a series of successive motor steps, thus enabling precise signatures of neuron presence that algorithmically replicate the intuitive comparisons being performed by trained human investigators. We systematically explored this parameter space, varying the number of consecutive 2 μm steps over which pipette resistance values would be considered, and also varying the numerical threshold that the pipette resistance would have to increase over these steps in order for a neuron detection to be concluded, aiming to maximize the success of manually establishing whole-cell patch clamping for each

neuron-hunting procedure. We found analysis of only 2 consecutive motor steps (i.e., pipette resistance data over 4 μm of travel) to yield noisy data, and 4 consecutive steps (i.e., over 8 μm of travel) to detect the neuron too late to get good recordings, perhaps because the cell was stretched. Thus, we focused our analysis on pipette resistance sequences taken over 3 consecutive steps (6 μm). Because the measurement-to-measurement variability on consecutive motor steps (see above) was about 136 kΩ, we chose to investigate thresholds of pipette resistance increase between the first and third step of 150, 200, 250, 300, 350, and 400 kΩ. We found that first-to-third step differences of at least 200-250 kΩ yielded patchable neurons at success rates of 40-45% (11 cells out of 25 were manually successfully gigasealed and broken-into). In contrast, 3-step sequences with <200 kΩ thresholds or >300 kΩ thresholds had much lower success rates of manual gigasealing and breaking-into (5-15% yields; 4 out of 27), perhaps due to errors in neuron detection or approach (false positives for the lower thresholds; cell stretching for the higher thresholds). Thus, we chose for the robot a 200 kΩ threshold for pipettes of 3-5 MΩ initial resistance, and 250 kΩ for pipettes of 5-9 MΩ initial resistance. In the final robot validation test set (**Table 2.2**), we found that this neuron hunting algorithm converged upon targets within the localized region 93% of the time (114 targets detected out of 123 total trials); of these 114, 47 cells ultimately resulted in a patch recording (cell-attached or whole-patch patched), or a yield of 41% - similar to the 40-45% rate obtained during the pilot studies using manual validation, mentioned earlier in this paragraph.

For comparison purposes, we evaluated the value of observing heartbeat modulation as an indication of neuronal detection. According to ref.[19, 66], "*The best predictor of the pipette having made contact with a neuronal membrane was pulsation of the reduced current pulse at heartbeat frequency… Slow changes in current pulse amplitude that lacked the rhythmic modulation rarely resulted in neuronal recordings… one of the trademark characteristics of the 'strike' of the pipette against neuronal material is pulsation of the recorded current at heartbeat frequencies. In our experience this is the best indicator of the patch pipette making contact with neuronal material. While there were instances in which this pulsation was due to contact with non-neuronal membranes, presumably glia or blood vessels, this occurred less than 5% of the time.*" In order to determine whether heartbeat modulation of pipette currents was also a good indicator of neuronal detection in our hands, we used the autopatching robot to record $n$ = 17 neurons, keeping attuned to the presence or absence of heartbeat modulation. All 17 neurons patched exhibited, at the point of completion of the "neuron hunting" stage, a prominent heartbeat modulation (see **Fig.2.3.2 a-c** for examples), in full accordance with the Margrie et al. paper. Thus, in principle, heartbeat modulation could be added as a confirmatory check in the algorithm, although we did not find it necessary; it appears that our algorithms' search for a monotonically increasing pipette resistance recapitulates the same essential process that takes place in the heartbeat detection procedure.

We note that we often saw heartbeat modulation sometimes, but not always, when the patch pipette was 10 μm away from the neuron (e.g., five 2 μm steps before the pipette halted and the "neuron hunting" stage ended; **Fig. 2.3.2c**); this occurred 6 out of

the 17 times, and may indicate that heartbeat modulation may occur even before the pipette resistance increases, and thus when a neuron has not been quite detected. (This neuron-selectivity that our algorithm encapsulates may explain why ~90% of the structures we patched were neuronal, with only ~10% glial.

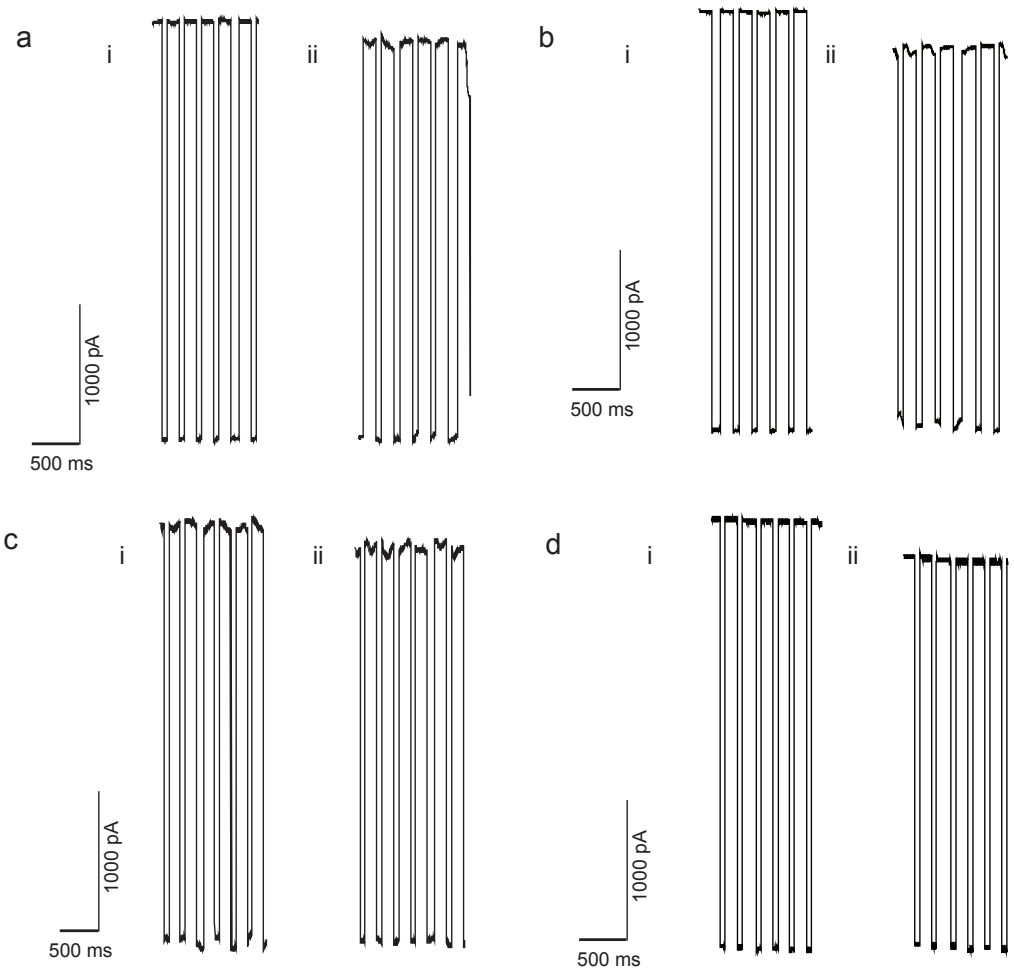


**Figure 2.3.2. Evaluating raw current traces recorded during "neuron hunting" stage.** Shown are patch pipette currents obtained when a square voltage wave (10 Hz, 10 mV during "neuron hunting" stage) is applied to the pipette in voltage clamp mode. The *left* traces in **a-d** are current traces measured 10 mm before the pipette was stopped at the end of "neuron hunting" to attempt "gigasealing". The *right* traces in **a-d** are current traces measured at the point the pipette was stopped at the end of neuron hunting. Trials **a-c** culminated in successful whole cell patch clamp recording, while **d** did not result in

successful gigaseal, and subsequently was unsuccessful in establishing whole cell as well. Comparing the successful trials, while the *left* traces in **a** and **b** show no heart beat modulation at distance from the neuron**,** the *left* trace in **c** shows heartbeat modulation of the current traces even 10 μm away from point of stoppage. The *right* traces in **a-c** all show prominent heartbeat modulation at the point of stoppage; this is not seen in the *right* trace in **d.**

Why so few glia and non-excitable structures? It is possible that we are actually encountering a lot of these, but we are not sealing well on to them with our current pipette shape and search algorithm. Remember, although most of the cells we patched indeed were neurons – the patch algorithm did not form good gigaseals typically ~50% of the time – and those targets may be with connective tissue, glia, blood vessels, etc. This is consistent with the strong neuron selectivity of papers such as ref. as mentioned above.) Notably; we also analyzed $n = 26$ attempts in which neuron hunting halted on an object (perhaps a cell, or a piece of connective tissue), but which did not yield a gigaseal (e.g., **Fig. 2.3.2d**); in 24 such cases (such as the one shown in **Fig.2.3.2 d right**), there was no heartbeat modulation; in the remaining two cases, extreme heartbeat modulation was seen (perhaps suggesting a blood vessel to be there). Thus again, heartbeat modulation could be used to confirm our algorithm, but given the complexity in automating heartbeat modulation analysis (heartbeat, after all, varies greatly in shape and frequency from cell to cell, mouse to mouse, and depending on anesthesia protocol), we decided to stick with the simpler-to-automate monotonic pipette resistance_criterion for our algorithm. It is possible, however, given our independent confirmation of the heartbeat modulation criterion, that heartbeat modulation, given its prominent visual pattern, is still one of the best methods for human use for neuron detection. In principle,

future versions of the algorithm that take heartbeat modulation into account, might enable failed gigaseal trials to be ended early, thus saving several seconds per cell of time, and speeding up the robot still more.

The gigaseal formation stage (stage 3, **Fig 2.2.2** and **Fig 2.3.1**) was adapted from the best practices of prior protocols, aiming for a stereotyped sequence of steps amenable to automation. The motor was switched off after neuron hunting completion, and a 10 second wait period was imposed to see if the pipette resistance decayed back to baseline (this happened 1 time out of the 114 successful hunts; the motor simply reactivated and the neuron-hunting phase resumed). Then the positive pressure was released, suction pressure was applied if the gigaseal was not spontaneous, and the holding potential was reduced slowly to -65 mV (see **Fig. 2.3.1**, "gigaseal formation" for the detailed description of the series of steps). If a gigaseal was not apparent at the end of this procedure, the algorithm was halted (although, these could be considered loose-cell attached patches – of interest because of the excellent single cell isolation offered, even if subthreshold and synaptic events are not observable as in the whole-cell case); else, the gigaseal was left until it plateaued for at least 10-15 seconds (see **Fig. 2.4.1** for example). In the final robot validation test set (**Table 2.2.1**), of the 114 targets detected by "neuron hunting", 52 formed gigaseals (46% yield) under the operation of the robot.

The final stage was break-in (stage 4), and again, we aimed for a procedure that would be easily and objectively automated. The robot applied suction for periods of 1 second, and then precisely activated the "zap" function of the patch amplifiers (a 200 μs

voltage pulse to 1 V), repeatedly every 5 seconds until the whole-cell configuration was obtained. In this scenario, we reserved the judgment of the whole cell state for a human observer, who could then halt the program, because we were seeking to analyze the quality of our recordings; the stereotyped changes due to the cell capacitance and resistance being appended to the pipette are also quantifiable to the extent of yielding automation of program cessation, if desired. In the final robot validation test set, the 52 gigasealed neurons were split into two sets: 28 underwent break-in with the robot, and 24 were manually broken-into in order to evaluate the success of our automated break-in procedure. Out of the 28 automatically broken-in trials, 23 successfully attained whole-cell mode (82% success); failures (5 cells) were stringently defined as a lack of break-in, "losing" the cell within 5 minutes of attaining whole-cell recording, or exhibiting >500 pA of holding current (at -65 mV). For the 24 other cells, we achieved manual whole-cell break-in in 100% of the cells using standard methods, applying brief suction pulses in rapid succession[66].

We incorporated a second method of automated in vivo patching using suction pulses to achieve the break-in step (algorithm described in **Fig. 2.3.3**).

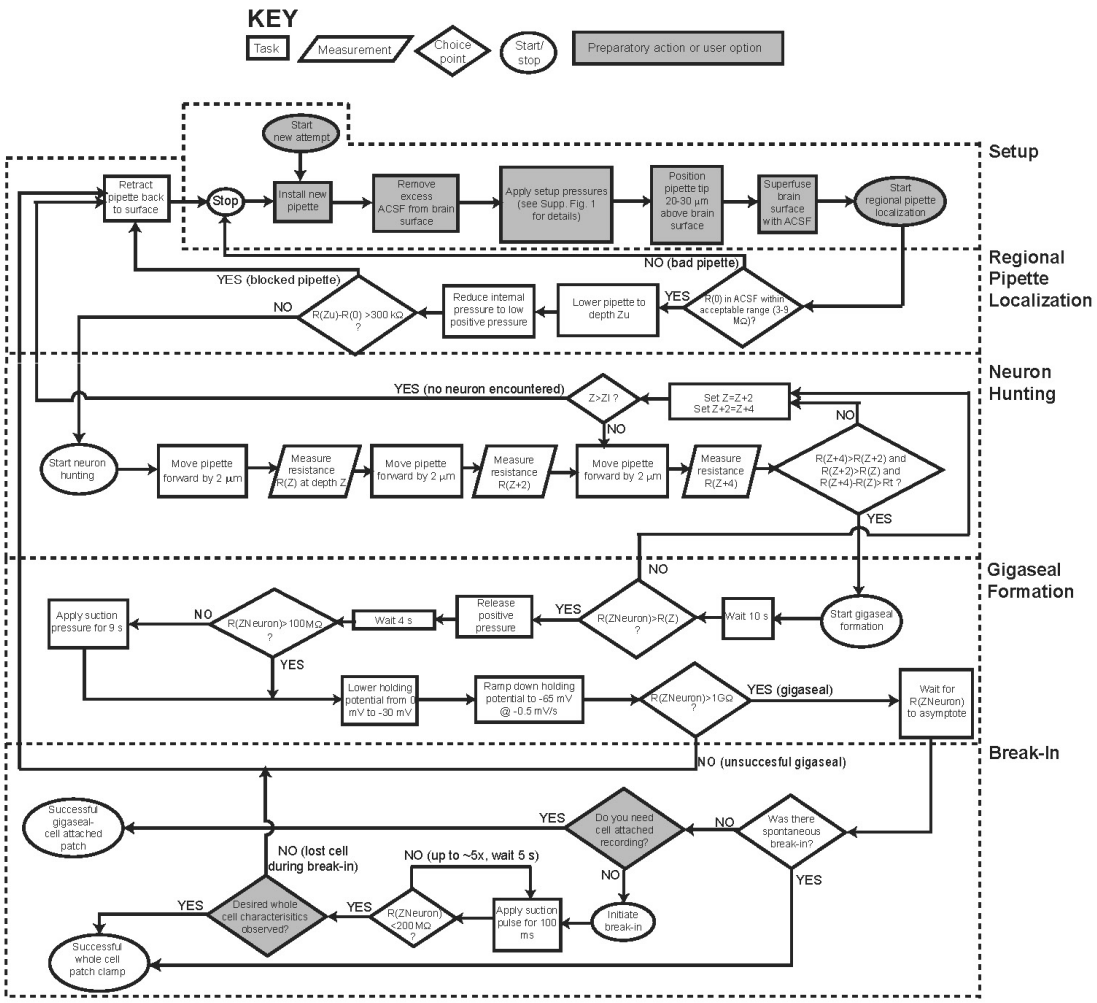


**Figure 2.3.3. The algorithm of Fig. 2.3.1, modified to use suction pulses instead of "zap", to break in.** The algorithm for automated *in vivo* patch clamping when using "suction pulses" for the break-in stage, rather than "zap," to establish the whole cell state. All symbols, shadings, headers, etc. are as in **Fig. 2.3.1.**

Once the gigaseal is established, the experimenter needs to manually increase the suction pressure in the suction port (**Fig. 2.2.1 Fig. 2.12.1**) to –150 to –250 mBar; alternatively, an additional valve and an additional pressure source could be utilized. When activated, the robot applies suction for a period of 100 ms, repeatedly, every 5 seconds, until whole cell configuration is established. Out of the 30 trials where the 'suction pulse' method was employed to break-in, 25 successfully attained whole-cell

mode (83.3%). It is clear that the objective and systematic analysis of how *in vivo* patch clamping occurs, coupled to precision measurement and well-timed robotic control of pipette movement and pressure control, enables automation of the steps at which humans ordinarily require extensive practice to master.

### 2.4. Timecourse of operation of the autopatcher, and quality of patch outcomes

A representative autopatcher run, plotting the pipette resistance versus time, is shown in **Fig. 2.4.1A**, with key events indicated by Roman numerals; raw current traces resulting from the continuously applied voltage pulses, from which the pipette resistances were derived, are shown in **Fig. 2.4.1B**. The key neuron detection step, in which the robot tracks the pipette resistance across three consecutive 2 μm steps, and then halts movement upon detection of the sequence of changes described above, occurs between events *i* and *ii*. Note the small visual change in pipette currents observed in the raw traces between *i* and *ii* (**Fig. 2.4.1Bi** vs **Bii**); the ability of the robot to detect this small change, and halt pipette motion immediately, helped to greatly increase yield, as described above. At event *iii*, the autopatcher releases positive pressure, and the gigaseal process begins, assisted by the application of suction at event *iv* because the robot detected that seal resistance was not increasing quickly enough. At event *v*, the holding potential jumps down to -30 mV, and then ramps down to -65 mV, event *vi*. At event *vii*, the gigaseal has fully asymptoted, and the user has the option to halt the program (for gigaseal cell-attached patch) or launch the break-in procedure (for whole cell patch clamp).

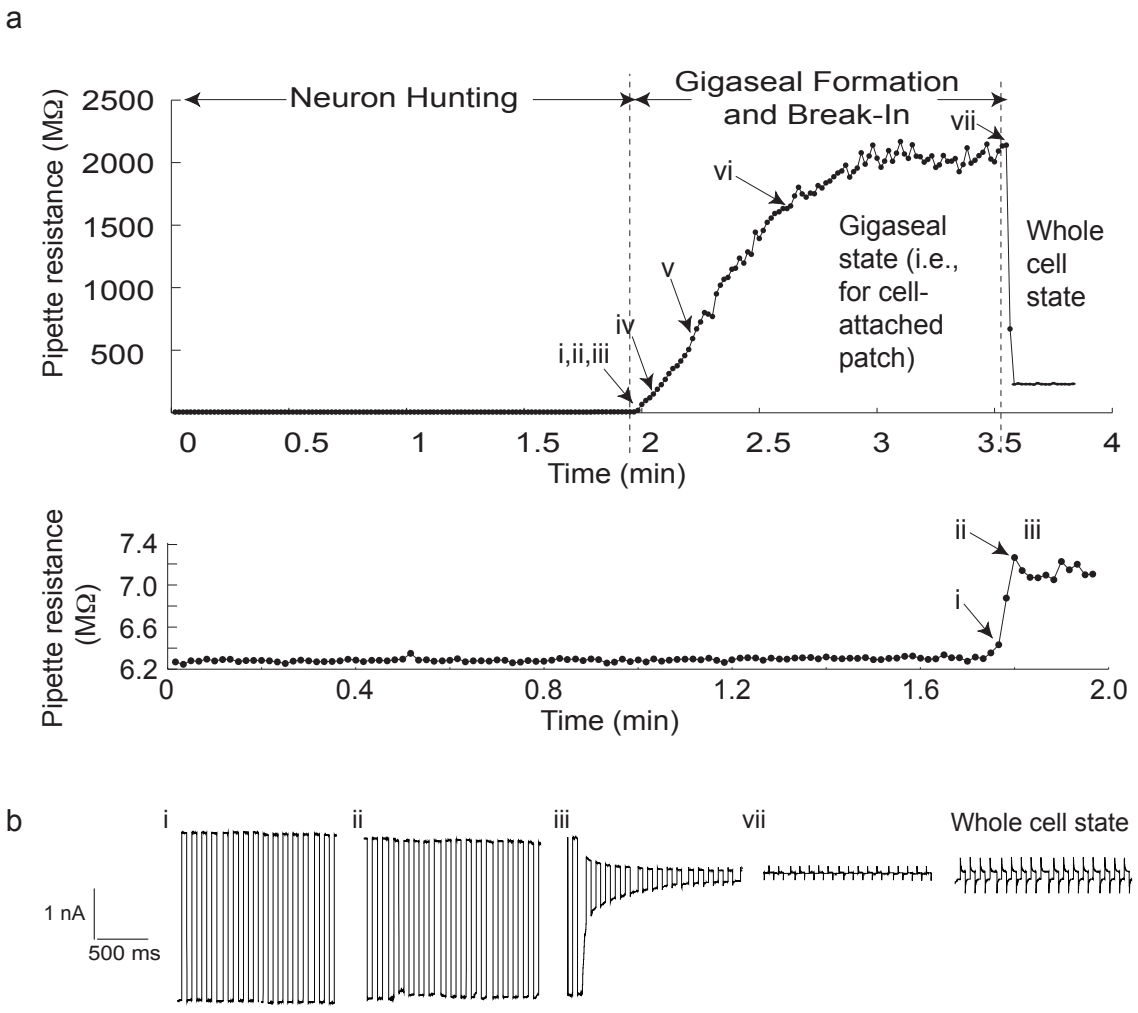


**Figure 2.4.1. Timecourse of autopatcher operation.** **A**, Representative trajectory of pipette resistance (the key parameter analyzed to control robot operation throughout the algorithm of **Fig. 2.3.1 and Fig. 2.3.3**) throughout a successful whole-cell patch clamp experiment performed on the autopatcher, starting with the "neuron hunting" stage and ending with successful whole cell attainment, ***top:*** The entire process from start of neurons hunting to break in, ***bottom:*** focusing on the smaller resistance changes in the neuronhunting stage. Stages are indicated at top (neuron hunting, etc.); Roman numerals flag specific events within those stages. i, the first of three resistance measurements that indicate the threshold of detection of a neuron; ii, the last of three resistance measurements that indicate the threshold of detection of a neuron; iii, the point at which positive pressure is released during gigaseal formation; iv, the point at which suction is applied during gigaseal formation; v, the point at which holding potential starts to ramp down from -30 mV to -65 mV; vi, the point at which holding potential hits -65 mV; vii, the point at which break-in occurs. **B**, Raw traces showing the currents observed going

through the patch pipette, while a square voltage wave (10 Hz, 10 mV) is applied to the pipette, at the events flagged by the corresponding Roman numerals in **A**. The resistances used throughout the algorithm for decision-making are computed by taking the average of the resistances calculated (using Ohm's law, R = (peak V)/(peak I)) from each set of five successive voltage pulses.

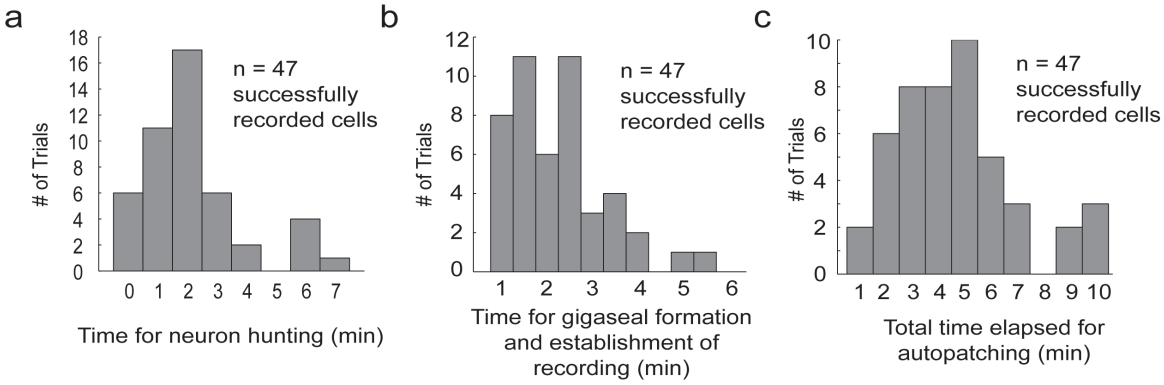


**Figure 2.4.2: Time durations of neuron hunting and gigasealing: A**, Histogram of execution times of the "neuron hunting" stage, showing the duration of operation of neuron hunting for the n = 47 targets successfully gigaseal-cell-attached-patched and whole cell patched **B**, Histogram of execution times of the "gigaseal formation" and "break-in" phases, if the latter applied, for the n = 47 cells for which we obtained successful cell-attached or whole-cell recordings. Note: the "break-in" phase lasts typically just 1-10 seconds, so whole-cell recordings usually take only a little longer to obtain than do cell-attached recordings, and thus both sets of times are pooled, for simplicity, in the current histogram. **C**, Histogram of execution times for the total autopatcher algorithm starting from neuron-hunting and ending with patch attainment (i.e., the sum of the times plotted in **A** and **B**).

The entire process takes about 3.5 minutes for this cell; for the gigaseal cell-attached and whole-cell patched neurons studied in detail here, the population mean and standard deviation was 5.1 $\pm$ 1.8 minutes from the beginning of neuron hunting to the establishment of recording (**Fig. 2.4.2C**; n = 47 neurons). The neuron-hunting stage took on average 2.5 $\pm$1.7 minutes (**Fig. 2.4.2A**, n = 47), with the time to find a target that later led to successful gigaseal not differing significantly from the time to find a target that

does not lead to a gigaseal ($p > 0.80$; t-test; n = 67 unsuccessful gigaseal formation trials), that is, failed trials did not take longer than successful ones. The gigaseal formation took 2.6 $\pm$ 1.0 minutes (**Fig. 2.4.2B**), including for the whole cell autopatched case the few seconds required for break-in; failed attempts to form gigaseals were truncated at the end of the ramp down procedure and thus took ~85 seconds. These durations are similar to those obtained by trained human investigators practicing published protocols[37].

**2.5 Quality of the recordings obtained by the autopatcher.**

Neurons recorded using the autopatcher in whole cell mode exhibited, in current clamp, voltage traces of sufficient quality to perform experiments involving either control of the neuron (top traces in **Fig. 2.5.1A** and **2.5.1B**, showing responses of cortical neurons and hippocampal neurons respectively, to current injection), or passive observation of the neuron (bottom traces in **Fig. 2.5.1A** and **2.5.1B**). For example, rhythmic changes in resting potential reminiscent of up and down states were clear in cortical recordings (**Fig. 2.5.1A**, bottom traces), but less so in the hippocampus (**Fig. 2.5.1B**, bottom traces).

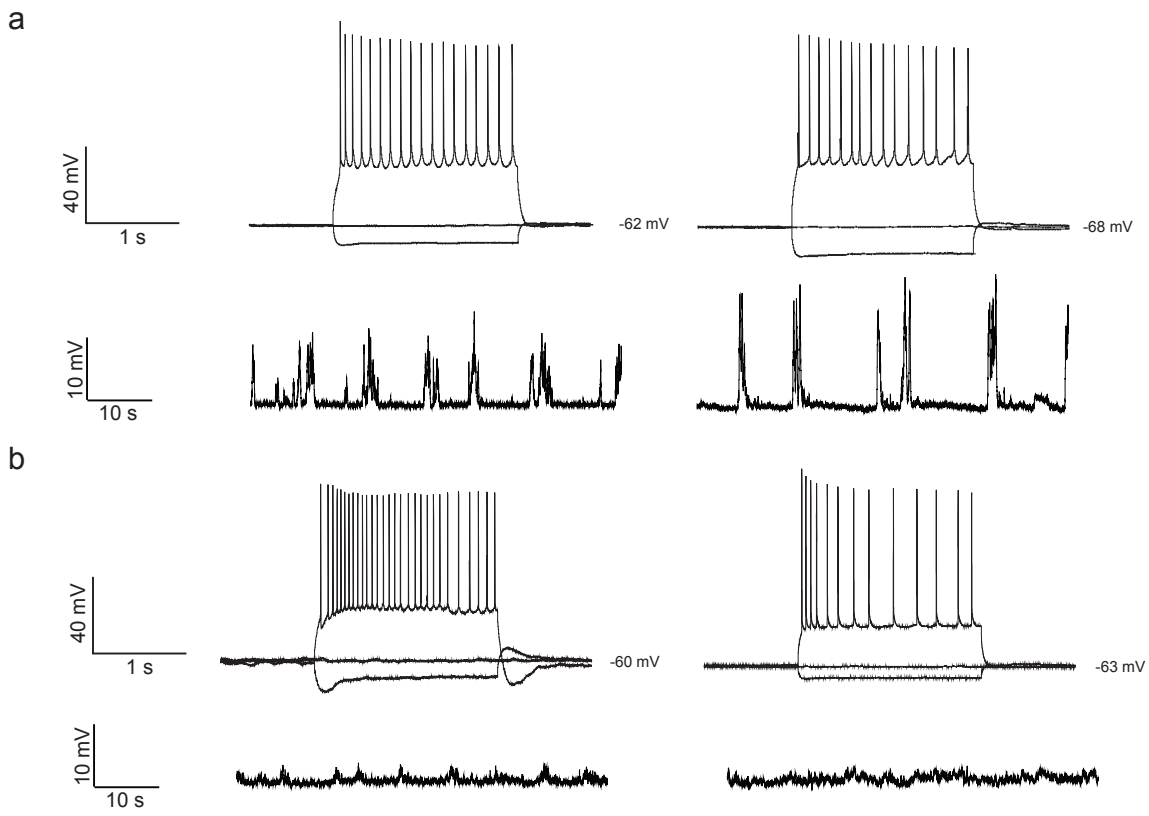


**Figure 2.5.1. Examples of data acquired from autopatched cells. A**, Current clamp traces during current injection (*top*; 2 s-long pulses of -60, 0, and +80 pA somatic current injection, for both cells), and at rest (*bottom*; note significantly compressed timescale relative to the top trace), for two cortical neurons for which whole cell patch clamp was established via autopatcher. **B**, Current clamp traces during current injection (*top*; 2 s-long pulses of -60, 0, and +40 pA somatic current injection, for the left cell, and -60, 0, and +100 pA, for the right cell), and at rest (*bottom*; note significantly compressed timescale relative to the top trace), for two hippocampal neurons for which whole cell patch clamp was established via autopatcher.

We evaluated a number of measures of whole cell patch clamp quality (**Fig. 5**) for neurons obtained at various depths, both in the cortex and in the hippocampus (n = 23 neurons, closed symbols).

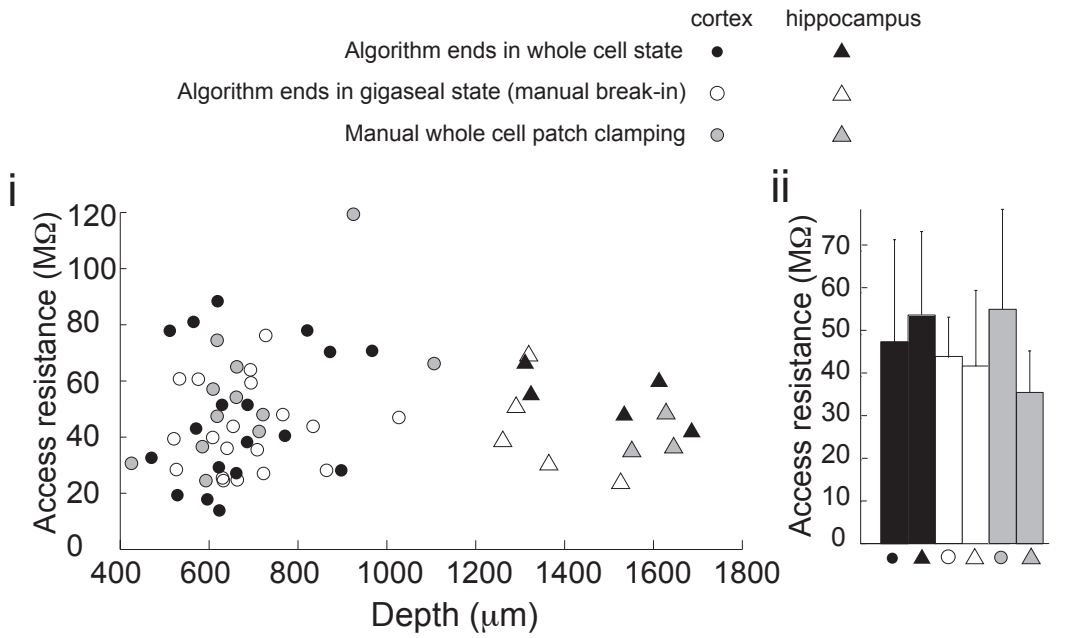


**Figure 2.5.2. Access resistance of *in vivo* neural whole cell recordings. A**, **I**, Plot of the access resistances obtained versus pipette depth and **ii,** bar graph summary of access resistances (mean ± std. dev.), for the final robot validation test set of automatically whole-cell patched neurons (closed symbols; n = 23), for the final robot validation test set of automatically cell-attached patched neurons (open symbols, n = 24, showing the data acquired after manual break-in following the conclusion of the automatic establishment of the gigaseal cell-attached state) and comparative results from completely manual whole cell patch clamping (grey symbols, n = 17), for cortical neurons (circles; anteroposterior, 0 mm relative to bregma; mediolateral, 0-1 mm left or right of the midline; neuron hunting begins at Zu = 400 μm depth) or hippocampal neurons (triangles; anteroposterior, -2 mm relative to bregma; mediolateral, 0.75-1.25 mm left or right of the midline; neuron hunting begins at Zu = 1100 μm depth).

As mentioned above, we also manually broke into the cells that were obtained in gigaseal cell-attached mode (n = 24 neurons, open symbols), to evaluate the quality of the cells that were recorded in cell-attached mode, since few quality measures are available in cell-attached mode. All parameters are reported in uncompensated form (e.g., no series resistance or capacitance compensation), obtained using the conventional patch clamp

software after autopatcher program completion. The first parameter we evaluated (**Fig. 2.5.1**) was the resultant pipette access resistance after obtaining whole cell mode; typical ranges obtained *in vivo* for blind whole-cell recording by trained human investigators are 40-120 MΩ (in cortex of young rats[60]), 20-30 MΩ (in olfactory bulb of young mice[60]) and 35-60 MΩ (in hippocampus of adult mice[61]) . Our pipette access resistances were 48.0 $\pm$ 24.5 MΩ (n = 18, auto-whole-cell patched, cortex), 44.5 $\pm$ 14.9 MΩ (n = 19, auto-gigaseal-cell-attached patch followed by manual break-in, cortex), 54.4 $\pm$ 9.6 (n = 5, auto-whole-cell patched, hippocampus), and 39.5 $\pm$ 17.8 MΩ (n = 5, auto-gigaseal-cell-attached patch followed by manual break-in, hippocampus), squarely in the ranges above. We performed a linear regression of pipette access resistance vs. neuron recording depth, and saw no relationship ($R^2$ = 0.007, p > 0.08), suggesting that our robot performed similarly at depth as at the surface.

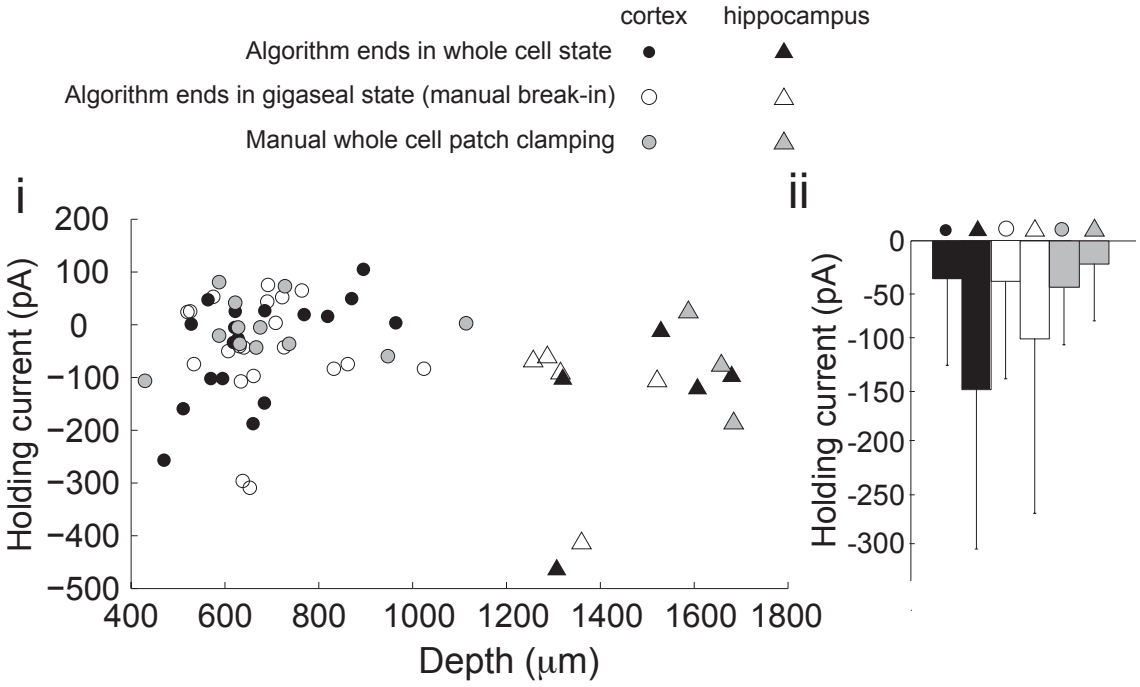

**Figure 2.5.3. Holding currents of *in vivo* neural whole cell recordings.** **A**, **I**, Plot of the holding currents needed to hold the neurons at -65 mV in voltage clamp mode versus pipette depth and **ii,** bar graph summary of holding currents (mean ± std. dev.), for the final robot validation test set of automatically whole-cell patched neurons (closed symbols; n = 23), for the final robot validation test set of automatically cell-attached patched neurons (open symbols, n = 24, showing the data acquired after manual break-in following the conclusion of the automatic establishment of the gigaseal cell-attached state) and comparative results from completely manual whole cell patch clamping (grey symbols, n = 17), for cortical neurons (circles; anteroposterior, 0 mm relative to bregma; mediolateral, 0-1 mm left or right of the midline; neuron hunting begins at Zu = 400 μm depth) or hippocampal neurons (triangles; anteroposterior, -2 mm relative to bregma; mediolateral, 0.75-1.25 mm left or right of the midline; neuron hunting begins at Zu = 1100 μm depth).

Similarly, we evaluated the holding current required to keep the neuron at -65 mV (**Fig. 2.5.3**) and the neuron resting potential when zero current is injected (**Fig. 2.5.4**). Commonly, the goal is to obtain cells that have a membrane potential lower than -55 mV[24, 31, 37, 60, 61, 66]. The mean and standard deviation of the holding currents, across both regions and conditions, was -63 ± 124 pA, and the resting potential was -61.9 ± 7.1 mV (n = 47). Finally, we analyzed the holding times over which we could record cells.

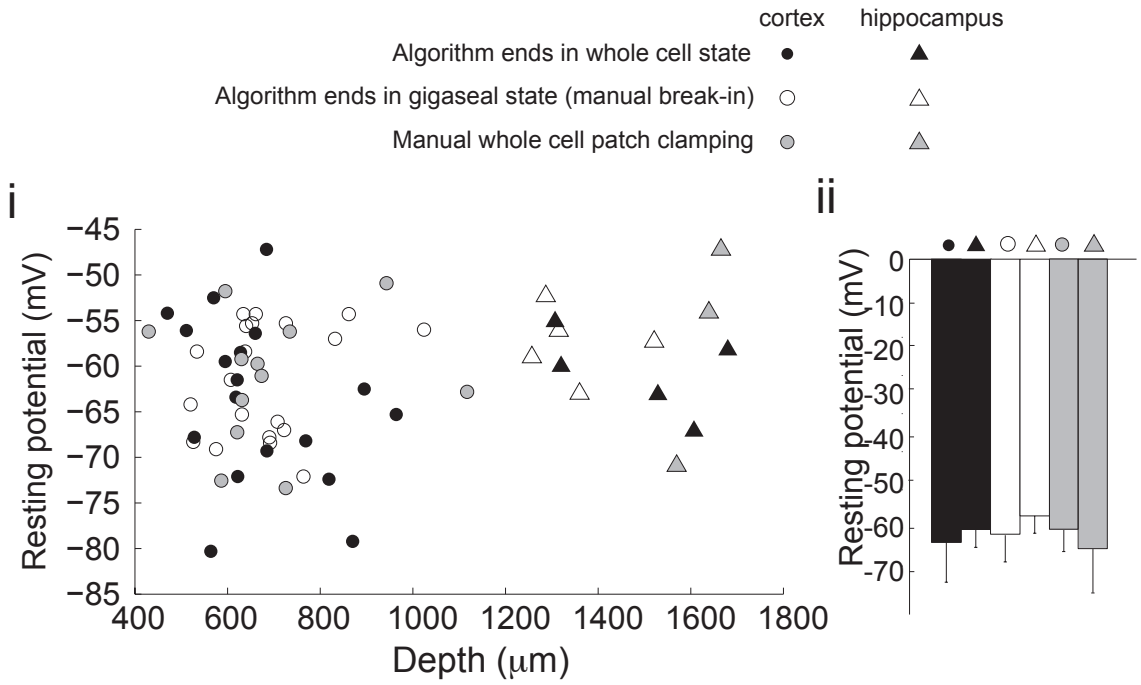


**Figure 2.5.4. Resting membrane potentials of *in vivo* neural whole cell recordings.** **A**, **I**, Plot of the resting membrane potentials in current clamp mode versus pipette depth and **ii,** bar graph summary of holding currents (mean ± std. dev.), for the final robot validation test set of automatically whole-cell patched neurons (closed symbols; n = 23), for the final robot validation test set of automatically cell-attached patched neurons (open symbols, n = 24, showing the data acquired after manual break-in following the conclusion of the automatic establishment of the gigaseal cell-attached state) and comparative results from completely manual whole cell patch clamping (grey symbols, n = 17), for cortical neurons (circles; anteroposterior, 0 mm relative to bregma; mediolateral, 0-1 mm left or right of the midline; neuron hunting begins at Zu = 400 μm depth) or hippocampal neurons (triangles; anteroposterior, -2 mm relative to bregma; mediolateral, 0.75-1.25 mm left or right of the midline; neuron hunting begins at Zu = 1100 μm depth).

Out of the 47 cells from which we obtained stable recordings, we terminated 14 recordings early (30-45 minutes) in order to try for more cells; for the remaining 33 cells, the recordings lasted 56.6 ± 44.2 minutes (with 25 cells lasting longer than 30 minutes), comparable to or exceeding the performance of trained human investigators.

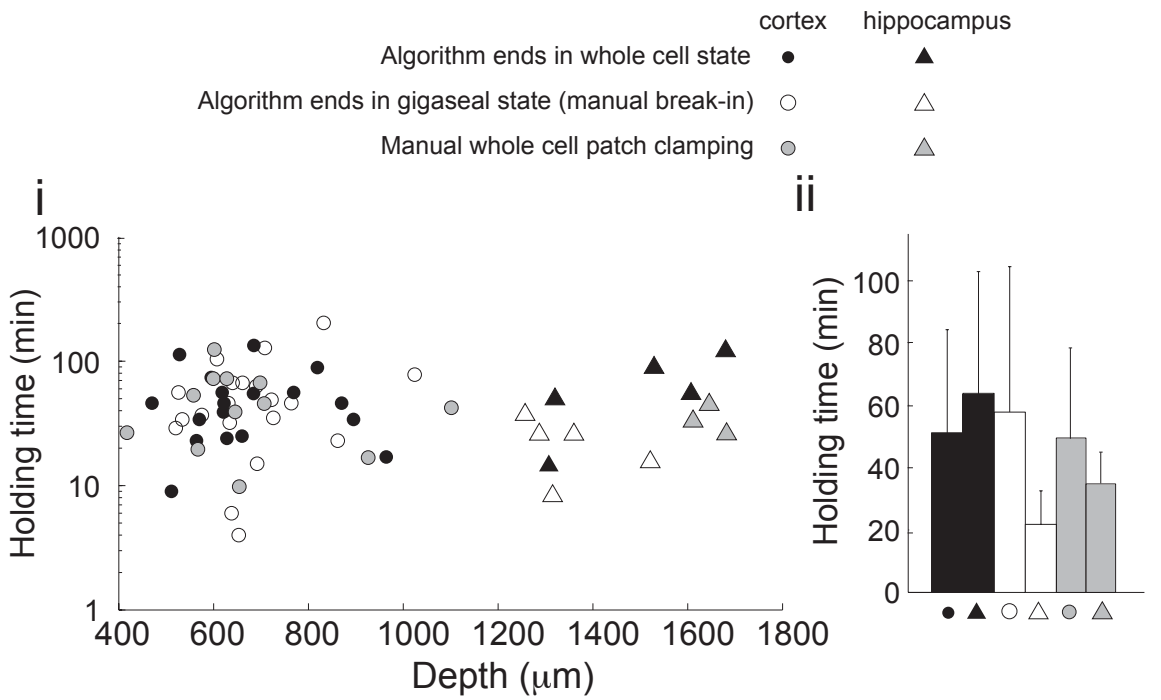


**Figure 2.5.5. Holding times of *in vivo* neural whole cell recordings.** **A**, **I**, Logarithmic plot of the holding currents needed to hold the neurons at -65 mV in voltage clamp mode versus pipette depth and **ii,** bar graph summary of holding currents (mean $\pm$ std. dev.), for the final robot validation test set of automatically whole-cell patched neurons (closed symbols; n = 23), for the final robot validation test set of automatically cell-attached patched neurons (open symbols, n = 24, showing the data acquired after manual break-in following the conclusion of the automatic establishment of the gigaseal cell-attached state) and comparative results from completely manual whole cell patch clamping (grey symbols, n = 17), for cortical neurons (circles; anteroposterior, 0 mm relative to bregma; mediolateral, 0-1 mm left or right of the midline; neuron hunting begins at Zu = 400 μm depth) or hippocampal neurons (triangles; anteroposterior, -2 mm relative to bregma; mediolateral, 0.75-1.25 mm left or right of the midline; neuron hunting begins at Zu = 1100 μm depth). Shown are both recording times which were terminated early, as well as recording times terminated by spontaneous loss of the cell.

Finally, we summarize the cell membrane characteristics as well as the gigaseal resistances obtained in the three different methods that were used in **Fig. 2.5.6**.

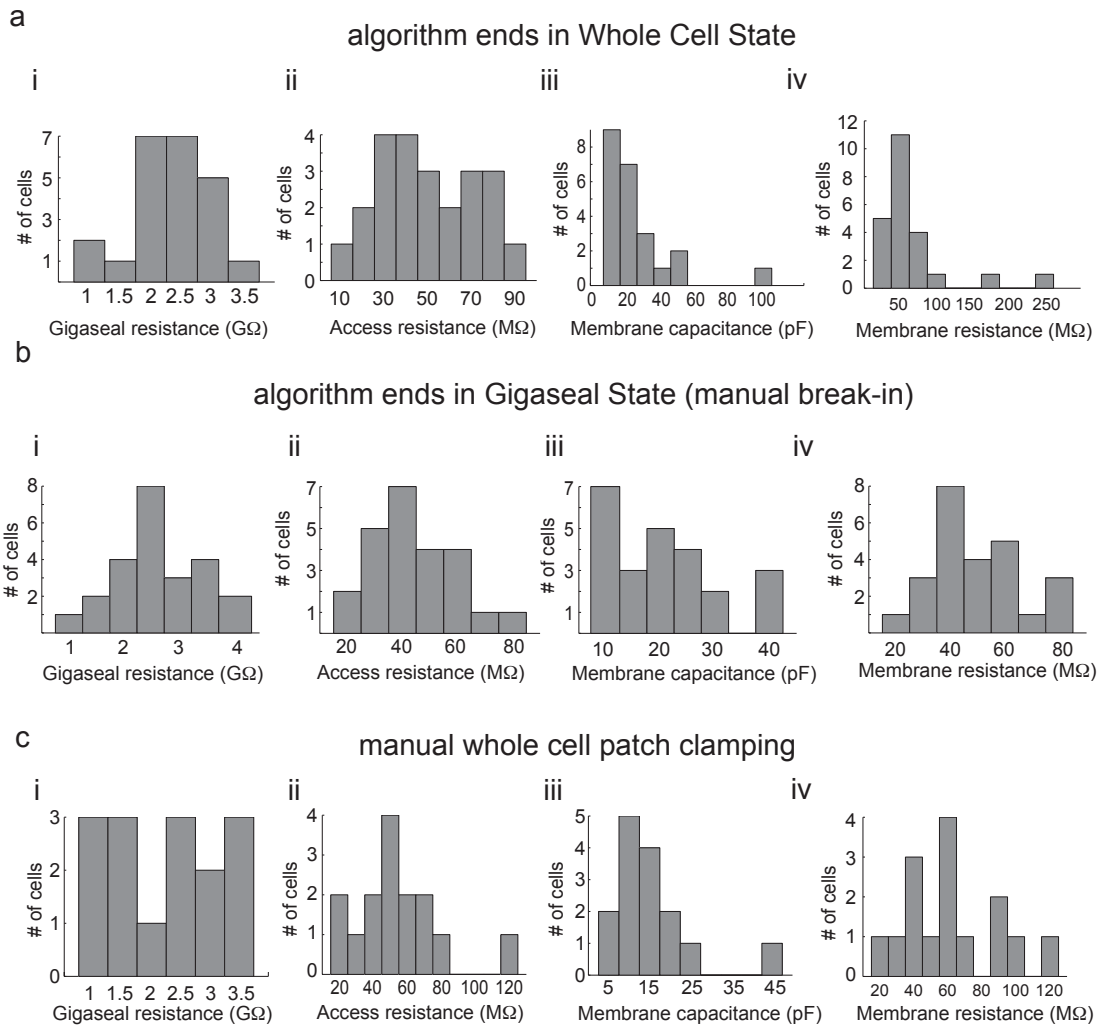


**Figure 2.5.6 Cell characteristics after completion of autopatching or manual patching using the algorithm of Fig. 2.3.1.** Histograms summarizing the whole cell patch clamp properties of the neurons described in **Figure 2.3.1** for which recordings were either automatically established in (**a**) whole cell state ($n$ = 23 cells), or (**b**) gigaseal state followed by manual break-in to verify cell properties ($n$ = 24 cells), or (**c**) fully manual whole cell patch clamping ($n$ = 15 cells), measured in voltage clamp at –65 mV, including **i**, gigaseal resistance after gigaseal formation, **ii**, access resistance after break-in (~5 minutes after break-in), **iii**, cell membrane capacitance, and **iv**, cell input resistance.

A single robot might be capable of recording 50-100 cells a day, and a single human operator should be able to run several robots. Thus, new kinds of experiment, like

the systematic classification of cell types by their electrophysiological properties, in a diversity of behavioral and brain disorder contexts, might be possible. We note that the gigaseal resistances, membrane capacitances, and membrane resistances of the neurons both auto-whole-cell patched (**Fig. 2.5.2**) and manually broken into after auto-gigaseal-cell-attached patching spanned the ranges of what we would expect given prior cortical and hippocampal patching experiments[37, 60, 61, 66, 69], suggesting that with automation, the robot did not incur sacrifices in cell quality.

## 2.6. Statistical comparison of quality of autopatched neurons with fully manual patched neurons.

Comparing the cell quality metrics between the $n$ = 23 auto-whole cell patched neurons and the 15 *fully* manually patched neurons. No difference between auto-whole-cell patched and fully manually patched neurons was noted for access resistances (two-way ANOVA; main effect of method of patching, $F_{1,33} = 0.92$, $P = 0.5116$; main effect of region (cortex vs hippocampus), $F_{1,33} = 1.73$, $P = 0.4175$; interaction, $F_{1,33} = 0.14$, $P = 0.706$, holding current (two-way ANOVA; main effect of method of patching, $F_{1,33} = 0.83$, $P = 0.5382$; main effect of region, $F_{1,33} = 0.12$, $P = 0.7819$; interaction, $F_{1,33} = 0.38$, $P = 0.5432$), or resting membrane potential (two-way ANOVA; main effect of method of patching, $F_{1,33} = 1.16$, $P = 0.4758$; main effect of region, $F_{1,33} = 0.72$, $P = 0.5539$; interaction, $F_{1,33} = 5.873$, $P = 0.0218$). Out of the 47 neurons from which we obtained stable recordings, we terminated 14 recordings early (30-45 minutes) in order to try for more cells; for the remaining 33 cells, the recordings lasted 56.6 $\pm$ 44.2 minutes (**Fig. 2.5.5**). No difference in cell holding times was noted between auto-whole-cell patched

and fully manually patched neurons (two-way ANOVA; main effect of method of patching, $F_{1,33}$ = 3.19, $P$ = 0.3279; main effect of region, $F_{1,33}$ = 0.19, $P$ = 0.7317; interaction, $F_{1,33}$ = 1.08, $P$ = 0.3016). Finally, no difference between auto-whole-cell patched and fully manually patched neurons was noted for gigaseal resistance (two-way ANOVA; main effect of method of patching, $F_{1,33}$ = 1.85, $P$ = 0.1809; main effect of region, $F_{1,33}$ = 0.12, $P$ = 0.7267; interaction, $F_{1,33}$ = 6.02, $P$ = 0.0192), cell membrane capacitance (two-way ANOVA; main effect of method of patching, $F_{1,33}$ = 0.96, $P$ = 0.9578; main effect of region (cortex vs. hippocampus), $F_{1,33}$ = 2.91, $P$ = 0.09628; interaction, $F_{1,33}$ = 0.7, $P$ = 0.4021), or cell input resistance (two-way ANOVA; main effect of method of patching, $F_{1,33}$ = 1.47, $P$ = 0.2327; main effect of region, $F_{1,33}$ = 0.25, $P$ = 0.2417; interaction, $F_{1,33}$ = 0.06, $P$ = 0.8182).

### 2.7. The cell types patched by the autopatcher

Using the cell type criteria of references[70, 71], we found that of the 47 autopatched neuronal recordings from cortex and hippocampus analyzed in **Fig. 2.5.1, Fig. 2.5.2, Fig. 2.5.3, Fig. 2.5.4** and **Fig. 2.5.5,** 68% (32/47) exhibited regular spiking (RS) characteristics, 4% (2/47) exhibited burst firing patterns, 13% (6/47) exhibited irregular spike characteristics, 4% (2/47) exhibited spikes followed by smaller spikelets suggestive of back propagation of action potentials in dendritic recordings, and 2% (1/47) had accelerating spike firing characteristics. In 9% (4/47) of the neurons, steady current injection resulted a in single action potential followed by plateaued depolarizing current, with no further spike firing, indicating fast adapting neurons. It is likely that all cell recording strategies have some bias in what kinds of cells they record; extracellular

recording methods, for example, might favor neurons capable of creating large extracellular fields that result in easily sortable spikes for example (papers such as ref. [26] comment on how difficult it is to record small neurons like cerebellar granule cells via extracellular recording). A recent *in vivo* patch clamping paper, ref. [72] points out, *"Most of the recorded cells were pyramidal cells and their recovered morphologies typically included an apical dendrite ..."*, which would be consistent with our apparent high yield of neurons, especially pyramidal neurons, as noted in this paragraph and in the fills (**Fig 2.8.1**).

## 2.8. Morphology of autopatched neurons via biocytin filling

In a subset of experiments we added 0.1-0.5% biocytin to the intracellular pipette solution to attempt filling the neuron with biocytin for morphological analysis. Once whole cell configuration was established, the cells were typically held in this configuration for atleast 10 minutes, giving enough time for the biocytin in the intracellular solution to diffuse into the cell. At the end of the recordings the pipette was withdrawn slowly at the rate of 3 μm/s for a distance of 150 μm, which typically resulted in the formation of an outside out patch. As demonstrated previously, this technique can be used to reseal the cell membrane and confine the diffused biocytin to the recorded cell. After the experiment, this biocytin filled cell could be visualized after immunohistochemical staining. **Figure 2.8.1** shows some representative confocal microscope images of biocytin filled neurons obtained using this technique. We were able to recover and identify the morphology of neurons unambiguously in 72% (n= 15

out of 21 filled cells) of the trials. In other trials, the background staining resulting from the intracellular pipette solution ejected out of the pipette under high pressure during the initial descent to depth ("Regional pipette localization" stage) made it difficult to isolate the single neuron recorded from.

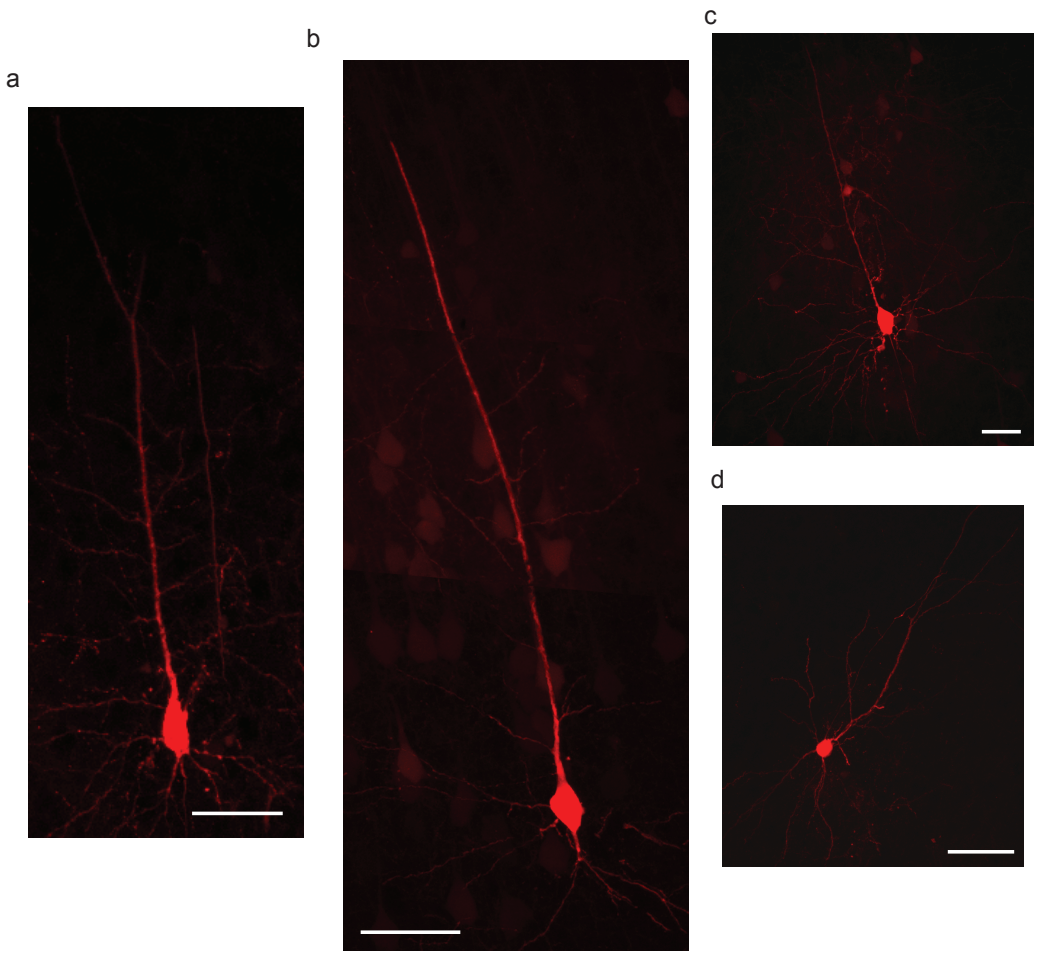


**Figure 2.8.1. Neurons filled with biocytin, and visualized with Alexa 594-streptavidin, after recording by the autopatching robot.** Each panel shows a neuron recorded at 500-800 μm depth below the brain surface, 0-2 mm left or right of midline, 0-2 mm anterior of bregma. Scale bars, 50 μm.

## 2.9. Results from recordings where the autopatcher used suction pulses as a method for breaking in

As an alternate method, we iterated a second algorithm that used 200-500 ms pulses of suction (-150 to -200 mBar) to break in to the cells after gigaseal was obtained. We obtained stable whole cell recordings from 25 neurons in the cortex at depths ranging from 400 μm to 1000 μm. The access resistances, the holding currents, the holding potentials are plotted against the recording depth as shown in Fig. 2.9.1. We did not see any differences in these parameters when compared to the neurons that were broken in using the suction with zap method, presented before. We did not characterize the holding times of these neurons, as its is expected that they will have similar times to the previous method. Instead we limited these recordings to 10 minutes, and attempted to estimate the success success rates that can be obtained along the whole time of the experiment. This is plotted in **Fig. 2.9.1d**. It can be seen that the success rate of the recordings can be as high as 60% in the first hour after the acute craniotomy is opened, and deteriorates over time, possibly because of tissue damage, greater motion artifacts of the brain as the animal goes deeper into anesthesia.

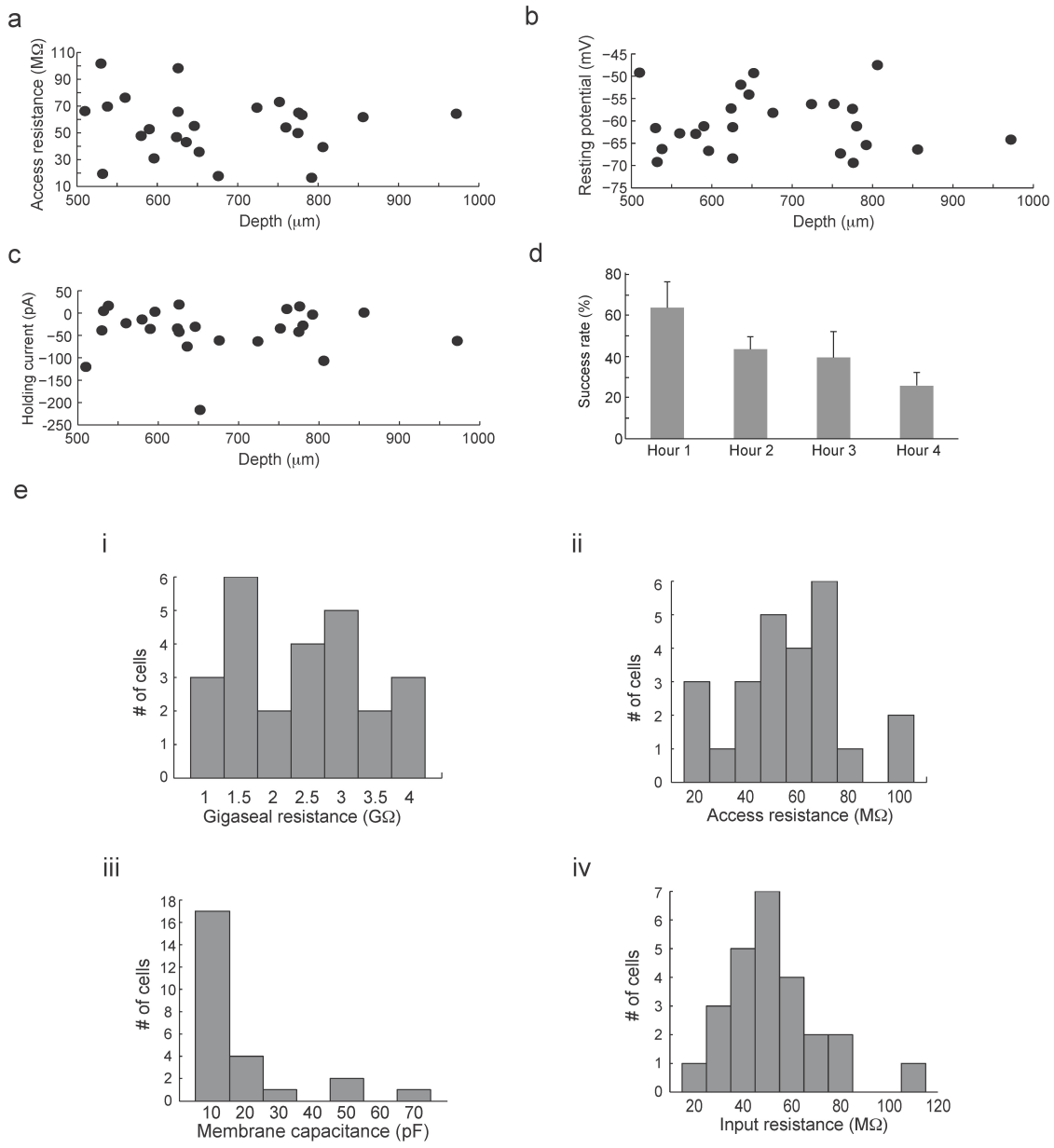


**Figure 2.9.1. Quality of recordings obtained using the autopatcher using the 'suction pulses' method for break-in and achieving the whole cell state, as described in Fig. 2.3.3.** (**a**) Plot of the access resistances obtained versus pipette depth for set of neurons for which whole cell state was established using the algorithm of **Fig.2.3.3**, in which the "zap" is replaced by suction pulses. $n$ = 25 cortical neurons were successfully broken in to, out of 30 successful gigaseals, out of 61 total attempts starting with regional pipette localization (anteroposterior, 0 mm relative to bregma; mediolateral, 0-1 mm left or right of the midline; neuron hunting begins at 400 mm depth). Thus the break-in rate was 83% of the gigasealed neurons (not different from the break-in rate for zap-mediated break in, **Fig. 2.3.1**; chi-square = 0.001, $P$ = 0.8023), and total yield from start of the

algorithm was 41%. (**b**) Plot of the resting potentials obtained versus pipette depth, for the neurons described in **a**. (**c**) Plot of the holding currents obtained versus pipette depth for the neurons described in **a.** The recordings lasted at least 15 minutes, but we terminated the recordings early in order to focus more on the understanding of whether suction pulses would work in the autopatcher algorithm. (**d**) Bar graph of average success rates obtained in each hour of recording after surgery ($n$ = 3 experimental sessions; plotted is mean + standard deviation). (**e**) Histograms summarizing the whole cell properties of the automatically whole-cell patched neurons broken in using suction pulses method, showing good quality recordings equivalent to those obtained by zap method of break-in, measured in voltage clamp at –65 mV, including **i**, gigaseal resistance after gigaseal formation, **ii**, access resistance after break-in (~5 minutes after break-in), **iii**, cell membrane capacitance, and **iv**, cell input resistance.

### 2.10. Throughput of the autopatcher

Is the autopatcher a "high throughput" machine? Perhaps, not in terms of sheer speed per cell (currently), although certainly the autopatcher can sustain its work without getting tired or bored, as a human might. We did a series of experiments, automatically recording in each of 3 mice, 7-8 successfully whole cell patch clamped neurons (total for the 3 mice, 22 successes), out of 16-20 attempts (total for the 3 mice, 52 attempts; yield, 42%); surgeries would take 41 + 6 minutes beginning from anesthesia of the mouse and ending with the exposed brain ready for recording; then, for each cell, pipette filling and installation (removing any used pipette, of course) would take 2 ± 0.4 minutes, followed by the autopatcher establishing whole cell patch clamp in 5 ± 2 minutes. We limited the recording time for each cell to 15 minutes, arbitrarily, but shorter or longer times may be of course utilized, depending on the science at hand. Thus, the amount of time required to record n neurons successfully, for a desired recording time T, would be approximately:

40 + n / .42 * 7 + n / .42 * T minutes

The surgeries, of course, could be done in advance to equip mice with headplates to minimize day-of-recording time expenditure. Thus, during an 8 hour day, ~25 neurons might be successfully recordable in a single mouse, if the recording times were very short; this doesn't take into account the important consideration of cell displacement that could result from an electrophysiological experiment, thus reducing yield over time. Strategies can be devised to limit the impact of cell displacement or damage from impacting yield, for example, patching neurons in higher regions before patching those in lower ones. The autopatcher travels, on average, 150 ± 112 microns in the cortex during the neuron hunt phase, before hitting the neuron ($n$ = 22 cells); this short travel distance suggests that the pipette might well be hitting the very first cell that it is allowed to encounter (e.g., is approaching under low pressure). Smaller diameter pipettes, even down to 100-200 mm in diameter, are easily available (albeit more difficult for humans to handle), and so this might not be a fundamental limit on scale. Or, it is possible that patching neurons in varying brain regions could result in very high fidelity recordings, although again, the science would have to match with this goal.

Also important to note: if it takes 2 minutes to load a pipette, and 5 to obtain a cell and another T minutes to do a recording, it would in principle be possible for a single individual to run (5+T)/2 rigs at once; for 15 minute recording times, that would make for 10 rigs being simultaneously controlled by one employee.

### 2.11. Recordings in awake, headfixed mice using the autopatcher

As a final note, we attempted to use the same algorithm described previously in Fig. 2.3.1 and Fig. 2.3.3 to record from headfixed awake mice. These experiments were conducted in n=2 mice. We obtained stable whole cell recordings from 3 neurons (out of 18 attempts). A representative voltage trace recorded from a cortical neuron in current clamp mode is shown in **Fig. 2.11.1.** We were able to record from these neurons for 3, 25, and 31 minutes which indicates that it is possible to get stable recordings in awake headfixed preparations, although the low yield indicates further work needs to be done to develop algorithms that can be used to account for higher degree of motion of the brain, which is an artifact of the awake state.

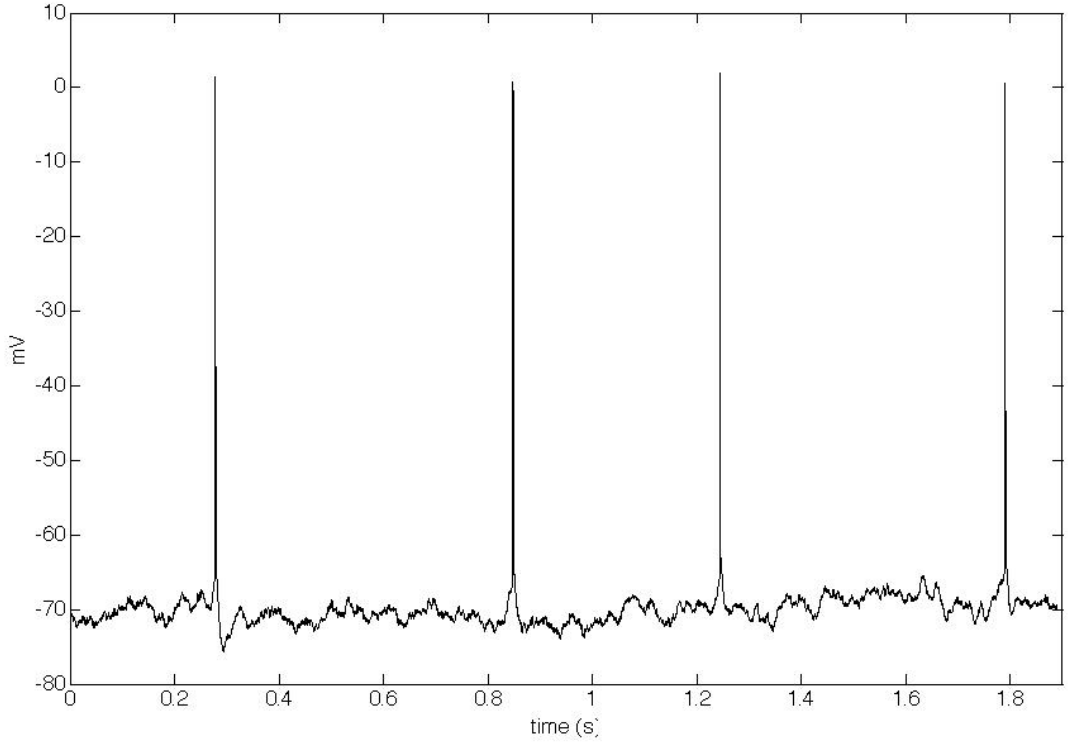


**Figure 2.11.1: Recordings obtained with the autopatcher in awake headfixed mice:** A representative voltage trace recorded in current clamp mode from a neuron in the

motor cortex. The recording remained stable for 28.4 minutes. Access resistance 46.2 MΩ, membrane resistance of 74.9 MΩ, and membrane capacitance 23.6 pF.

## 2.12. Experimental Methods

### 2.12.1 Surgical procedures

All animal procedures were approved by the MIT Committee on Animal Care. Adult male C57BL/6 mice (Taconic), 8-12 weeks old, were anesthetized using ketamine/xylazine (initially at 100 mg/kg and 10 mg/kg, and redosed at 30-45 minute intervals with 10-15% of the initial ketamine dose as needed, using toe pinch reflex as a standard metric of anesthesia depth). The scalp was shaved, and the mouse placed in a custom stereotax, with ophthalmic ointment applied to the eyes, and with Betadine and 70% ethanol used to sterilize the surgical area. Three self-tapping screws (F000CE094, Morris Precision Screws and Parts) were attached to the skull and a plastic headplate affixed using dental acrylic, as previously described[73]. Once set (~20 minutes), the mice were removed from the stereotax and placed in a custom-built low profile holder. A dental drill was used to open up a craniotomy (1-2 mm diameter) by thinning the skull until ~100 μm thick, and then a small aperture was opened up with a 30 ga needle tip. It is critical to ensure that bleeding is minimal and the craniotomy is clean, as this allows good visualization of the pipette, and minimizes the number of pipettes blocked after insertion into the brain. The dura was removed using a pair of fine forceps. The craniotomy was superfused with artificial cerebrospinal fluid (ACSF, consisting of 126 mM NaCl, 3 mM KCl, 1.25 mM $NaH_2PO_4$, 2 mM $CaCl_2$, 2 mM $MgSO_4$, 24 mM

$NaHCO_3$, and 10 mM glucose), to keep the brain moist until the moment of pipette insertion.

For experiments where we attempted awake patch clamp recordings, the animal was anesthetized using 1-2% isoflurane, and surgical procedures for headplate fixing was carried out as described above with the animal administered with analgesic analgesic buprenorphine subcutaneously (0.1 mg/kg) and 1-2 mg/kg Meloxicam subcutaneously, as a supplementary analgesic. The mice were allowed to recover from surgery for 2-3 days before the recordings were attempted. On the day of the recordings, the animals were anesthetized for a second time with 1-2% isoflurane, and the craniotomy performed. The animals were headfixed in the custom low profile holder and allowed to recover from anesthesia, before the commencement of the autopatcher recordings.

### 2.12.2 Experimental Methods: Electrophysiology.

Borosilicate glass pipettes (Warner) were pulled using a filament micropipette puller (Flaming-Brown P97 model, Sutter Instruments), within a few hours before beginning the experiment, and stored in a closed petri dish to reduce dust contamination. We pulled glass pipettes with resistances between 3-9 MΩ. The intracellular pipette solution consisted of (in mM): 125 potassium gluconate (with more added empirically to bring it up to ~290 mOsm), 0.1 $CaCl_2$, 0.6 $MgCl_2$, 1 EGTA, 10 HEPES, 4 Mg ATP, 0.4 Na GTP, 8 NaCl (pH 7.23, osmolarity 289 mOsm), similar as to what has been used in the past[74]. For biocytin staining, 500 μM of Alexa Fluor 594 biocytin, sodium salt (Invitrogen) was added to the pipette solution. We performed manual patch clamping

using previously described protocols[60, 66], with some modifications and iterations as explained in the text, in order to prototype algorithm steps and to test them.

### 2.12.3 Experimental Methods: Robot construction

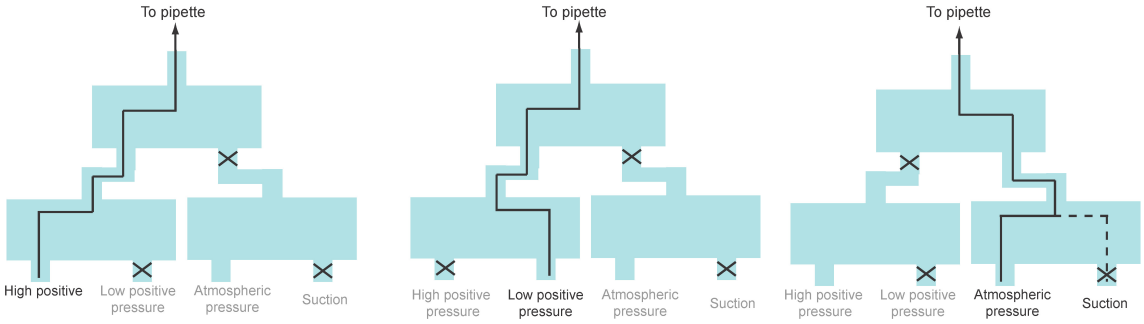


**Figure 2.12.1 Diagram depicting configurations of the three pneumatic valve bank during the stages of autopatcher operation, depicted in Fig. 2.2.1.** "x" represents closed valve; line depicts connectivity of volumes at the same pressure. **A**, During regional pipette localization, positive pressure (800-1000 mBar) is connected to the pipette. (This is the configuration realized when the valves are not powered.) **B**, During neuron hunting, low positive pressure (25-30 mBar) is connected to the pipette. **C**, During gigaseal formation, suction pressure (-15 to -20 mBar; dotted line) or atmospheric pressure (solid line) is applied. During break-in, suction pressure is also applied.

We assembled the autopatcher (**Fig. 2.2.1**) through modification of a standard *in vivo* patch clamping system. The standard system comprised a 3-axis linear actuator (MC1000e, Siskiyou Inc) for holding the patch headstage, and a patch amplifier (Multiclamp 700B, Molecular Devices) that connects its patch headstage to a computer through a Digidata 1440A analog/digital interface board (Molecular Devices). For programmable actuation of the pipette in the vertical direction, we mounted a programmable linear motor (PZC12, Newport) onto the 3-axis linear actuator. The

headstage was in turn mounted on the programmable linear motor through a custom mounting plate. The programmable linear motor was controlled using a motor controller (PZC200, Newport Inc) that was connected to the computer through a serial COM port. An additional data acquisition (DAQ) board (USB6259, National Instruments Inc) was connected to the computer via a USB port, and to the patch amplifier through BNC cables, for control of patch pipette voltage commands, and acquisition of pipette current data, during the execution of the autopatcher algorithm. During autopatcher operation, the USB 6259 board sent commands to the patch amplifier; after acquisition of cell-attached or whole-cell-patched neurons, the patch amplifier would instead receive commands from the Digidata. The patch amplifier streamed its data to the analog input ports of both the USB DAQ and the Digidata throughout and after autopatching. For pneumatic control of pipette pressure, we used a set of three solenoid valves (2-input, 1-output, LHDA0533215H-A, Lee Company). They were arranged, and operated, in the configuration shown in **Fig. 2.12.1**. The autopatcher program was coded in, and run by, Labview 8.6 (National Instruments). The USB6259 DAQ sampled the patch amplifier at 30 KHz and with unity gain applied, and then filtered the signal using a moving average smoothening filter (half width, 6 samples, with triangular envelope), and the amplitude of the current pulses was measured using the peak-to-peak measurement function of Labview. During the entire procedure, a square wave of voltage was applied, 10 mV in amplitude, at 10 Hz, to the pipette via the USB6259 DAQ analog output. Resistance values were then computed, by dividing applied voltage by the peak-to-peak current observed, for 5 consecutive voltage pulses, and then these 5 values were averaged. Once the autopatch process was complete, neurons were recorded using Clampex software

(Molecular Devices). Signals were acquired at standard rates (e.g., 30-50 KHz), and low-pass filtered (Bessel filter, 10 KHz cutoff). All data was analyzed using Clampfit software (Molecular Devices) and MATLAB (Mathworks). For detailed notes on the hardware installations and software operations, please refer to the **Appendix A - Autopatcher User Manual**.

### 2.12.4 Experimental Methods: Autopatcher Operation

At the beginning of the experiment, we installed a pipette and filled it with pipette solution using a thin polyimide/fused silica needle (Microfil) attached to a syringe filter (0.2 μm) attached to a syringe (1 mL). We removed excess ACSF to improve visualization of the brain surface in the pipette lowering stage, and then applied high positive pressure (800-1000 mBar), low positive pressure (25-30 mBar), and suction pressure (-15 to -20 mBar) at the designated ports (**Fig. 2.2.1 and 2.12.1**) and clamped the tubing to the input ports with butterfly clips; the initial state of high positive pressure was present at this time (with all valves electrically off). We used the 3-axis linear actuator (Siskiyou) to manually position the pipette tip over the craniotomy using a control joystick with the aid of a stereomicroscope (Nikon). The pipette was lowered until it just touched the brain surface (indicated by dimpling of surface) and retracted back by 20-30 micrometers. The autopatcher software then denote this position, just above the brain surface, as $z = 0$ for the purposes of executing the algorithm (**Fig. 2.3.1 and 2.3.3**), acquiring the baseline value $R(0)$ of the pipette resistance at this time (the z-axis is the vertical axis perpendicular to the earth's surface, with greater values going

downwards). The pipette voltage offset was automatically nullified by the "pipette offset" function in the Multiclamp Commander (Molecular Devices). We ensured that electrode wire in the pipette was well chlorided so as to minimize pipette current drift which can affect the detection of the small resistance measurements that occur during autopatcher operation. The brain surface was then superfused with ACSF and the autopatcher program was started. For detailed notes on the hardware installations and software operations, please refer to the **Appendix A -Autopatcher User Manual**.

### 2.12.5 Experimental Methods: Histology and Imaging.

At the end of the experiment, mice were euthanized while anesthetized via standard means (cervical dislocation or transcardial perfusion). For experiments with biocytin filling of cells, mice were perfused through the left cardiac ventricle with ~40 mL ice-cold 4% paraformaldehyde in phosphate buffered saline. Perfused brains were then postfixed overnight in the same solution at $4^{o}$C. The fixed brains were incubated in 30% sucrose solution until cryoprotected. The brains were flash frozen in isopentane and dry ice, and sectioned using a cryostat (Leica) at $-20^{o}$C. Slices were mounted in Vectashield with DAPI (Vector Labs), covered using a coverslip and sealed using nail polish. Imaging was done with a confocal microscope (Zeiss) using 20x and 63x objective lenses, and maximum intensity projections taken using the confocal software.

## 2.13. Conclusions

Whole-cell patch clamp electrophysiology enables high signal-to-noise cellular electrical recording, and also enables anatomical visualization of the morphology of cells, as well as extraction of cell contents for molecular analysis. Here we report an algorithm, and a robot suited for performing the algorithm, for automatically patch clamping cells in the living brain with yields, speeds, and quality levels comparable to or exceeding what trained human investigators can perform. The algorithm involves precision measurements, including measurements of sequences of pipette electrophysiological events, as well as precision movements, such as being able to halt pipette movements immediately following detection of such events. The algorithm also involves temporally precise control of pressure, essential for enabling pipettes to descend to depth and for high-fidelity cell-attached and whole-cell recordings to be obtained. The algorithm takes advantage of the power of simple robotic design principles, for example the ability to analyze temporal trajectories of quantitative data (in a fashion that is difficult for humans), and performing fast actuation events triggered by these analyses. Importantly, the finding of the algorithm itself would have been difficult without a robotic platform for evaluating systematically the parameters governing the success of *in vivo* patch clamping. Thus, we anticipate that other applications of robotics to the automation of complex neuroscience experiments will be possible, and facilitated by the realization that a cycle of innovation in which the engineering and science iterate is useful in the discovering and creation of scientifically impactful technologies.

Some aspects of *in vivo* patching had been standardized prior to this paper. For example, pipette solutions must have osmolarity and pH defined within strict numerical

limits. Most other aspects of patch clamping, however, have been regarded as human skills requiring dynamic evaluation of situations and adaptation to complex *in vivo* events. Here we find that the decisions to be made, and the measurements and analyses leading to these decisions, can be codified in algorithmic form. With a single set of thresholds of detection, protocols for achieving seals, and criteria for gauging the progress from one stage of the patch process to another, we were able to record cells in both the hippocampus and the cortex (despite the algorithm having been derived from cortical experiments alone), implying a degree of generality to the algorithm here described. For cells that are vastly different from cells of the hippocampus and cortex, e.g. cerebellar granule cells whose small size requires high resistance pipettes[26], or cells in non-brain structures (e.g., [75]) or in other species such as Drosophila (e.g., [76]), it is likely that the precise parameters utilized might need to be adjusted. The iterative process utilized to derive the algorithm above, however, is in part automated by the existence of the robot – for example, the robot may be able to track yields and adaptively modify parameters if the recordings are failing at too high a rate. The fact that the robot automates the process, reduces the cost of iteration, as well as the skill required to iterate – opening up methodology invention itself to a broader population.

We chose to automate blind whole cell patch clamping because of its versatility, inexpensiveness, and power. Using just the resistance of the pipette as the core measure governing decision making, we were able to hunt for cells and establish recordings, even deep within intact tissue. Two-photon targeted patching[24, 31] and other targeted methods[25] enable high quality recordings of fluorescently delimited cells, but have not been

automated, and are also expensive. In vitro autopatching, in which a cell is sucked onto a microfabricated pore, or other equivalent protocols are performed, has been available for years[51, 77-80] , but cannot be applied easily to intact tissue samples, such as living brain, due to the physical strategies employed by these earlier technologies. Our robot may open up many new frontiers in biology, bioengineering, and medicine in which the assessment of the properties of single cells, embedded within intact tissue, is desired but has not been achievable in a systematic high-throughput fashion. For example, analyzing how different cells in a neural circuit respond to a drug in specific brain states, performing electrical characterizations of cells in tissues removed during surgery, determining how different individual cells within a tumor biopsy sample vary in gene expression, and assessing how tissue-engineered organs vary in cell to cell composition, may provide fundamental new capabilities in diagnostics, personalized medicine, and drug development. The ability to determine whether a recorded cell is of a given cell class, using optical activation of specific cells within that class as a way of indicating the identity of those cells[81], would be aided by the ability to rapidly patch cells, thus enabling optogenetic[74, 82-84] cell identification. The autopatcher robot's pipette can potentially be integrated with capillary systems for liquid chromatography and mass spectrometry for single cell proteomic analysis[85, 86]. Automation both speeds up processes and reduces the skill levels required, enabling for example a single robot operator to control many rigs; these effects will greatly broaden the number of fields for which single-cell analyses in intact tissue are applicable.

Our device is based on a relatively inexpensive modification to a conventional patch rig, and thus can easily be incorporated into existing labs' setups. Such a rig is capable of enabling the recording of many dozens of cells per experiment in an automated fashion, but higher throughput devices and devices with new features would expand the power of this robotic approach even further. For example, given that only a single linear drive is required, a head borne version for freely moving animals (e.g., building off the protocols described by Lee et al. [36]) might be easily achieved. Image-guided versions may be developable, which use microscopy to identify targets, but then use the autopatcher algorithm to detect the cell membrane, obtain the seals, and achieve whole-cell access. The ability to automatically make micropipettes in a high-throughput fashion[87], and to install them automatically, might eliminate some of the few remaining steps requiring human intervention. As a final example, the ability to actuate many pipettes within a single brain, and to perform massively recordings of neurons or other cells within a single living network, may open up the ability to analyze neural computations and other biological phenomena with great accuracy. The algorithmic nature of the procedure we describe here, and the simple robotics needed to implement it, not only open up many kinds of scientific investigation, but also empower new kinds of neuroengineering to be contemplated and pursued.

# CHAPTER 3

# INTEGRATION OF AUTOMATED PATCH CLAMPING ROBOT WITH OPTOGENETICS

## 3.1. Introduction

The cells in the brains exhibit a vast diversity of gene expression profiles, morphological properties and electrophysiological properties. Much of the current work in systems neuroscience is aimed at revealing how these different cell types of the brain work together in circuits to implement brain computations as well as how different cell types go awry in brain disorders. Establishing the causal roles specific cells types play on neural circuit dynamics requires tools that can monitor the electrophysiology of neurons at the single cell resolution while at the same time allowing the perturbation of activity of these specific neuronal cell types in a spatio-temporally precise manner. The recent developments on the field of optogenetics has allowed neuroscientists to study causal relationships between neural networks and behavior in a manner that previously was not possible. Optogenetic tools are able to activate and silence specific neuronal populations of the brain, in a temporally precise and rapidly reversible fashion via light activation. Specifically, the *in vitro* and *in vivo* expression of the light-responsive protein, channelrhodopsin-2 (ChR2)[88], archaerhodopsin-3 (Arch)[74, 89], and Halorhodopsin-57

(unpublished) in genetically-targeted neurons enables them to be depolarized (ChR2) or hyperpolarized (Arch, Halo57) by pulses of blue and green and red light, respectively. Current techniques used to measure the activity of single cells *in vivo* during optogenetic stimulation are predominantly extracellular; and rely on spike timing and spike waveform characteristics of optically perturbed cells to determine their cell type. These are however, subjected to sampling biases and vary depending on brain state and region. Intracellular techniques such as whole cell patch clamping, on the other hand, enable single cell isolation as well as the measurement of sub-threshold membrane potential deflections in individual cells. This property can thus be used along with optogenetics to identify cell types being recorded from by directly measuring induced photocurrents or lack there of, due to light stimulation.

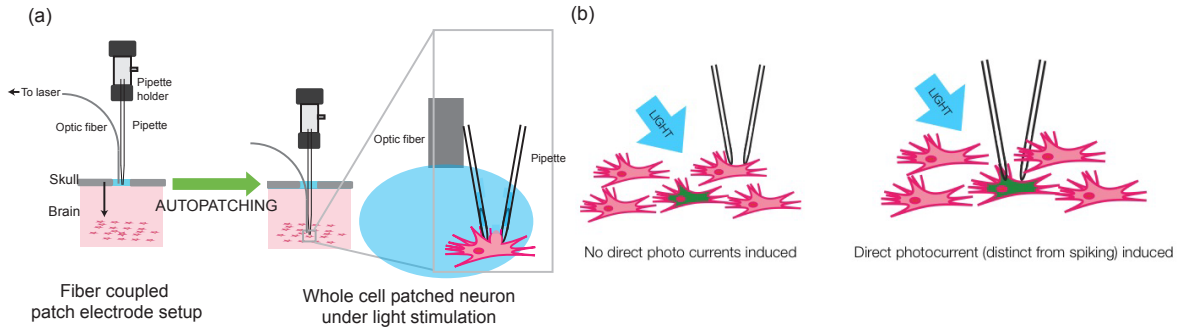


**Figure 3.1: (a)** Schematic of a fiber coupled patch electrode mounted on a robot for automated whole cell patch clamping[90]. (b) Cartoon illustration of optogenetically driven cell type identification *in vivo*. While extracellular recording pick up multiple units, the ability to patch cell enables direct measurement of evoked photo-currents, presence or absence of which indicates the neuron type being recorded from.

We demonstrate here the integration of optogenetic tools with the autopatcher: a robot for automated whole cell patch clamping of neurons in vivo[90]. We used this

integrated system to record from neurons expressing ChR2, Arch, as well as Halo-57. Using the autopatcher, is possible to distinguish between opsin expressing and non-expressing cells simply by measuring the direct photocurrents that are induced by photostimulation in the former via whole cell recording. We report of performance of this integrated system in measures of yield and quality of recordings. We further demonstrate the utilization of the autopatcher as a high-throughput system for characterizing optogenetic molecules *in vivo*.

## 3.2. Materials and Methods

### 3.2.1 Cell type specific targeting of optogenetic molecule

Neurons in the brain can be targeted with optogenetic molecules via several means. To illustrate the feasibility of targeting specific cell types we targeted Arch, a light-driven silencing opsin, to serotonergic neurons of the dorsal raphe nucleus (DRN) by injecting a Cre recombinase-dependent AAV vector (AAV-FLEXArch-GFP) into the dorsal-raphe nucleus (DRN) of knock-in mice that selectively express Cre in tryptophan hydroxylase (TPH; the rate-limiting enzyme for serotonin synthesis)-positive neurons. We examined the specificity and extent of Arch-GFP expression by analyzing the overlap of viral GFP expression with TPH immunofluorescence. The ChR2 experiments were conducted in transgenic mice that express ChR2 under the Thy1 factor (Thy1-ChR2)[91]. We also used the autopatcher to characterize *in vivo*, the performance of a Halo-57 that was virally delivered using AAV8-CAG-FLEX-Halo57-KGC-GFP-ER2 vector in CamKII-Cre transgenic mice.

### 3.2.2 Integration of optical stimulation hardware with Autopatcher

The optic fiber is aligned parallel to the glass electrode of an Autopatcher and fixed by wrapping heat shrink tubing around the fiber and electrode and heating it for 2-3 seconds (Fig. 1a). It allows the center of a 200 μm diameter optical fiber to be positioned ~800 μm from the tip of glass electrode that is used for patching and deliver light powers up to 20 $mW/mm^2$ at the recorded neuron for optogenetic stimulation. For patch clamping, the fiber coupled glass electrode is positioned 20-30 μm above the brain surface and automated whole cell patch clamping is carried out as described in Chapter 2 [90]. All surgical procedures are as described previously[90], with the exception of the craniotomy preparation. For parallel insertion of the optic fiber along with the patch electrode, we opened up rectangular craniotomies with dimensions ~1mm x 2mm. The concept of cell type identification of recorded cells via optical stimulation is illustrated in **Figure 3.1b**.

## 3.3. Results

The integrated system shown in **Figure. 3.1** can be used to reliably obtain whole cell recordings from anesthetized mouse during optical stimulation. Shown in **Figure 3.2a** is a representative trace of a well-isolated single unit recording in cell-attached patch mode from an Arch expressing serotonin neuron in the DRN. Onset of green light stimulation (532nm wavelength) as indicated by the green bar resulted in photo-inhibition of spiking activity. We observed up to 87.09 ± 2.10% photoinhibition of firing rate

relative to baseline (n = 11 recordings, 3 mice). In contrast, light delivery to the DRN in non-transduced mice had no significant impact on spiking activity (2.00 ± 0.32 Hz firing rate at baseline versus 2.09 ± 0.27 Hz firing rate during light; P = 0.504, paired t-test; n = 11 recordings, 3 mice; Fig. 2B), of the activity of putative DRN serotonergic neurons. Faster spiking GABAergic neurons within the DRN did not show any photoinhibition, enabling us to positively identify serotonin neurons via light stimulation.

We have also successfully autopatched neurons expressing Halo-57 in the motor cortex (M2, depths 500-800 mm, n=4 neurons, 3 mice) and orbitofrontal cortex (OFC, depth 900-1200 mm, n=3 neurons, 2 mice), with a success rate of 32% (9 successful / 28 attempts). This is comparable to the success rate we reported previously with the standalone autopatcher[90]. **Figure 3.2c** shows the current clamp recordings showing hyperpolarizing membrane potential hyperpolarization induced in neurons recorded from M1 when red light laser (635 nm wavelength) was switched on. We compared the hyperpolarization of membrane potential between neurons of M2 and OFC in **Figure 3.2d**. This data indicates that the level of opsin expression can vary significantly from brain region to region, for the same gene delivery technique and further systematic studies will need to be done to characterize other existing optogenetic molecules and their efficacy *in vivo*. Finally, shown in **Figure 3.2e** is current clamp recording from a layer-5 neuron in motor cortex (M1) of a Thy1-ChR2 transgenic mouse. At an estimated 20 $mW/mm^2$ light power at the recording neuron, it is possible to elicit single spikes from 10 ms light pulses.

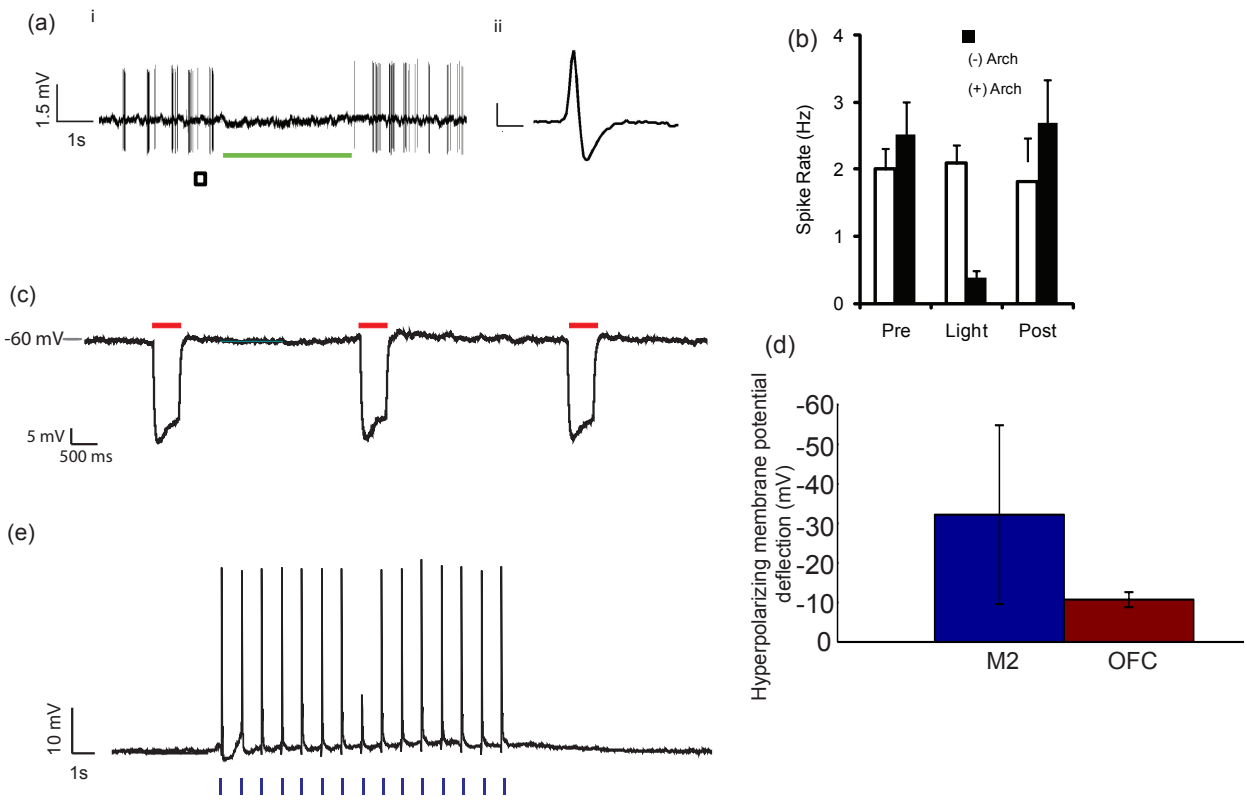


**Figure 3.2: Simultaneous patch clamping recording and optogenetic stimulation *in vivo:*** (a) (i) Representative waveform of an *in vivo* loose-cell attached recording from the dorsal raphe nucleus (DRN) of a SERT-Cre mouse. Due to the depth of the DRN, these recordings were obtained manually. (ii) scaled up view of a single action potential. (b) Bar plot of mean firing rate of the neurons before during and after light stimulation. The recordings revealed that 30 s 532-nm illumination potently reduced mean spiking frequency in Arch (+), but not Arch (-), SERT-Cre mice. (c) Raw trace of current clamp recording from a Halo-57 positive neuron showing hyperpolarizer potential during red light stimulation. Comparison between hyperpolarization in M2 and OFC neurons at same light stimulation power. (e) Raw voltage traces in current clamp showing spike evoked at 1 Hz using blue light pulses of 10 ms

### 3.4. Conclusions

The integration of automated *in vivo* patch clamping robot with optogenetic stimulation hardware has resulted in a high-throughput tool for the characterization of optogenetic molecules *in vivo*. We have demonstrated that this integrated system can be used with the same efficiency as a standalone autopatcher, and can be used to characterize a variety of optogenetic molecules *in vivo* expressed both in transgenic animals as well those delivered via viral vector techniques. The ability to measure direct induced photocurrent due to light stimulation allows on-the-fly, unambiguous cell type identification of recorded neurons *in vivo*. This can be used to study the role of specific cells types in neuronal network dynamics, at a resolution that was previously not possible. Aside from high resolution electrophysiology capabilities that allow measurement of subthreshold membrane potential fluctuation events, whole cell patch clamping has the additional capabilities of allowing single cell morphological reconstruction via biocytin staining[90] as well as the ability to isolate the mRNA of recorded cells for transcriptomic analysis[14]. When these capabilities are combined with optogenetics, it is possible to have a relatively complete characterization of the neurons; bridging the intrinsic properties of the neuron, its connectivity and the causal role its plays in local circuit dynamics.

# CHAPTER 4

# MULTIPATCHER: A ROBOT FOR AUTOMATED PATCH CLAMPING OF MULTIPLE NEURONS *IN VIVO*

## 4.1 Introduction

In **Chapter 2** of this thesis, we described a method by which patch clamping *in vivo* was reduced to a computer algorithm that controlled the "autopatcher", a robot capable of conducting blind *in vivo* patch clamping in an automated fashion[90]. We demonstrated the utility of the autopatcher in obtaining recordings in both the cortex and hippocampus of the anesthetized mouse brain, achieving high yields (~30% of overall attempts) and recording qualities were comparable to those of trained humans. The algorithmic nature of the procedure and the simple robotics needed to implement the autopatcher opened up the ability to actuate many pipettes within a single brain, and to perform parallel recordings of neurons or other cells within a single living network. Building off our discovery that blind *in vivo* whole-cell patching could be reduced to a reliable and stereotyped algorithm, we used the core hardware and software components of the single channel autopatcher and developed the "multipatcher", a robot capable patch clamping sets of neurons simultaneously *in vivo*. As a demonstration, we built a multipatcher consisting of four independently controlled patch pipettes. This

multipatching robot was capable of achieving stable whole cell recordings from pairs and triplet of neurons, with a 59% success rate of whole cell recordings from one or more neurons, and a 30.7% success rate of recording from two or more neurons. The trials typically took just 2-3 minutes for each channel, and taking 10 - 11 minutes for a full trial. Simultaneous whole cell recordings could be carried from these neurons for up to 90 minutes. The algorithms used for multipatching can be generalized to control arbitrarily large number of electrodes; additionally, the high yield, throughput and automation of complex set of tasks enables a practical solution for conducting patch clamp studies in potentially dozens of interconnected neurons *in vivo* for the first time. This will enable a more systematic assessment of how neurons work together to implement computations, and how they malfunction in diseased states.

### 4.2 Multipatcher: a robot for parallel patch clamping of multiple neurons *in vivo*

The multipatcher robot shares many of its core components with single channel autopatcher[90] (**Fig. 4.2.1**). Each recording probe is a glass pipette with a fine tip, and filled with conductive saline solution. A silver chloride wire is inserted inside the pipette electrically connects the conductive solution to an amplifying headstage. Each headstage is mounted on a programmable linear motor, which is in turn held in place using a 3-axes linear manipulator. The assembly of the programmable linear motor, and the 3-axes linear manipulator make up the end actuator modules, four of which are arranged in a radial

pattern so as to be able to position an array of 4 pipettes, with their distal ends in close proximity to each other.

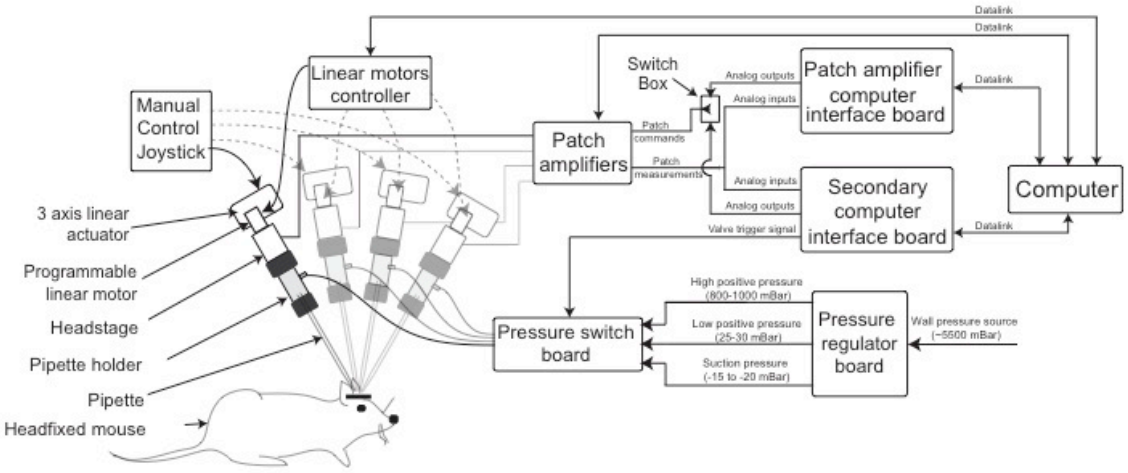


**Figure 4.2.1**: **Schematic of the robotic system used to perform the multipatching algorithm** (**Fig. 4.2.2** and **Fig. 4.3.2**). The system consists of 4 end actuator modules each consisting of a 3 axes linear actuator and an additional programmable linear motor. Conventional *in vivo* patch setup compnents i.e., pipette, pipette holder, headstage, are mounted on the end actuator modules as shown. For simplicity, we have highlighted connections from only one such system to the patch amplifier, the motor controllers and the joystick. The same system can be in principle scaled up n-fold for a scaled up multipatcher hardware system. Each headstage is connected to a patch amplifier, which routes the signals to a computer via two computer interface boards. One board is dedicated for data acquisition, while a second one is used for executing the multipatching algorithm. A pressure switchboard with controllable bank of pneumatic valves, as well as analog pressure regulators is controlled using the secondary computer interface board. Actuation of motors is achieved using linear motor controller that is commanded by the computer, thus completing the closed loop control system.

The headstages communicate electrically with amplifiers and a computer interface board that both records the neural signals and delivers neural control signals to the headstages. Finally, there is a pneumatic pressure control system consisting of a pressure regulation board and a pressure switching board that takes in pressurized air stored in a large

reservoir and converts that into different regulated pressure states such as high positive pressure, low positive pressure and suction. These regulated pressure states can be applied to the pipettes at different time points during the multipatching process.

The process by which the multipatching robot establishes whole cell recordings in multiple neurons is illustrated in **Fig 4.2.1.** Before the robot is started, pipettes are installed in all the channels of the multipatcher, and the pressure set to high positive pressure state in all of them. The pipettes are then positioned in the craniotomy such that their tips enter and probe a brain area within a few hundred micrometers of each other (**Fig 4.2.2 i**). First, an initial assessment of the pipettes' electrical resistance is carried out to ensure the pipettes are within an acceptable range for patch clamping- typically between 3-9 MΩ. The robot then lowers all the pipettes in a serial fashion (**Fig 4.2.2 i-iv**) to the desired depths set by the experimenter. It is possible to localize different pipettes to different depths within the cortex, for e.g. both layer 2/3 and layer neurons.

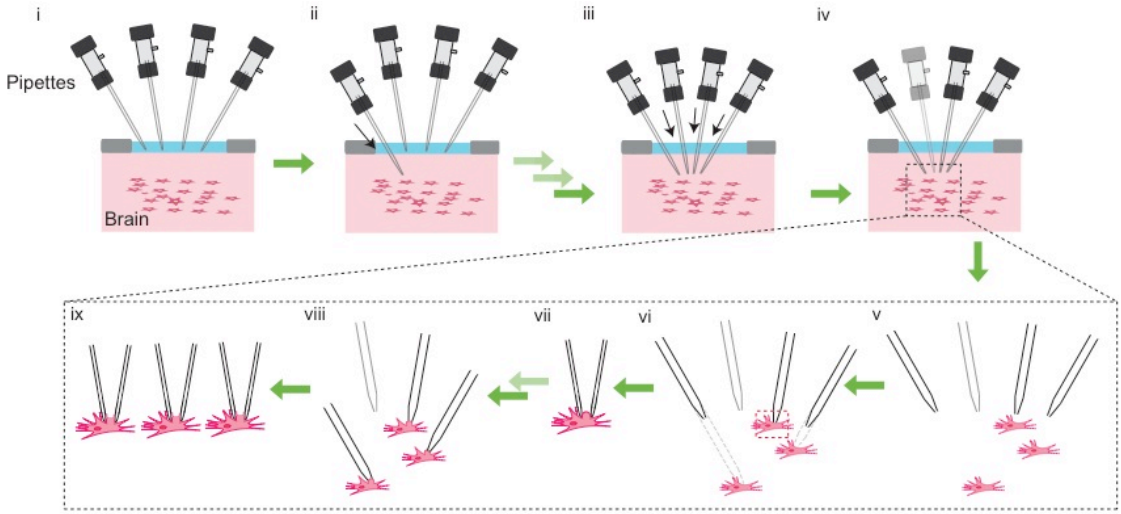

**Figure 4.2.2: Algorithm for multipatching:** The different stages of the *in vivo* multipatching process which we optimized building upon the autopatcher algorithm ([90], **Chapter 2**): **i** to **iv** execute the "regional pipette localization," in which the pipettes is lowered to the respective target areas in the brain. At the end of the regional pipette localization stage, clogged pipettes are deactivated indicated by the faded pipettes in subsequent stages (**iv** to **ix**). In steps **v** to **viii** the robot enters the "neuron hunting and gigasealing mode" in which the pipettes are advanced in small increments, until each detects a neuron via signature changes in pipette resistance; at which time, the pipettes stop moving and "gigaseal formation" (**vii**) is attempted. This process is repeated until a gigasealing formation attempt is made in all the active channels, after which "break-in" is used to synchronously break into all gigasealed neurons to get to whole cell configuration (**ix**).

Once all the pipettes have been lowered, they are checked for tip fouling or blockage. If pipettes have clogged or fouled tips, the corresponding channels are deactivated, and play no further part in the multipatching process (**Fig 4.2.2 iv**). The robot then moves all the pipettes in active channels in small incremental steps (2-3 μm), after which it sends a series of predefined square wave voltage pulses (e.g. 10 mV at 10 Hz, with offset voltage set at 0 mV) to the different pipettes, and measures the resultant current traces. This is used to compute the resistance values of the pipettes. This two-step process is repeated while looking for signature trends in resistance traces in one or more channels that indicate suitable contact with a neuron for patch clamping (**Fig. 4.2.2 v** and **vi**; analogous to the "neuron hunting" stage in the autopatcher operation, **Section 2.2**). After detecting this signature, the robot halts the movement of pipettes in all channels, and attempts to establish a gigaseal in the channel(s) that have encountered a neuron (the "gigasealing" stage in the autopatcher, (**Fig.4.2.2 vii**). After a gigasealing attempt has been carried out in a particular channel, its motor is deactivated, and the rest of the pipettes resume neuron hunting. This process is repeated until all the pipettes have

encountered neurons and attempted gigasealing (**Fig. 4.2.2 vi-viii**). At this point, the channels that have successfully formed gigaseals are selected and the robot applied pulses of suction until it successfully breaks into the gigasealed cells (the "synchronized break-in" stage, **Fig 4.2.2 ix**).

The ability of the robot to perform these stereotypical tasks in an automated and parallel fashion results in a degree of scalability that human operators find hard to perform manually. Simultaneous, parallel execution of multiple time-point tasks such as lowering multiple pipettes in small increments; monitoring of resistance values in multiple channels and identification of signature neuron contact trends become increasingly complex tasks for human experimenters and thus become unmanageable to perform manually when the number of pipettes is scaled beyond even 2-3 channels. Further, automation enables a fine control of the time scales over which different tasks and decisions are executed. For example, it is possible to synchronize events such as breaking in to multiple neurons so that the all the gigasealed neurons can obtain whole cell state at the same time, thus enabling the experimenter to maximize the time duration of simultaneously whole cell recordings, and normalizing that effects of cell dialysis which occurs starting from the moment intracellular access is obtained.

In the next section, we will describe in detail, the construction of the robot. But first we summarize the performance of the multipatching robot. We validated the performance of a 4-channel multipatching robot in the cortex of anesthetized mice. The multipatcher, running the algorithm shown in **Fig. 4.2.2,** obtained successful whole cell recordings in 1 or more channels 58.9% of the time (n = 23 out of 39 trials, n=7 mice).

We defined success as being able to hold a cell in current clamp mode with under 500 pA of injected current for at least 5 minutes.

Out of these 23 trials, the multipatcher successfully recorded from pairs of neurons in 11 trials and from a triplet of neurons in one trial. Thus overall, the multipatcher was able to establish successful whole cell recordings from multiple neurons 30.76% of the time (12 out of 39 attempts). The ability to record from pairs and triplets of cells simultaneously demonstrate the scalability of the multipatching robot algorithm; by increasing the number of controllable pipettes, even higher numbers of simultaneous whole cell recordings can be obtained. In these trials, overall, 17.9% of the pipettes got blocked (n= 28 of 156 pipettes in n=39 trials), a percentage that is comparable to those obtained when using the single channel autopatcher[90]. The entire multipatcher trial from start of regional pipette localization to end of break-in took on an average 10.45 $\pm$ 2.56 minutes. Thus, per channel, the multipatcher requires 2.61 $\pm$ 0.64 minutes, again, comparable to the time taken by the single channel autopatcher to establish whole cell recordings.

### 4.3 Multipatcher robot construction

We assembled the multipatcher hardware by using the basic template of the autopatcher robot described in **Chapter 2** (See **Section 2.10.3**) and replicating the end actuators four fold. Modifications were made to the pneumatic systems such that a central

pressure control system could be used for independent pressure modulation in all four channels. These are described in detail below.

### 4.3.1 Actuator system

The pipette actuator modules were of the same configuration as the single channel system. Briefly, each module comprised a 3-axis linear actuator (MPC285, Sutter Instruments Inc) for holding the patch headstage (**Fig. 4.3.1**). For programmable actuation of the pipette in the tilt axis, we mounted a programmable linear motor (PZC12, Newport) onto the 3-axis linear actuator. The tilt axis actuator was mounted at an angle of 45 degrees to the vertical. The headstage was in turn mounted on the programmable linear motor through a custom mounting plate. Four such actuator modules were placed in close proximity to each other in a radial fashion as shown in **Fig 4.3.1 b** and **Fig. 4.2.1**. In this configuration, it was possible to position four patch pipette tips in an array of 1mm x 1mm on top of the brain surface (**Fig 4.2.1 c** and **Fig 4.2)**. It is desirable to get the pipette tips as close to each other as possible, so as to target neurons within the same microcircuit (<200 μm).

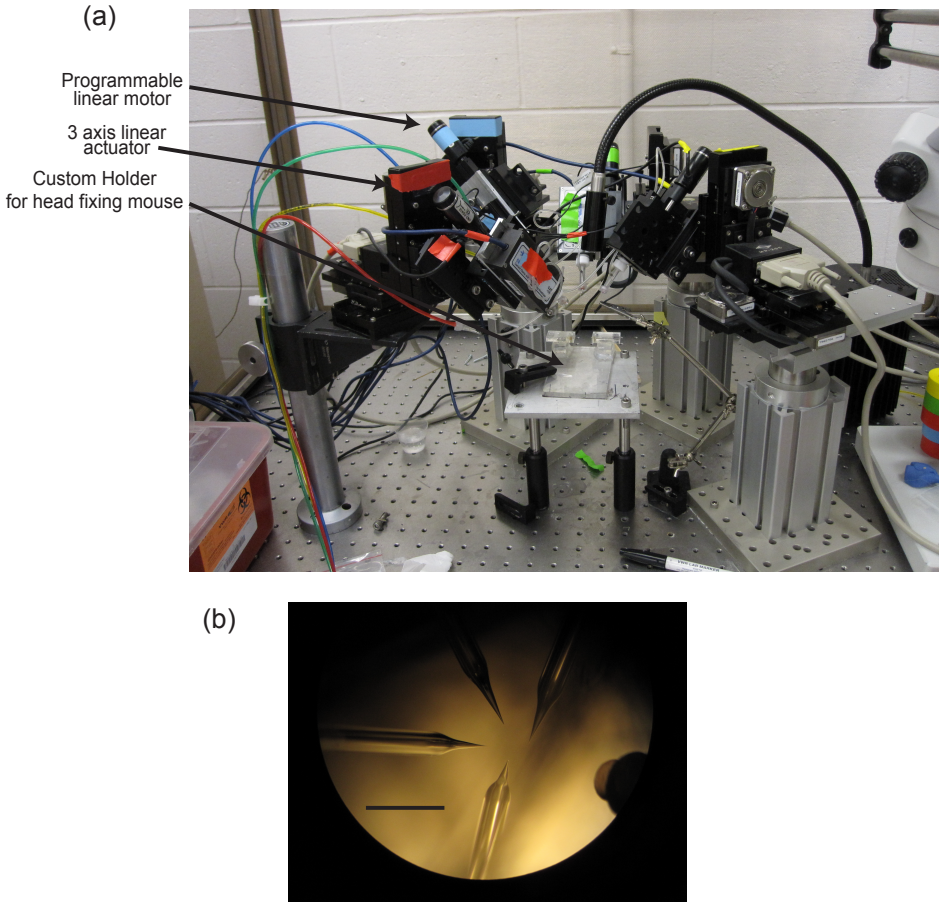


**Figure 4.3.1: Photograph of the multipatcher robot's end actuator modules,** showing **(a)** 4 actuator modules forming an asymmetric array for actuating pipettes. The anesthetized mouse if head fixed using the custom holder, and pipettes are positioned using the stereomicroscope for visualization. (b) Photomicrograph of a set of 4 pipettes tips positioned within a 1mm square area for targeting the same brain region in the cortex. Scale bar indicates 1.5 mm.

With an angled approach, if the pipettes were lowered into the brain to depths > 700 μm, the pipettes could be positioned within a millimeter of each other with this current system. Positioning them closer, can sometimes result in pipettes colliding with each other during a trial, and was thus not attempted. The programmable linear motors in each of the four channels were connected to a multiplexing switchboard (PZC-SB,

Newport; **Fig. 4.2.1 and Fig 4.3.1**). All motors were controlled via a single motor controller (PZC200, Newport Inc). The PZC200 motor controller was in turn connected to the computer through a serial COM port. This architecture allowed up to 8 channels to be selected and controlled by the switch box using a single serial port in the computer.

### 4.3.2 Signal Interfacing with computer

Signals from the headstages were sent to two 2-channel patch amplifiers (Multiclamp 700B, Molecular Devices) that connected patch headstages to a computer through a Digidata 1440A analog/digital interface board (Molecular Devices) (**Fig. 4.2.1**). In a similar fashion to the autopatcher, we used an additional data acquisition (DAQ) board (cDAQ-9174 chassis with modules NI 9215 for analog inputs and NI 9264 for analog outputs, National Instruments Inc) was connected to the computer via a USB port, and to the patch amplifier through BNC cables, for control of patch pipette voltage commands, and acquisition of pipette current data, during the execution of the multipatcher algorithm. During autopatcher operation, the cDAQ-9174 board sent commands to the patch amplifier; after acquisition of cell-attached or whole-cell-patched neurons, the patch amplifier would instead receive commands from the Digidata. We used a software-controlled co-axial BNC relays (CX230, Tohtsu) for driving signal switching between the cDAQ-9174 and the Digidata. The patch amplifier signals were split and streamed simultaneously to the analog input ports of both the cDAQ-9174 and the Digidata throughout and after autopatching. The multipatcher program was coded in,

and run Labview 2011 (National Instruments). The cDAQ-9174 sampled each channel of patch amplifiers at 15 KHz and without any applied scaling factor, and then filtered the signal using a moving average smoothening filter (half width, 6 samples, with triangular envelope), and the amplitude of the current pulses was measured using the peak-to-peak measurement function of Labview. During gigasealing operations, where currents of the orders of 5-10 pA were measured, an additional exponential filter (decay rate = 0.001 seconds) was used to filter out any stray pipette capacitance traces. For resistance measurements, the amplifiers were set in voltage clamp mode using the Multiclamp commander software (Molecular Devices). Square wave of voltage traces were applied: 10 mV in amplitude, at 10 Hz, to the pipettes via the cDAQ-9174 analog outputs. Resistance values were then computed, by dividing applied voltage by the peak-to-peak current observed, for 5 consecutive voltage pulses, and then these 5 values were averaged. During gigasealing and break-in stages of the robot operation, offsets ranging from 0 to -70 mV were applied to the 10 mV, 10 Hz square waveforms to apply the requisite holding potentials needed by the multipatcher algorithm. Multipatched neurons were recorded using Clampex software (Molecular Devices). Signals were acquired at standard rates (e.g., 30-50 KHz), and low-pass filtered (Bessel filter, 10 KHz cutoff). All data was analyzed using Clampfit software (Molecular Devices) and MATLAB (Mathworks).

### 4.3.3 Pneumatic system

The pneumatic system consisted of two boards: an analog pressure regulator board and a pressure switching board. The pressure regulator board is shown in **Fig 4.3.2.** It consists of three manual pressure down-regulators (Mcmaster Carr) connected to a common wall pressure source outputting a pressure of ~5500 mBar. The wall pressure was down regulated to three levels 1 Bar, 100 mBar and ~500 mBar. The 1 Bar regulated pressure was connected to an electronic pressure regulator (990-005101-015, Parker) for setting to high positive pressure state (i.e. 800-1000 mBar). The 100 mBar regulated pressure was similarly connected a second pressure regulator (990-005101-002, Parker) for setting the low positive pressure state (15-20 mBar). The ~500 mBar regulated pressure was connected to venturi vacuum generator (AVR038H, Air-Vac) which generated a vacuum pressure of 300 mBar that was connected to an electronically controlled vacuum pressure regulator (990-005203-005, Parker).

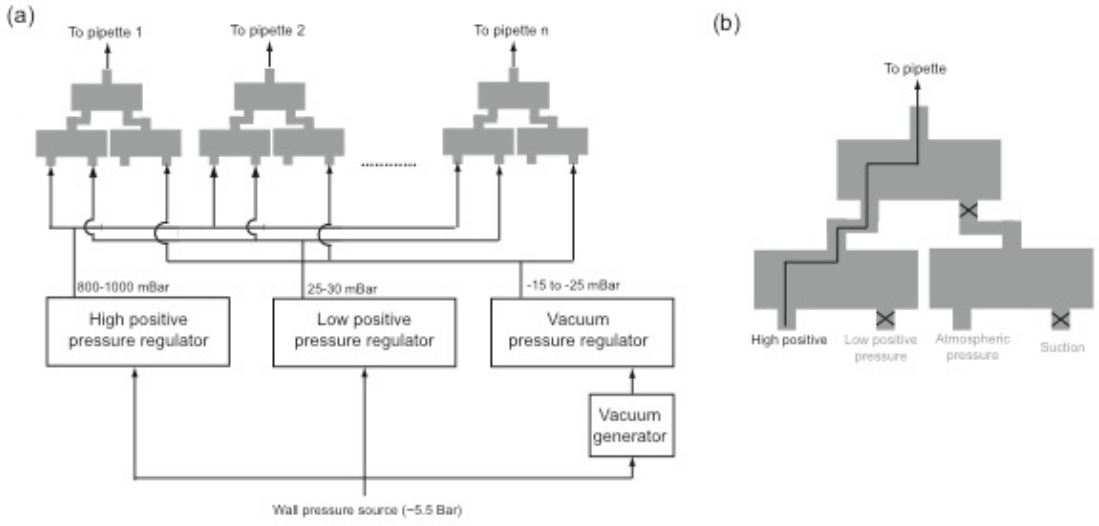


**Figure 4.3.2: Schematic of the pneumatic:** (a) Shows the regulation of pressure to different pipettes using a common pressure source. The wall pressure source is down regulated, or converted to a vacuum pressure and routed to the designated input ports of

the valve switching board. Each valve switching board consists of multiple valve banks **(b)** that can be controlled using the secondary digitizer (See **Fig. 4.2.1**) to set a desired pressure state in a pipette. In this particular example, the valves are set such that the high positive pressure is output to the pipette.

The pressure outputs of the three electronic pressure regulators' were controlled using analog voltages (0-5 V) set manually using potentiometers at 800 mBar (high positive pressure), 20-25 mBar (low positive pressure state) and -15 to -25 mBar (suction state). For breaking in, the suction pressure was set to vacuum pressures between -150 mBar to -250 mBar. The pressures outputs where measured using digital manometers (4756-FM, Dwyer) and connected to the input manifolds of the pressure switchboard.

The pressure switchboard consisted of 4 sets of valve banks, with each valve bank, consisting of 3 solenoid valves (2-input, 1-output, LHDA0533215H-A, Lee Company) as shown in **Fig. 4.3.2 b.** The input ports in each of the three valves making up the valve bank can be closed or opened using a TTL command from the secondary interface board.

### 4.4 Derivation of an algorithm for multipatching

The algorithms for multipatching *in vivo* were formulated using the autopatcher algorithm as a basic template and modifying it for parallel control of multiple pipettes. Here, we describe the iterative process utilized for developing these algorithms. The primary objective of any algorithm used for parallel patch clamping *in vivo* is to establish

whole cell recordings from as many neurons as possible, ideally ensuring arbitrary scalability in a short time period. It was immediately apparent to us that the simplest implementation of a parallel patch clamping system was to introduce *n* number of fully independent autopatcher units simultaneously into the brain, with the physical constraint being the placement of the pipettes in the desired positions in the brain. Such an independently deployed system would ensure that *n* number of channels conduct autopatching trials in the same average time as it would take for a single channel autopatcher ($5 \pm 1$ minute[90]). However, this strategy encountered two issues. Firstly, the movement of motors during neuron hunting resulted in electrical noise, and when coincident with the resistance measurements in other channels, thus resulting in errors. Thus, the resistance measurement events in all channels needed to be synchronized during the entire process of neuron hunting. Secondly, this approach did not take into consideration brain tissue displacement caused by the motion of multiple pipettes in brain. For establishing stable gigaseals, it is critical to prevent any relative motion between the pipette tip and the cell during the gigasealing process[60, 92]. Since encountering a neuron during blind *in vivo* patch clamping is a random process, in a system with multiple autopatchers running independently, different pipettes encounter neurons at different time points. Movement of pipettes seeking neurons during neuron hunting cause tissue displacement, which would hinder the proper establishment of gigaseals in pipettes that had already encountered neurons. Large displacements could also dislodge neurons that were fully gigasealed onto pipettes. Thus we pursued strategies to minimize the amount of tissue displacement during the neuron hunting and gigasealing stages of the algorithm execution.

One of the steps taken to mitigate the tissue displacement issue was to perform the regional pipette localization step for all the electrodes in one single step. Thus, each pipette can be lowered to the desired depth, and then neuron hunting in all channels can start simultaneously. This is shown in the "regional pipette localization" section of the multipatcher algorithm flowchart (**Fig. 4.4.1 i-iv**). Once the pipettes have been installed and positioned in the craniotomies, the multipatcher program is started. At this point the depths for all the pipettes $Z_{0i}$ ($i$=1,2,3 and 4) are denoted as zero by the program. Then the baseline pipette resistances $R_{Z0i}$ in the ACSF or saline bath are recorded (**Fig. 4.4.1 i**). The pipettes are then lowered to the desired depths at a speed of ~200 mm/s[90] (**Fig. 4.4.1 ii-iv**). Pipettes in different channels can be lowered to different desired depths, thereby allowing simultaneous recordings from different layers of the cortex, or even different regions of the brain. Once lowered to depth, the pressures in the pipettes are decreased to low positive pressure state (~20-25 mBar) and the pipette resistances $R_{ZUi}$ assessed for a second time. The values of $R_{ZUi}$ and $R_{Z0i}$ are compared and if resistance increases greater than 0.35 MΩ are detected in any of the channels, the pipette tips are deemed blocked or fouled and those channels are deactivated as denoted by the low opacity pipette in **Fig. 4.2.2 iv**. These channels play no further part in the multipatcher trial. If all pipettes are found to be inadequate for patching, the program stops, and a new trial has to be started. We found that pipettes got fouled at a rate of 18.2% (n=28 out of 156 pipettes in 39 trials), which is comparable to the rate of pipette blockage in the autopatcher. By lowering all the pipettes into the regions of interest in a single step, large macroscopic displacements of pipettes (and the corresponding tissue displacement) are eliminated.

This completes the "regional pipette localization" stage of the multipatcher algorithm. The multipatcher now has to seek out neurons to gigaseal and break in establish whole cell recordings. We proceeded to explore three different algorithms shown in **Fig. 4.4.1**.

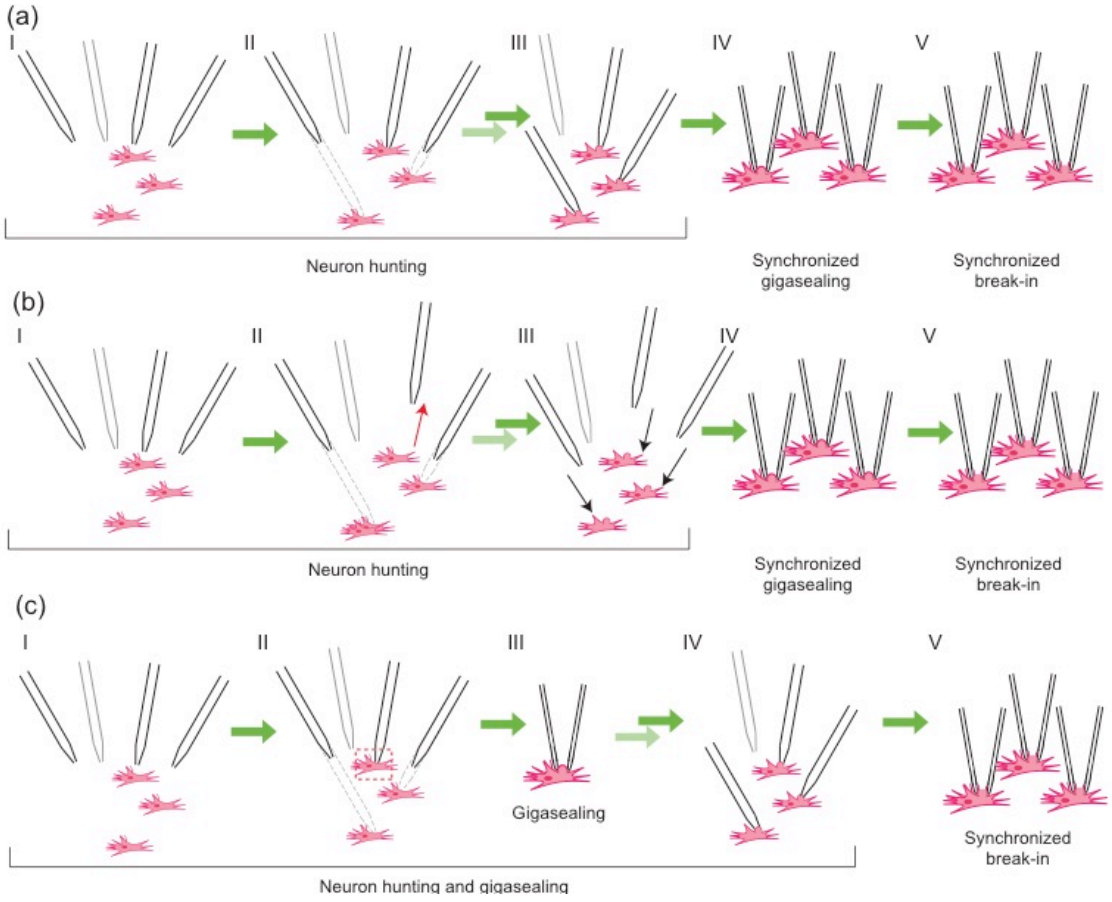


**Figure. 4.4.1: Multipatcher algorithm iterations:** We explored different means to achieve the end whole cell state in all pipettes in as synchronized a manner as possible. Algorithms (a) and (b) where all cells reached gigasealed state synchronously while (c) where only the break-in stage was synchronized. In all cases, pipettes faded out represent those that were deactivated at the end of the regional pipette localization stage and play no part in these algorithms. In (a) each pipette stops when neurons are encountered, in (b) the pipettes are retracted back by a fixed distance after contact, and in (c) pipettes attempt gigasealing immediately upon encountering neurons.

Two factors needed to be taken into consideration while formulating algorithms for the subsequent stages of patch clamping. Firstly, it is advantageous to perform all the steps of neuron hunting, gigasealing and break-in in a parallel manner, so as to reduce the time duration of the experiment. Secondly, as we scale up the number of channels, the supporting hardware required for independent pressure control scales up proportionally. Each channel of the multipatcher requires three solenoid valves and three corresponding TTL control channels. Thus for n number of channels, this number would be 3n. When we are dealing with large number of channels (>50), it become impractical to have independent control over the pressures for each individual channel. One way to simplify this requirement is to synchronize the gigasealing events of all the channels. In this way, the pressures of all the systems can be switched between different states at the same time, i.e. from low positive to atmospheric pressure, followed by suction application using just one set of solenoid switch valves.

Hence, we first implemented a simple extension of the autopatcher algorithm shown in **Fig 4.4.1 a**. The active pipettes were first actuated in steps of 2 μm, followed by an assessment of their pipette resistances. This process was repeated iteratively, until one or more pipettes encountered a neuron (**Fig 4.4.1a i** and **ii**) as detected by the criterion used by the autopatcher, i.e. monotonic increase in pipette resistance greater than 250 kΩ over two consecutive actuation steps. Once a neuron was detected, the corresponding motor was simply deactivated and the rest of the pipettes continue the process of neuron hunting, until all pipettes encountered neurons and stopped (**Fig 4.4.1a iii** and **iv**). At this time, the pressure in all the pipettes was simultaneously released and gigasealing was attempted in a manner identical to the autopacher. This algorithm is

identical to that employed by the autopatcher, but for the different times waited before release of positive pressure for gigasealing in different channels. In 19 trials (in n= 3 mice) where three or more active pipettes performed the neuron hunting and gigasealing tasks, the multipatcher established successful gigaseals 22% of the time (15 out of a total of 68 attempts in 19 trials; 8 out of 76 pipettes were deactivated at the end of regional pipette localization stage due to tip blockage). The pipettes reaching neurons last, and thereby immediately going into gigasealing successfully formed gigaseals 36.8% of the time (7 out of 19 attempts). In the rest of attempts, successful gigaseals were formed 16.3% of the time (8 out of a possible 49 attempts). This number is significantly lower that what was previously using the autopatcher[90]. We analyzed the resistance traces in this second set and found that in some of the traces, the resistance values decreased to the baseline readings obtained before contact with a neuron, during the course of waiting for pipettes in other channels (20% of the time, 10 out of 49 trials). This indicates that the tissue displacements caused by motion of other pipettes in the brain was large enough to dislodge neurons from the optimum relative positions with respect to the neurons for gigasealing. Further, only 20.5% (8 out of the remaining 39) of the pipettes established successful gigaseals, even when elevated resistance readings (indicating contact with a neuron) were observed. We hypothesized that the constant exposure of the neurons to the intracellular pipette solution ejected out of the pipette, when waiting for the rest of the channels to find neurons, possibly had a deleterious effect on the neurons and resulted in lower rates of gigasealing.

To mitigate this effect, we implemented a second algorithm shown in **Figure 4.4.1b.** In this procedure the multipatcher proceeded along the same lines as the previous

algorithm, until a neuron was encountered at one of the channels, at which time, the pipette was retracted by 30 μm, and stopped (**Fig 4.4.1b ii**). We chose a value of 30 μm because, that was the minimum distance the pipettes needed to be retracted before the resistance measurement decreased to the average baseline value (n=15 trials). This would position the tip at a distance where the ejection of the intracellular solution has no effect. This process was repeated for all the active pipettes, such that at the end of neuron hunting, the relative positions of all the pipettes, and the corresponding neurons they encountered were the same (~30 μm, after accounting for tissues displacement) (**Fig 4.4.1b iii**). As a final neuron-hunting step, all pipettes were moved forward by the same distance (30 μm), and gigasealing attempted synchronously (**Fig 4.4.1b iii-v**). This algorithm yielded a success rate for gigasealing of ~20% (12 out of 59 attempts in 17 trials, with 9 pipettes deactivated at the end of regional pipette localization stage due to tip blockage). Again, this was much less than what we would expect when using the autopatcher algorithm. We analyzed the resistance measurement traces for this algorithm, along similar lines to the previous algorithm described above and found that after the final neuron hunting step when all pipettes advanced forward by 30 μm, resistances went back to the elevated values indicated by contact with neurons in only 45.7% (27/59 attempts), again indicating that tissues displacement effects were in play.

As a third iteration, we implemented the algorithm shown in **Figure 4.4.1c.** As it has been observed previously, once gigasealed cell attached or whole cell stage has been achieved, the configuration is remarkably stable against motion artifacts. This has been used previously to record in the whole cell state from head fixed rodents[36, 37, 60, 61, 66], freely moving animals[35, 36, 93]. Several groups have also shown that it is possible to carry

out loose cell attached recordings for tens of minutes to hours[94]. Further, from whole cell stage, pipettes can be retracted for up to 50-60 μm before an outside out patch is established[95]. Using this property, a third algorithm was explored where in, once a pipette encountered a neuron, the program pauses neuron hunting in all channels and attempts gigasealing in the channel that has encountered a neuron.

This is shown in **Fig 4.4.1c**. once the robot enters the neuron hunting and gigasealing stage (**Fig 4.4.1c v-viii**), it lowers pipettes in the active channels forward by 2 μm in a serial fashion. This is followed by assessment of the resistances of pipettes. These two tasks are performed repetitively, while constantly looking for time-series trends in resistance measurements that are indicative of contact with a neuron. These trends are typically monotonic increases in pipette resistance over 0.2- 0.25 MΩ within three measurements (See **Section 2.4** in **Chapter 2**). Whenever a channel positively encounters a neuron, pipette actuation in all channels is stopped and gigasealing protocol is initiated.

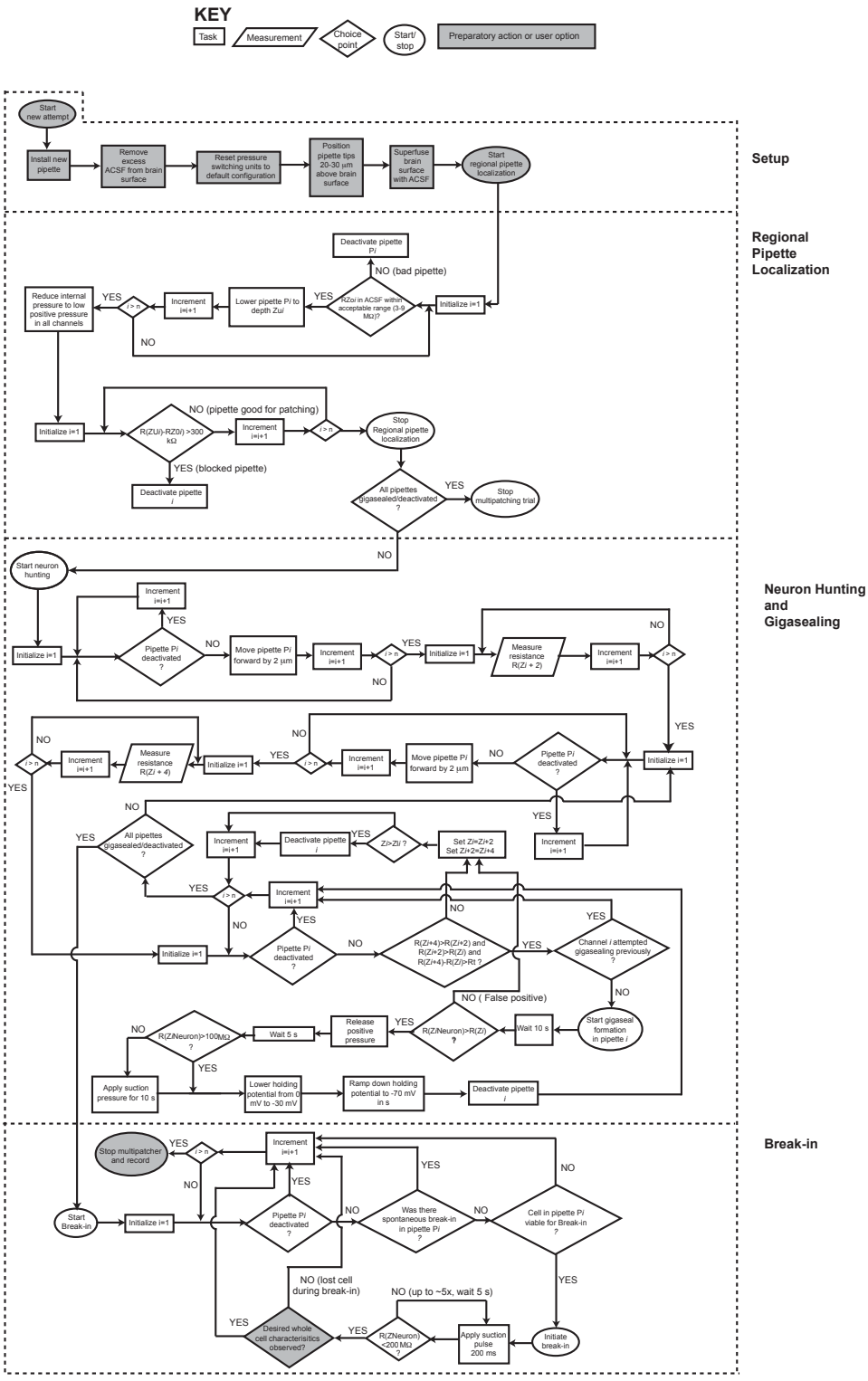


**Figure 4.4.2: The complete algorithm for automated *in vivo* multipatching:** The dotted lines frame separate each of the stages of the algorithm; within the dotted line

frames, symbols representing tasks, measurements, and choice points are indicated, along with text explaining the individual steps and consequences of decisions (see "KEY" for definition of symbols). Abbreviations: ACSF, artificial cerebrospinal fluid; $RZ0_i$, resistance of pipette *i* at depth Z in the brain; $ZU_i$ , upper depth limit of the region targeted by the regional pipette localization stage of each pipette *i*; $R(Zi_{Neuron})$, pipette resistance at the depth at which the neuron is being recorded (which will vary over time, as the later stages of the process, gigasealing and breaking-in, occur); Rt, pipette resistance threshold for neuron detection. The blocks shown in grey are manual tasks that are carried out by the experimenter, and the blocks in white are those executed by the computer.

The multipatcher waits 10 seconds to see if the pipette resistance decays back to baseline value. If it does, the program restarts neuron hunting. Otherwise, the program releases positive pressure in the pipette, waits 5 seconds, and applies suction pressure for 10 seconds. Once the suction pressure is released, the holding potential is stepped down to -30mV, and ramped down from that value to -70mV over the next 30 seconds. This completes the "gigasealing" attempt for that pipette (**Fig 4.4.1c iii**). Once the gigasealing protocol is completed in a particular channel, the neuron is held at a holding potential of -70 mV, the motor is deactivated and neuron hunting is re-started in the remaining active channels. This process is repeated until all the active channels have encountered neurons and undergone gigasealing (**Fig 4.4.1c iv**).

**Table 4.1:** Pressure and time setting for iterative achieving successful break in, causing as minimal perturbation to the cell.

| | 200 ms | 250 ms | 300 ms | 350 ms | 400 ms | 450 ms | 500 ms | 750 ms | 1000 ms |
|---|---|---|---|---|---|---|---|---|---|

| | | | | | | | | | |
|---|---|---|---|---|---|---|---|---|---|
| 150 KPa | Attempt 1 | Attempt 2 | Attempt3 | Attempt4 | Attempt5 | Attempt6 | Attempt 21 | Attempt 22 | Attempt 23 |
| 200 KPa | Attempt 7 | Attempt 8 | Attempt9 | Attempt10 | Attempt11 | - | Attempt24 | Attempt 25 | Attempt 26 |
| 250 KPa | Attempt 12 | Attempt 13 | Attempt14 | Attempt15 | Attempt16 | - | - | - | - |
| 300 KPa | Attempt 17 | Attempt 18 | Attempt19 | Attempt20 | - | - | - | - | - |

At this point of time, the multipatcher attempts break in (**Fig 4.4.1c v**). The user can choose the channels in which break-in needs to be executed. We used an iterative method where in the duration of the suction pulses, and the applied pressures were incremented in each successive attempt, until a successful break-in was formed (**Table 4.1**). Using this algorithm, we were able to get successful gigasealed cell attached recordings from 35.93% of the active pipettes (46 out of 128 pipettes in 39 trials, 28 pipettes were deactivated at the end of the regional pipette localization stage). This was the highest yield we obtained from all three iterations and was thus used as the final generalized algorithm as shown in flow-chart form in **Figure 4.4.2**. Of the 46 neurons that were gigasealed, we established successful whole cell recordings in 36 neurons, achieving a break-in success rate of 78.2%. Finally, we were able to establish successful whole cell recordings from multiple neurons, i.e. 2 or 3; we were not able to achieve whole cell recordings in all 4 pipettes in any of the trials; in 30.7% (12 out of the 39 trials, with 11 recordings where pairs of neurons were connected, and 1 recording where a triplet of neurons were recorded) of the trials. While the algorithms were formulated

and tested using a 4-channel multipatcher system, they can in principle be applied to control arrays of arbitrarily large number of pipettes. More pipettes would ensure, higher success rate of obtaining multiple patch recordings.

### 4.5 Time course of Multipatcher operation

A representative trace of resistance readings recorded from the fours channels of the multipatcher during a full trial is shown in **Fig.4.5**. The resistance traces for channels 1,2,3 and 4 are shown in red, blue green and magenta respectively. The key events during the trial are denoted by Roman numerals. The detection of a neuron by channel 3 is shown by roman numeral **i**. Between **i** and **ii**, all pipettes paused neuron hunting and gigasealing was attempted in channel 3. The stereotypical gigasealing tasks were carried out in a similar fashion described in **Section 4.4**, At **ii**, set at -70 mV. The entire gigasealing process was programmed to execute in 60 seconds. At the end of 60 seconds, channel 3's motor was deactivated and the holding potential held at -70 mV as the rest of the channels resumed neuron hunting. At **iii** the robot detected contact with a neuron in channel 2. The same gigasealing steps described above for channel 3 were used for channel 1 between time-points **iii** and **iv**, resulting in an unsuccessful gigaseal formation. It must be noted here that gigasealing was attempted only for 35 seconds, as against the full 60 seconds routine. As it was clear that the cell would not gigaseal and the experimenter terminated the gigasealing attempt using a manual intervention mechanism in the software interface. At **iv** channel 2's motor was deactivated at the end of which the

holding potential was held at -70 mV, while channels 1 and 4 resumed neuron hunting. Between **v** and **vi**, the robot paused again, to successfully attempt a gigaseal formation in channel 1. Finally the same sequence of events applied to channel 4, and a successful gigaseal resulted between **vii** and **viii**. At **ix**, the gigasealed neurons attached to the patch electrodes in channels 1, 3 and 4 are broken into to establish whole cell patch recordings.

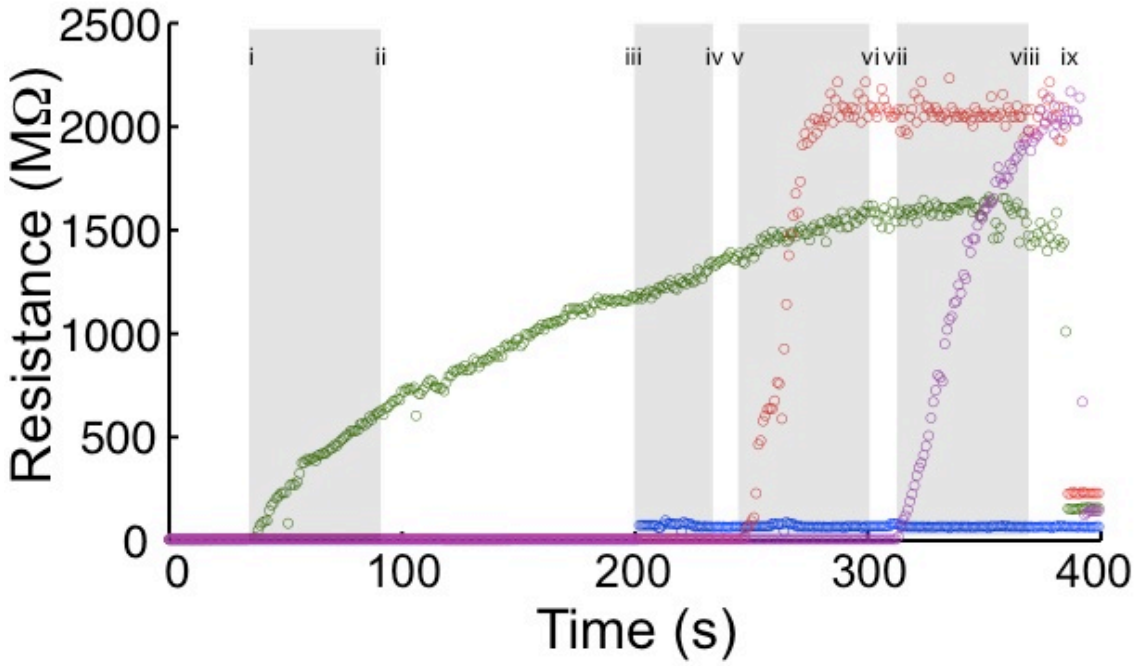


**Figure. 4.5:** Representative traces of pipette resistances recorded by the multipatcher during a successful multipatcher trial, during the neuron hunting and gigasealing stages. The traces from channels 1-4 are shown in red, blue green and magenta respectively. Key events are flagged by romal numerals, with time courses during gigasealing shaded in grey. At i channel 3 detects a neuron, and all pipettes stop advancing, and gigasealing is attempted between **i** and **ii**. At ii, motor in channel 3 is deactivated, and the pipette is held at -70mV holding, while the rest of the channels continue neuron hunting. This process is repeated every time a pipette encounters a neuron, and gigasealing is attempted between **iii** and **iv**; **v** and **vi**; and, **vii** and **viii**. **ix** is the point at which all channel that have successfully gigasealed are broken into, to get whole cell configuration.

An important distinction from the autopatcher algorithm is to be noted here. The time for execution of gigasealing tasks was fixed at 60 seconds, whereas in the autopatcher, break-in was initiated at the discretion of the experimenters. Thus, average gigasealing time reported for the autopatcher in chapter 2 is higher than 60 seconds. The gigasealing times recorded for autopatching[90] are the times taken for gigaseals to fully stabilize and asymptote, upon which break-in was initiated by the experimenter. In the multipatcher algorithm, we employed a fixed time for gigasealing with the cell being clamped at -70 mV holding potential at the end of the 60-second gigasealing routine. Thus, even as the program resumed neuron hunting with pipettes that were yet to encounter neurons, the gigasealed cell's(s') seal resistance continued to increase and finally asymptote due to the hyperpolarizing holding potential that was applied. This did not however apply to the channel that attempted gigasealing last for which the usual conditions used for autopatching were applied.

In a subset of the trials, we measured the time taken to fill, install and position the pipettes in a multipatching trial. For four channels, the average time taken for filling and installing pipettes was 12.48 $\pm$ 1.36 minutes (n=18 trials), and the time taken for the completion of multipatcher trials culminating in successful whole cell recordings recordings of one of more neurons was 10.45 $\pm$ 2.56 minutes (n=14 trials). Thus, for a single channel it takes 3.2 $\pm$ 0.31 minutes for pipette installation, and 2.61 $\pm$ 0.64 minutes for whole cell patch clamping as compared to the autopatcher (2.0 ± 0.4 for pipette installation and 5 ± 2 minutes for operation). The increased time for pipette installation per channel is due to the increased complexity of tasks involved in positioning the pipettes in close confinement. However, this is offset somewhat by the reduced time for

operation/channel mainly due to limiting the gigasealing operations of all but one channel to 60 seconds.

If the current system were to be scaled up for controlling higher numbers of pipettes, it is expected that installation and robot operation times would scale up proportionally, with the time for installation increasing more rapidly. Thus scaling up beyond 10-12 channels would necessitate a redesign of the actuation modules to enable quick replacement of pipettes for high-throughput operation.

### 4.6. Quality of patch recordings

Representative traces recorded from a triplet of neurons in current clamp mode are shown in **Fig. 4.6.1 a**. As observed previously with the autopatcher, a majority of the neurons exhibited up and down states, typical of cortical neurons under anesthesia. The up and down states in all neurons were highly correlated, as can be seen in **Fig. 4.6.1 b**. We injected currents in one or more neurons (**Fig. 4.6.2**), to evoke synaptic responses. We however did not see evoked synaptic currents in any of the paired recordings, possibly because we were still not within the range of distances where one would expect a high probability of synaptically connected neurons.

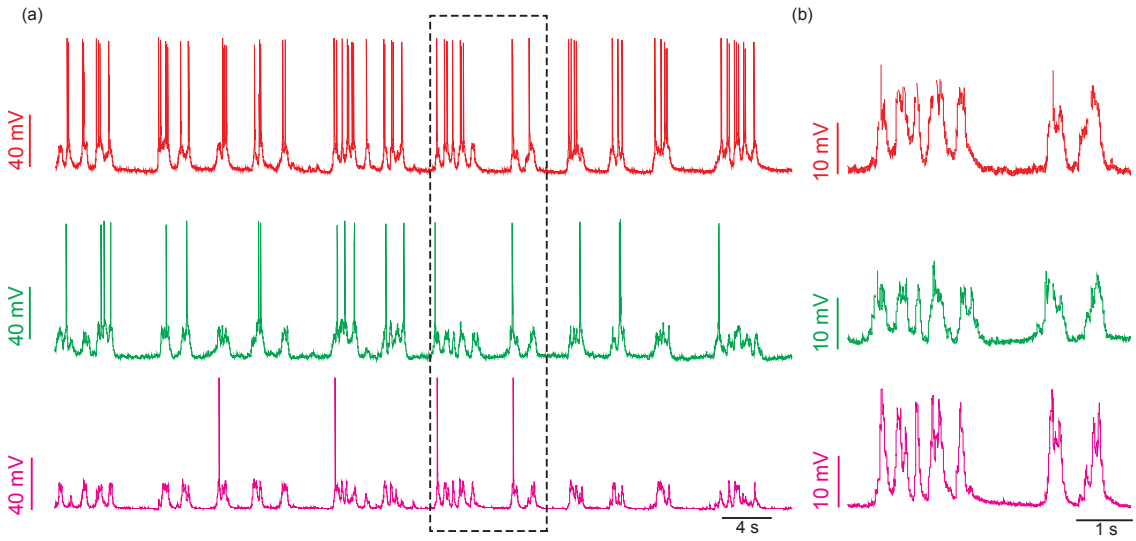


**Figure 4.6.1: Whole cell current clamp recordings:** Representative baseline spiking activity in current clamp mode, in three neurons that were simultaneously whole cell recorded using the multipatcher These recordings corresponds to the to the trial shown in **Fig 4.5**. (a) The three neurons were targeted in the motor cortex, ~ 700 micrometers from each other. Mean resting potentials for the neurons were -55.93 + 7.21 mV (*top*), -60.3 $\pm$ 4.52 mV (*center*) and -69.23 $\pm$ 4.58 mV (*bottom*) and (b) Zoomed in view of sub-threshold membrane potential fluctuations, during the time highlighted by the dashed box in **a**. Neurons recorded displayed a high degree of correlation in the up and down state fluctuations. Spikes in this time period have been truncated for better visualization.

We were able to record stably from multipatched cells for 56 $\pm$ 8 minutes (n=23 neurons), with recordings lasting for a maximum of 90 minutes. In the interest of throughput, we prematurely terminated the recordings in 5 trials (3 paired recordings, 2 single neuron recordings), before the whole cell recordings were lost, thus, the actual average recording time could have been higher.

Analyzing just the trials where multiple whole cell recordings were obtained, the mean and standard deviation of the access resistances obtained were 44.2 $\pm$ 17.6 MΩ (n= 23 neurons), the mean and standard deviation of the resting membrane potentials were -

62.2 ± 9.8 mV (n= 23 neurons), and the mean and standard deviation of the currents needed to hold the neurons at -65 mV in voltage clamp mode was -78.5 ± 55.2 pA (n= 23 neurons). All these values are comparable those obtained previously by us using the single channel autopatcher[90], suggesting that holding cells for prolonged periods of time (> 2-3 minutes) did not affect the quality of the whole cell recordings.( see **Section 2.5** ).

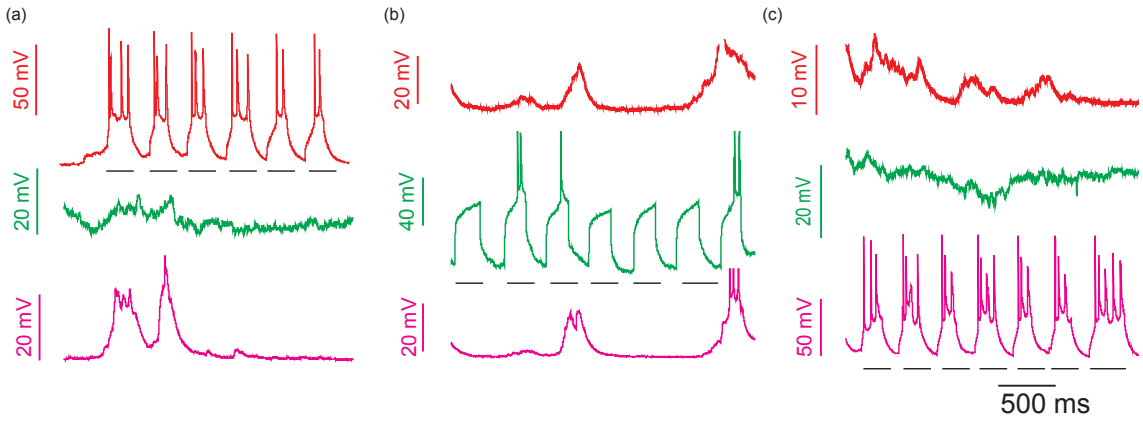


**Figure 4.6.2: Investigating synaptic connectivity between whole cell patched neurons:** Currents were injected in the neurons recorded in **Fig 4.6.1** to determine if they evoke synaptic currents in other neurons. **(a)** 80 pA of somatic current injection in the neuron shown in the top trace elicited no response in the other two cells despite spiking. (b) 120 pA current in the neuron recording shown in the middle trace, and (c) 60 pA current injection into the neuron recording shown in the bottom trace, again no synaptic response was evoked. This observation was consistent with other paired recordings. Black lines indicate time duration of injected currents, spikes if any in neurons that did not have any current injection were truncated, for better visualization of the sub-threshold current dynamics.

We grouped the whole cell patched neurons into those that were gigasealed immediately upon detection, and those that were held in gigasealed states for longer

periods of time during neuron hunting in other channels. Between these two groups, we compared the access resistances, and the resting membrane potentials; indicators of quality of the recording obtained. All parameters reported here are in the uncompensated form (i.e. no series resistance or capacitance compensation), obtained using the conventional patch clamp software after autopatcher program completion. Previous literature has suggested that holding neurons for prolonged periods of time in gigaseal cell attached state leads to higher access resistances[66]. Further, we also wanted to assess the effect if any, tissue displacement had on these gigasealed neurons. The mean and standard deviation of the access resistances were 49.4 $\pm$ 23.9 MΩ (n = 8 cells that were successfully broken into immediately upon establishment of gigaseal), and 41.4 + 14.6 49.4 $\pm$ 23.9 MΩ ( (n = 15 cells that were gigasealed held in that state when other channels were conducting neuron hunting). We found no statistically significant difference in the access resistances of the two datasets (t-test, $p > 0.86$).

## 4.7 Experimental Methods

### 4.7.1. Surgical Procedures

Surgical procedures were conducted similar to that described previously (see **Chapter 2**). All animal procedures were approved by the MIT Committee on Animal Care. Adult male C57BL/6 mice (Taconic), 8-12 weeks old, were anesthetized using ketamine/xylazine (initially at 100 mg/kg and 10 mg/kg, and redosed at 30-45 minute intervals with 10-15% of the initial ketamine dose as needed, using toe pinch reflex as a standard metric of anesthesia depth). The scalp was shaved, and the mouse placed in a

custom stereotax, with ophthalmic ointment applied to the eyes, and with Betadine and 70% ethanol used to sterilize the surgical area. Three self-tapping screws (F000CE094, Morris Precision Screws and Parts) were attached to the skull and a plastic headplate affixed using dental acrylic. Once set (~20 minutes), the mice were removed from the stereotax and placed in a custom-built low profile holder. A dental drill was used to open up 4 craniotomies (0.25 - 0.5 mm diameter, within a spacing of 1 mm) by thinning the skull until ~100 μm thick, and then a small aperture was opened up with a 30 gauge needle tip. Cortical craniotomies were opened at stereotaxic coordinates: anteroposterior, -1.5 to +0 mm relative to bregma; mediolateral, 1-3 mm left or right of the midline; neuron hunting typically began at a depth of ~ 400 μm depth. The dura was removed using a pair of fine forceps, or in some instances, not removed at all. For dampening the motion artifacts of the brain, we used 2% agarose to cover the brain surface. Experiments typically lasted 5 hours, at the end of which the mice were euthanized via cervical dislocation when fully anesthetized.

### 4.7.2. Electrophysiology

Borosilicate glass pipettes (Warner) with resistances between 3-9 MW, were pulled using a filament micropipette puller (Flaming-Brown P97 model, Sutter Instruments), and stored in a closed petri dish to reduce dust contamination. During each experiment we used atleast 60-70 pipettes. They were filled with intracellular pipette solution consisting of (in mM): 125 potassium gluconate (with more added empirically at

the end, to bring osmolarity up to ~290 mOsm), 0.1 $CaCl_2$, 0.6 $MgCl_2$, 1 EGTA, 10 HEPES, 4 Mg ATP, 0.4 Na GTP, 8 NaCl (pH 7.23, osmolarity 289 mOsm), as used in the past[90].

### 4.7.3. Multipatcher robot operation

The first step of the algorithm started with the pipettes having been installed in the holders. A program valve_reset.vi (See **Appendix B** – "Multipatcher User Manual") was executed in Labview to configure the pressure switching board to its default configuration, resulting all pipettes being maintained in high positive pressure state.

We used 3-axes linear actuators (Sutter Instruments) to manually position the pipette tips over the craniotomy (or multiple craniotomies) 20-30 mm above the brain surface using a control joystick with the aid of a stereomicroscope (Nikon). The pipette voltage offsets were automatically nullified by the "pipette offset" function in the Multiclamp Commander (Molecular Devices) and the **Multipatcher_ver1.0.vi** program initiated. A complete set of instructions on the use of the multipatcher software is described in **Appendix B** – "**Multipatcher User Manual**".

## 4.8. Conclusion

The multipatcher represents the first demonstration of a scalable platform capable of conducting multidimensional single cell measurements to the neuronal circuit level. For the first time a realistic solution for linking cellular level measurements to systems

level characterization in the intact brain has emerged. The algorithms developed for the multipatcher, build on the existing autopatcher algorithm that we have previously reported (**Chapter 2**), and takes into consideration the mechanical interactions of pipettes, and the surrounding brain tissue while being actuated. We found that the quality of recordings obtained with the mutlipatcher robot was comparable to the quality of recordings obtained with the single channel autopatcher system. When combined with custom hardware, it is thus scalable to control arbitrarily large numbers of pipettes in the intact brain. Further if the hardware can be miniaturized with better precision in placement within much smaller regions spanning local microcircuits[96, 97] (< 200 μm), it can be used to assess synaptic connectivity between neurons in a microcircuit in the intact brain. Multiple electrodes can also be used to record from varied interconnected regions of the brain, opening up possible experiments to assess how sub-threshold membrane potential fluctuations are correlated across these regions, such sensory thalamo-cortical circuits, or even more dynamic processes like memory formation.

The scalability in the electrode numbers means that the multipatcher can be used as a high-throughput tool for systematically obtaining large electrophysiological datasets for analyzing brain circuits. If combined algorithms that enable automated single cell RNA harvesting, the robot can be used to probe and obtain genetic information from large numbers of cells. Such a strategy can be generalized to other frontiers in biology, bioengineering, and medicine in which the assessment of the properties of single cells, embedded within intact tissue, is desired but has not been achievable in a systematic high-throughput fashion. For example, analyzing how different cells in a neural circuit respond to a drug in specific brain states, performing electrical characterizations of cells

in tissues removed during surgery, determining how different individual cells within a tumor biopsy sample vary in gene expression, and assessing how tissue-engineered organs vary in cell to cell composition, may provide fundamental new capabilities in diagnostics, personalized medicine, and drug development.

Further, the hardware architecture makes it amenable to integration with optical components for optogenetic stimulation[74, 98, 99]. This combined approach will enable assessments of the synaptic basis of how specific cell types coordinate network activity. The multipatcher opens up several interesting engineering challenges for scaling up. Currently, there are some limitations to the number of electrodes that can be simultaneously manipulated using these actuator systems due to their macroscopic scale. Attempting to build very larger arrays using conventional apparatus would run into stereotactic hindrance within 6-12 pipettes. Alternate strategies for miniaturizing the actuation systems, as well as using novel electrodes such as flexible fused silica pipettes[100] can be explored. Since patch pipettes can be used only once, scaled up multipatchers will require hundreds of pipettes to be fabricated, filled and assembled for each experiment (we currently use 60-70 pipettes in a typical day, taking ~1 hour to fabricate them). Thus developing a means to fabricate pipettes in an automated fashion[87] can be advantageous. The time taken to assemble these pipette arrays will also increase proportionally with electrode numbers. Thus, strategies for automated filling and assembly of pipettes will need to be explored. Alternately, protocols can be developed to re-use assembled multipatcher arrays by attempting to clean pipettes tips[101] or the hardware can be developed so as to allow robotic assembly of pipettes. Denser pipette arrays will increase the tissue displacement effects, and thus newer pipette geometries

with thinner shanks, will be needed. Finally, as the number of channels increase, the cost of the amplifiers will be significant. Thus, low cost amplifiers dedicated for patch clamping[102] need to be used to reduce the cost of patching.

# CHAPTER 5

# CONCLUSION AND FUTURE PERSPECTIVE

## 5.1. Conclusions

Whole-cell patch clamp recordings of the electrical activity of neurons *in vivo* exhibit signal quality and temporal fidelity sufficient to report synaptic and ion channel-mediated subthreshold events of importance for understanding not only how neurons compute during behavior, but how their physiology changes in disease states or in response to drug administration. However, *in vivo* patching requires skill, and the hardware required is specialized and expensive. Thus, *in vivo* patching has been utilized by a relatively small number of labs, and is usually regarded as a difficult technique. The ability to patch neurons *in vivo,* in an automated, inexpensive fashion, would broadly enable neuroscientists to examine how neurons within a network respond at the synaptic or ion channel level to behavioral or brain-state changes, how such subthreshold dynamics are altered in animal models of brain disorders, and how synapses and ion channels in specific cells function in the critical *in vivo* setting, and are affected by pharmacological agents. In this thesis, we demonstrate that the process of *in vivo* patch clamping can be reduced to a reliable algorithm that can be executed in closed loop by a robotic system, which we term the autopatcher.

This automated patch clamping robot achieves yields, quality and throughput that is comparable, or exceeds the capabilities of skilled human practitioners of this technique.

These recordings were firstly obtained in the cortex and hippocampus of adult anesthetized mice, and we have also shown that the same algorithms can be extended to obtain patch clamp recordings from awake, head fixed animals.

In chapter 3, we integrated the autopatcher with optical fibers and demonstrated that the algorithm continued to be robust enough such that the same algorithm without any modifications could be used to guide fiber coupled patch pipettes to record from neurons expressing optogentic molecules and measure evoked sub-threshold photocurrents. Finally, we extended the basic hardware and software components of the autopatcher to develop robotic systems with multiple pipettes that can be simultaneously controlled in a semi-parallel fashion to obtain recordings from pairs and triplets of neurons in anesthetized mice. This represents the first demonstration of a scalable platform capable of conducting multiple whole cell patch clamp measurements from neuronal circuits in the intact mammalian brain, and for the first time a realistic solution for linking cellular level measurements to systems level characterization in the intact brain has emerged.

## 5.2. Future perspectives

We have demonstrated that once an autopatching robot or multipatching robot is loaded with requisite pipettes filled with intracellular saline solutions, recordings can be obtained automatically. The current systems still need humans to prepare the patch electrdes and load then into the holders for each trial, a process that takes close to half the time taken to find a neuron and patch. Thus, all the tasks leading up to the process of

automated patch clamping such as the fabrication of patch pipettes, the filling of patch pipettes with intracellular pipette solution, the docking of patch pipettes in the holders, and subsequent positioning of the pipette tips at the surface of brain can also be automated to develop fully integrated robotic systems that can potentially run without human intervention throughout the entire length of the experiments. Such fully roboticized systems will enable a single human operator to control many rigs simultaneously, enabling the accumulation of large datasets, which are currently not possible with *in vivo* electrophysiology studies.

A current focus in systems neuroscience has been to determine the role played by specific cell types, in neuronal signal processing. While we have demonstrated automation of "blind" *in vivo* patch clamping, in our pilot experiments we have been successful in obtaining whole cell recordings in acute slices (data not shown). Thus the automated patch clamping systems can be combined with fluorescence imaging optics to obtain whole cell recordings from multiple fluorescently identified neurons from intact slices, with potential applications in circuit mapping, or by integrating the autopatcher/mulitpatcher with two-photon imaging systems, targeted patch clamping of specific identified cell types can be conducted *in vivo*.

Automation enables a fine degree of feedback control of the position and pressure states of the pipette, that is previously not possible by manual patch clamping. By incorporating advanced feedback algorithms and motion compensation mechanism so as to actuate the patch pipette in anticipation of brain motion, it is possible to develop

devices that can obtain whole cell recordings in conditions which a high degree of tissue movement, such as freely moving and behaving animals, where traditional static devices fail. For e.g., miniaturized head borne versions of the autopatcher actuators can be developed to enable patch clamp measurements from multiple neurons in freely moving animals, as demonstrated with single pipettes by Albert lee and colleagues, and advanced mechanisms for sensing and compensating for brain tissue displacement can be developed to conduct such recordings from awake behaving non-human primates: a feat that has not been possible thus far, due to the insurmountable challenges of tissue displacement.

As a final note, at a molecular neuroscience level, it is critical to be able to analyze how ion channels and receptors contribute to neural computational processes *in vivo*, because the levels of synaptic input, neuromodulator tone, and electrical activity impinging upon a specific neuron in the intact brain, in a specific behavior or disease context, may alter the performance and function of a given ion channel or receptor from what one might expect from purely in vitro studies. An understanding of the roles that ion channels and receptors play in intact brain networks (i.e., *in vivo*, and in the juvenile, adult, or aged brain), would greatly enhance our understanding of how a genetic or molecular change in an ion channel, results in a complex disease phenotype – important for guiding the way towards future therapeutic strategies. Variations of the transcriptomic make up of single cells effect such changes in ion channel and receptor compositions of single neurons. Thus, there is great need for high-throughput tools that enable the measurement of transcriptomic properties of individual brain cells so that

systematic and integrative characterizations of the cells in a brain circuit become possible. If the existing autopatcher algorithms can be equipped with feed back control algorithms to optimally harvest the single cell transctriptomes for qPCR and single cell RNA sequencing analysis and if combined with the scalable architecture the multipatcher, such a tool that uniquely suitable for conducting such single cell transcriptome harvesting studies from large numbers of neurons *in vivo* can be realized.

The richness of the electrophysiology data enabled by patch clamping has traditionally been a big incentive for neuroscientists to perform this art form. The idea of patch clamping as a tool for measurement of cellular phenomena has not gained traction in other areas of biology. Current methods (e.g. laser scanning micro-dissection) for isolating, categorizing and characterizing the cells in intact organ systems suffer from a lack of specificity and/or are low-throughput. The tools described above will have the necessary specificity (the ability to isolate single cells via access their cytosolic contents), and, importantly, high enough throughout (by means of automation and scalability) to transform the field of single cell analysis in the basic sciences as well as clinical fields. It will enable biologists and clinicians to take an intact organ system (e.g. a cancer tumor) and perform integrative analyses of single cells' gene expression profiles, morphologies, and, if relevant, electrophysiological characteristics. By enabling individuals to systematically accumulate datasets in the organ systems they study and in the states of interest (e.g., differentiating stem cell embryoid bodies), it will become possible to resolve the sources of cellular heterogeneity, and enable identification of rare and important cell types that is not possible with any of the existing techniques.

# APPENDIX A

# AUTOPATCHER USER MANUAL

**Parts list for Autopatcher setup**

1. Patch clamp amplifier: Multiclamp 700B (Molecular Devices)
2. Patch clamp headstage: CV-7B (Molecular Devices)
3. Primary computer interface board: Digidata 1440B (Molecular Devices)
4. Secondary computer interface board: NI USB-6259 (National Instruments)
5. 3 axes linear actuator for manual positioning: MX7600L (Siskiyou)
6. Programmable linear actuator with controller kit: PZC200-KT (Newport)
7. Linear stage: MX460A-X (Newport)
8. Electronic 2-way solenoid valves: LDA0533215H-A (Lee company)
9. BNC relay switch: (CX230, Tohtsu)

## A.1 Hardware Setup

### A.1.1. Installing programmable motor in standard in vivo electrophysiology setup

This will depend on the configuration of an existing setup. To install a programmable linear motor in our *in vivo* electrophysiology rig, we machined a custom dovetail groove mounting plate to fix the CV 7B headstage to the Newport linear stage that is controlled using the piezo-motor (Fig. 1.1).

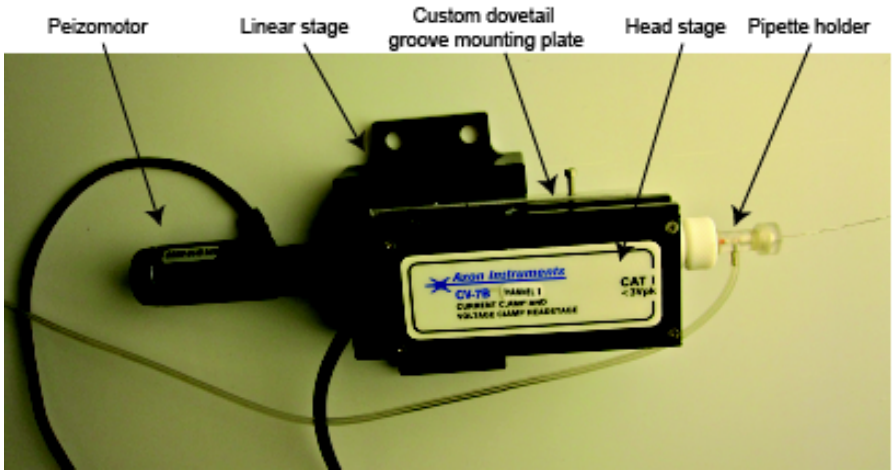


**Figure A.1.1:** Installing patch amplifier headstage onto to linear stage driven by peizomotor using a custom dovetail groove mounting plate

The entire assembly was then mounted onto the 3 axes linear actuator (Siskiyou Inc), as shown in Fig 1B in the main manuscript. The motor was connected to the controller and interfacing with the computer was done as per the instructions in the NanoPZ system user manual provided by Newport Corporation: ftp://download.newport.com/MotionControl/Current/MotionControllers/PZC200/Manual/NanoPZ.pdf

### A.1.2. Installing programmable pressure control valves

The circuit diagram for actuation of the solenoid valves is shown in Fig. 1.2. Instructions to make pneumatic connections are shown in Fig. 1 and described below:

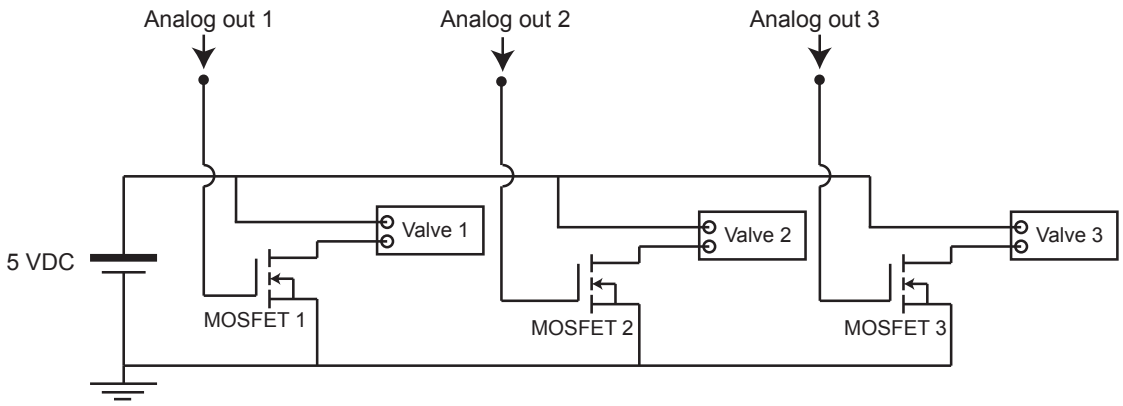


**Figure A.1.2:** Circuit diagram for controlling solenoid valves for pressure modulation

1) Connect the Common port (output) of Valve 1 to pipette holder.

2) Connect the Common port (output) of Valve 2 to normally open (N.O.) input port of Valve 1.

3) Connect the Common port (output) of Valve 3 to normally closed (N.C.) input port of Valve 1.

For port locations, see the mechanical drawing of the soleniod valves:

http://www.theleeco.com/PDF.nsf/2355f3df133a527185256c9300562a42/e8bb4dc1b62a5f54852569a6006b64d8/$FILE/LHDA0030000BA.pdf

For computer control of the bank of valves,

1) Connect Analog Out 1 (AO1) of the USB 6259 to Gate of MOSFET 1 to drive Valve 1.

2) Connect Analog Out 2 (AO2) of the USB 6259 to Gate of MOSFET 2 to drive Valve 2.

3) Connect Analog Out 3 (AO3) of the USB 6259 to Gate of MOSFET 3 to drive Valve 3.

### A.1.3. Interfacing Amplifier to computer

The signals for the Multiclamp 700B amplifier (Molecular Devices) are sent to and from two computer interface boards. The NIDAQ USB-6259 (National instruments) board is used to send signals to the amplifier during Autopatcher operation, and the Digidata 1440A is used for recording with commercial software Pclamp (Molecular Devices) once whole cell is obtained. For this dual interface:

1) Connect Analog Out 0 (AO0) of the NIDAQ USB-6259 to the channel A of the BNC relay switch.
2) Connect the Analog out 0 (AO0) of the Digidata 1440B to channel B of the BNC relay switch.
3) Connect the output of the BNC relay switch to the command input of the Multiclamp 700B amplifier.
4) Connect Digital Out Ch0 of the NIDAQ board to the BNC relay input.
5) Connect the primary scaled output of Multiclamp 700B to Analog IN 1 (AI 1) of the NIDAQ USB-6259 and analog input 0 (AI0) of the Digidata 1440B.

In its default configuration, the input command to the patch amplifier is sent from the NIDAQ board for automated patch clamping. Once a whole cell configuration is established, the "Record.vi" program can be run in labview to switch the inputs and data can be recorded in current clamp or voltage clamp using the clampex software.

### A.2. Initial Program Setup

The Autopatcher program has been developed in Labview 8.6 (National Instruments) programming environment running in a Windows XP operating system. The Autopatcher in its current form will thus require a version 8.6 or higher version of Labview to run. Install the NiDAQmx driver for the USB-6259 data acquisition board. It can be downloaded from:

http://zone.ni.com/devzone/cda/tut/p/id/6913

For serial communication with the motor controller, ensure labview VISA is installed.

It can be downloaded from:

http://joule.ni.com/nidu/cds/view/p/id/2659/lang/en

Follow the instructions below for setting up the program for automated whole cell patch clamping *in vivo*.

#### A.2.1. Establishing serial communication with motor controller

1. Open patch automation.lvproj in labview project manager window.

This contains all files that are called by the main program during autopatching. All files that need to be opened during the course of operation of the Autopatcher can be accessed using this project manager.

2. Open “VisaInit.vi”

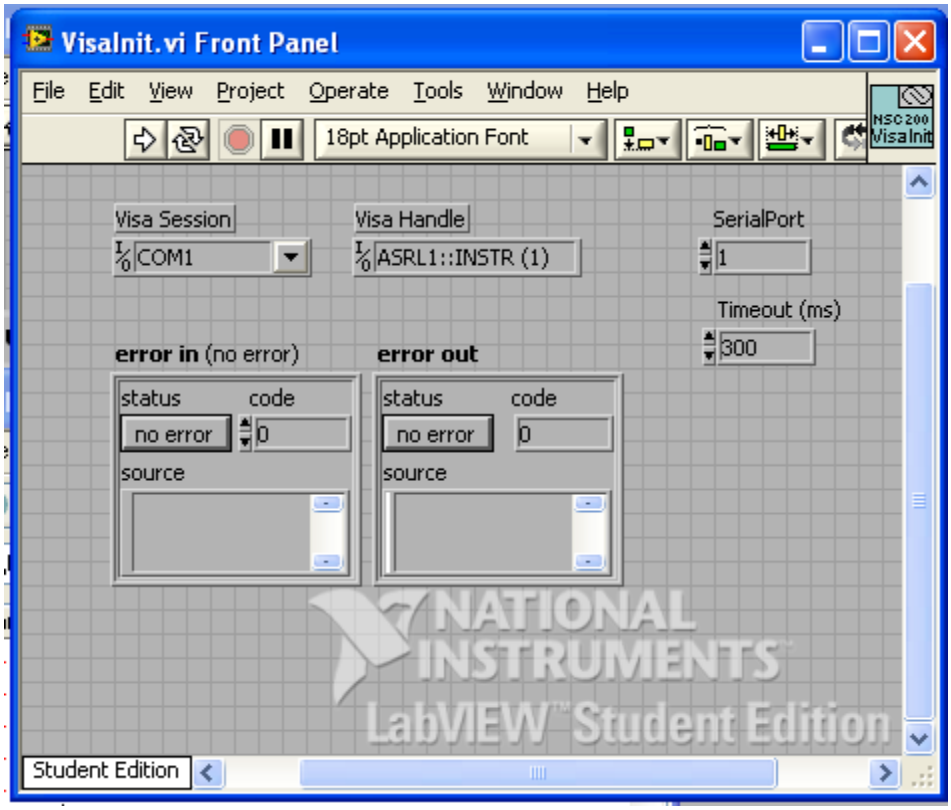


**Figure A. 2.1:** Screen shot of the “Visainit.vi” program that needs to be run to initiate serial communication with motor controller

3. Specify the COM1 port in the Visa Session and serial port number to which the motor controller is connected to in the computer, and run the program (Fig. 2.1).

NOTE: This needs to be done prior to the first Autopatcher program operation after every computer bootup.

## 2.2. User Settings in the "Autopatcher_ver1.0.vi"

4. From the same library, open "Autopatcher_ver0.1.vi"

The user interface for the Autopatcher program has 4 tabs: (a) Control panel, (b) Neuron hunt, (c) Seal formation and (d) Break-in.

### 2.2.1. Control Panel Tab Settings (Fig. 2.2.1)

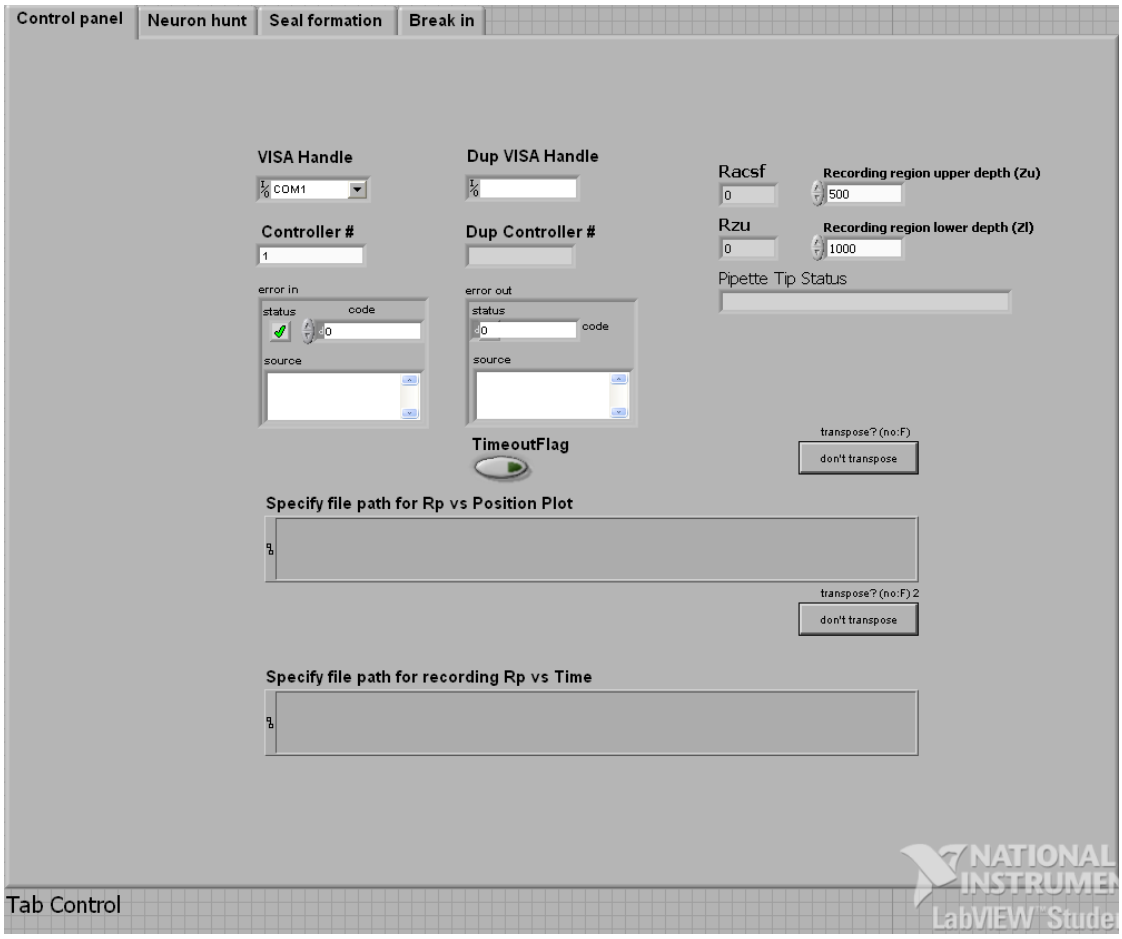


**Figure 2.2.1:** Computer screen capture of the Control panel tab of the Autopatcher program

1. Specify the COM port that was initialized in the "VisaInit.vi" program in the Visa Handle scroll down menu option.
2. Enter Controller number as 1.
3. Specify the upper depth (Zu in micrometers) of the region you want to record from.

4. Specify the lower depth (Zl in micrometers) of the region you want to record from. During operation, the Autopatcher will lower the pipette to Zu and start scanning for neurons. It will stop at Zl if no neuron is encountered in that range.
5. There are two file path dialog boxes to specify the location in which the plot of Pipette resistance as a funtion of depth (during neuron hunting) and pipette resistance as a function of time (during attempted gigaseal formation) are stored. Specify these file paths as needed.

### A. 2.2.2. Neuron Hunt Tab Settings (Fig. A.2.2.2)

NOTE: This is a debug-oriented version of the Autopatcher software, allowing parameters to be changed; since we never changed the parameters in all of our autopatching experiments, these parameters in principle could be hardwired into the code.

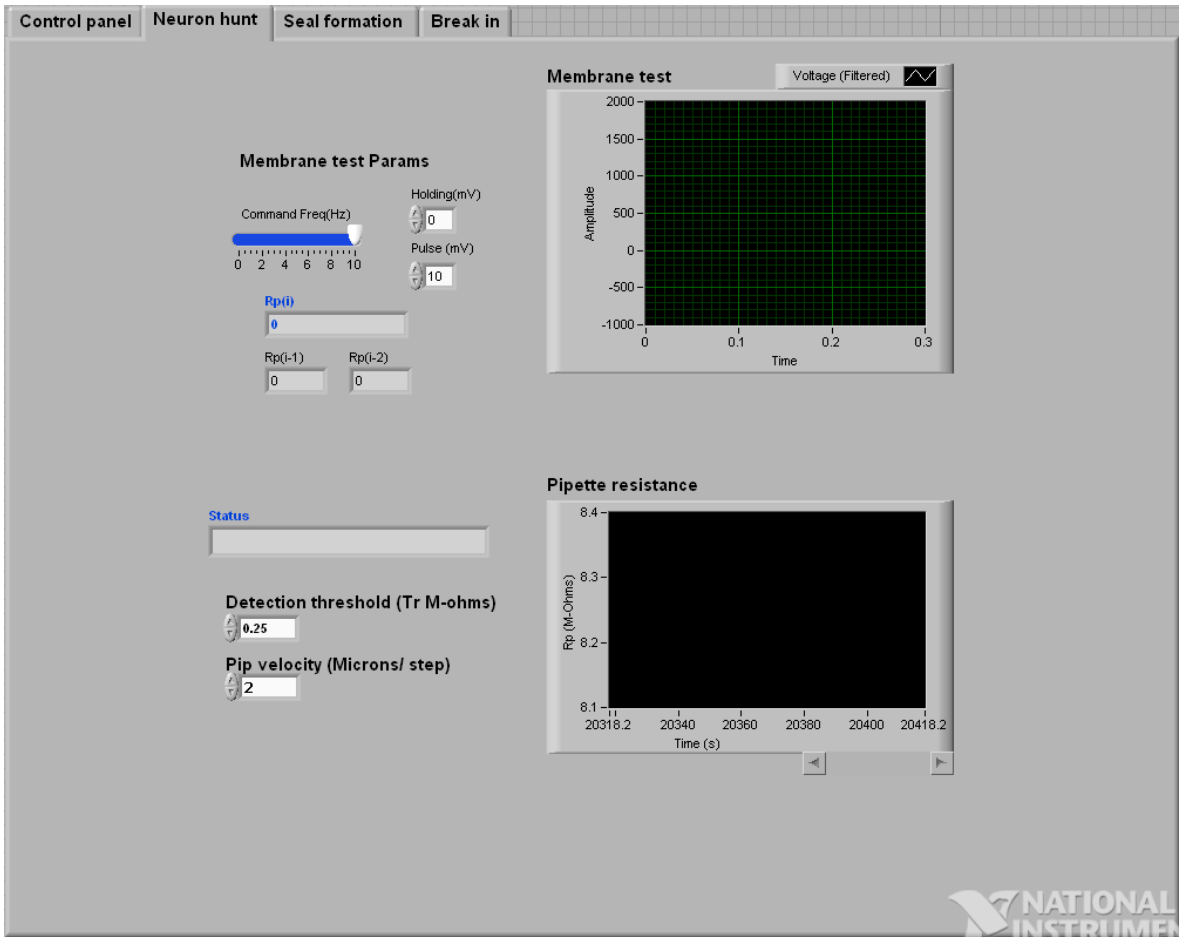


**Figure A.2.2.2:** Computer screen capture of the Neuron Hunt tab in the Autopatcher program

1. Specify the membrane test parameters in a manner similar to the Membrane test done in Pclamp. (e.g., Command frequency = 10 Hz, Holding = 0 mV, Pulse = 10 mV)
2. Set detection threshold between 0.2-0.3, as required.
3. Set pipette velocity at 2 micrometers/step.

NOTE: This tab displays the last three pipette resistance readings Rp (i), Rp (i-1) and Rp (i-2). Status bar indicates the current state of the program execution. (i.e., 'Hunting for neurons at desired depth' or 'Neuron found') Two graphical charts are provided that plot the currents flowing through the pipette (Membrane test) and the pipette resistance as a function of position in the brain.

### A.2.2.3. Seal Formation Tab Settings (Fig. 2.2.3)

NOTE: This is a debug-oriented version of the Autopatcher software, allowing parameters to be changed; since we never changed the parameters in all of our autopatching experiments, these parameters in principle could be hardwired into the code.

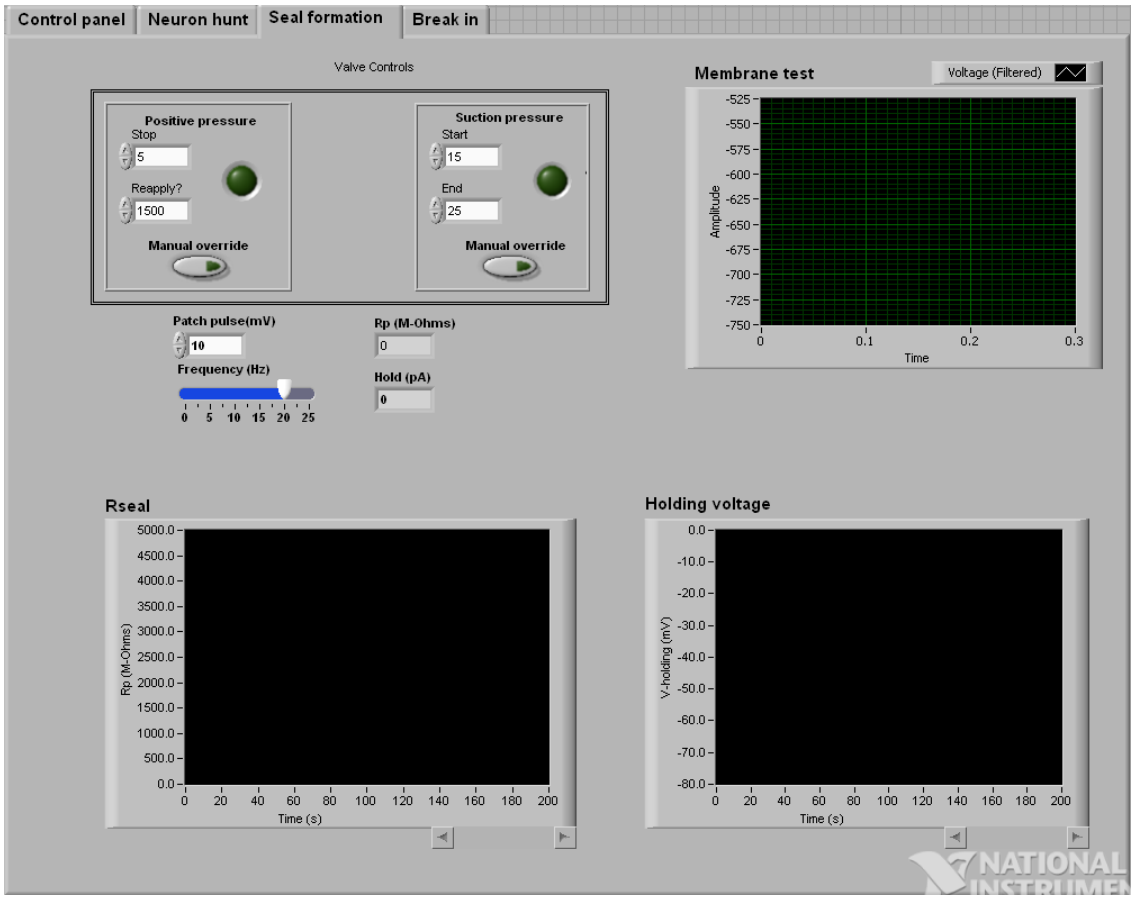


**Figure A.2.2.3:** Computer screen capture of Seal formation tab in Autopatcher program

1. Specify the membrane test parameters in a manner similar to the Membrane test done in Pclamp. (e.g., Command frequency = 10 Hz, Holding = 0 mV, Pulse = 10 mV)
2. Set the time at which positive pressure is released. In all our experiments it was set at 10 seconds. Similarly, set the time at which positive pressure needs to be reapplied if needed. In all our experiments, we set it at n arbitrarily large value (~1500 seconds).

3. Set the times at which suction pressures need to be applied and removed (15 s and 25 s respectively).

NOTE: In this tab, there are three graphical charts that plot the pipette resistance, the current flowing though the pipette during membrane test, and the holding potential. Two numerical indicators display the most recent pipette resistance (Rp) and holding current values.

### A.2.2.4. Break-in Tab Settings (Fig. A.2.2.4)

**NOTE:** This is a debug-oriented version of the Autopatcher software, allowing parameters to be changed; since we never changed the parameters in all of our autopatching experiments, these parameters in principle could be hardwired into the code.

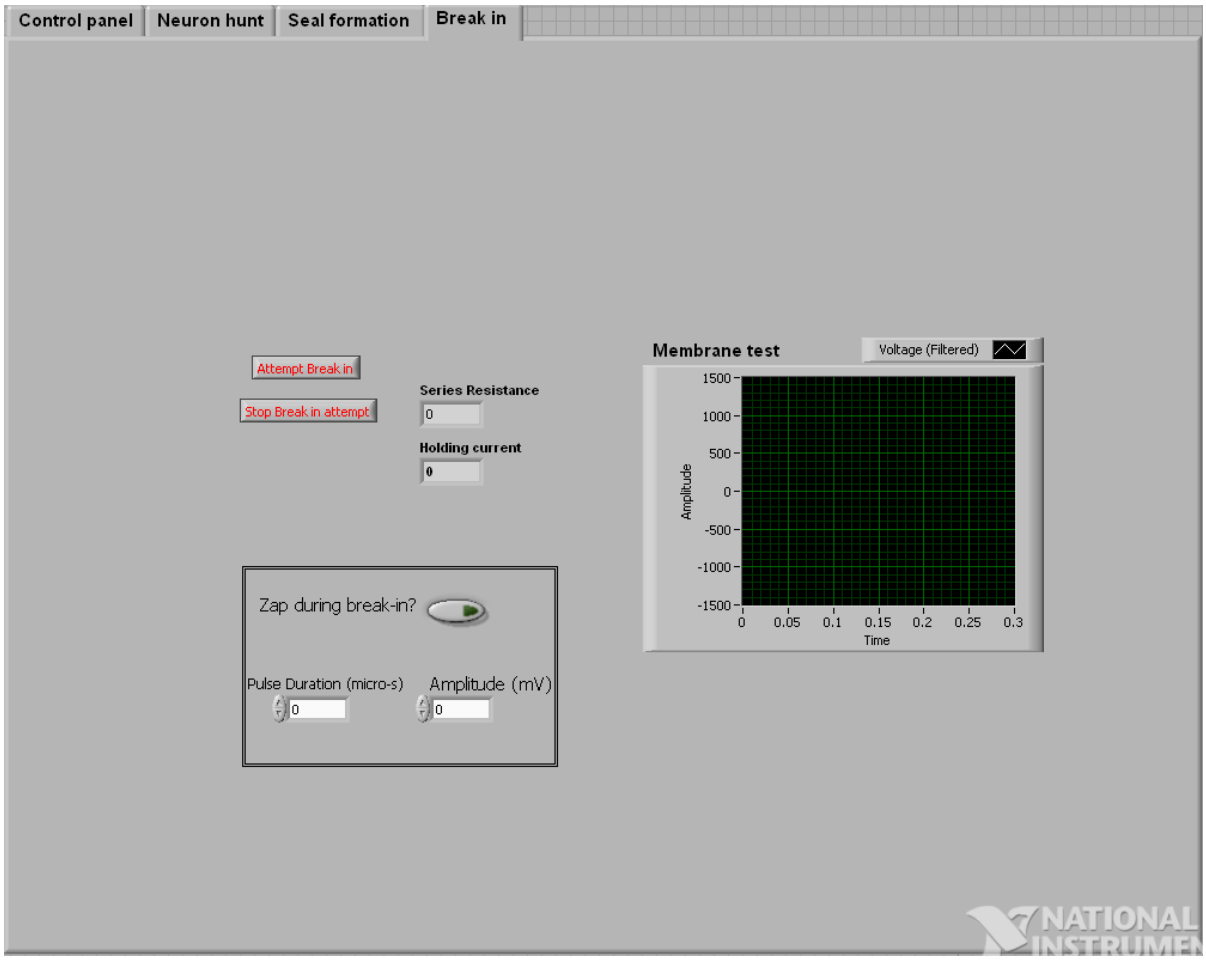


**Figure A.2.2.4:** Computer screen capture of Break-in tab in Autopatcher program

1. Specify whether you want to zap during break-in, or break-in using suction pulses only.
2. If zap function is used, specify the pulse duration (e.g,. 200 ms) and amplitude (e.g., 1000 mV)

NOTE: A graphical chart that displays the membrane current is provided to determine whether break-in has occurred or not.

Once these setting have been input for the first trial, they remain the same for the rest of the trials.

### A.3. Manual Tasks before running the Autopatcher program

1. Fill patch pipette with internal saline solution and install in pipette holder.
2. Open and run Valve "reset.vi" to reset all valves to default configuration.

3. Application of pressures:
    - **i.** Apply High positive pressure at N.O. port of Valve 2.
    - **ii.** Apply Low positive pressure at N.C. port of Valve 2.
    - **iii.** Apply suction pressure at N.C. port of valve 3.

In the default configuration, the valve system output high positive to the pipette to ensure that the tip does not get blocked accidently.

4. Position pipette in the center of the craniotomy, 20-30 micrometers above the brain surface using a stereomicroscope for visualization.
5. Open the Multiclamp 700B commander program. (See Fig. 3)
6. Make sure the amplifier is in Voltage clamp mode by selecting VC mode button.
7. Ensure Holding current is set at 0 mV.
8. Reset the pipette offset by using the Auto pipette offset function.
9. Neutralize for pipette capacitance by Auto correcting for Cp Fast and Cp.

The Autopatcher program can now be run for Automated whole cell patch clamping in vivo.

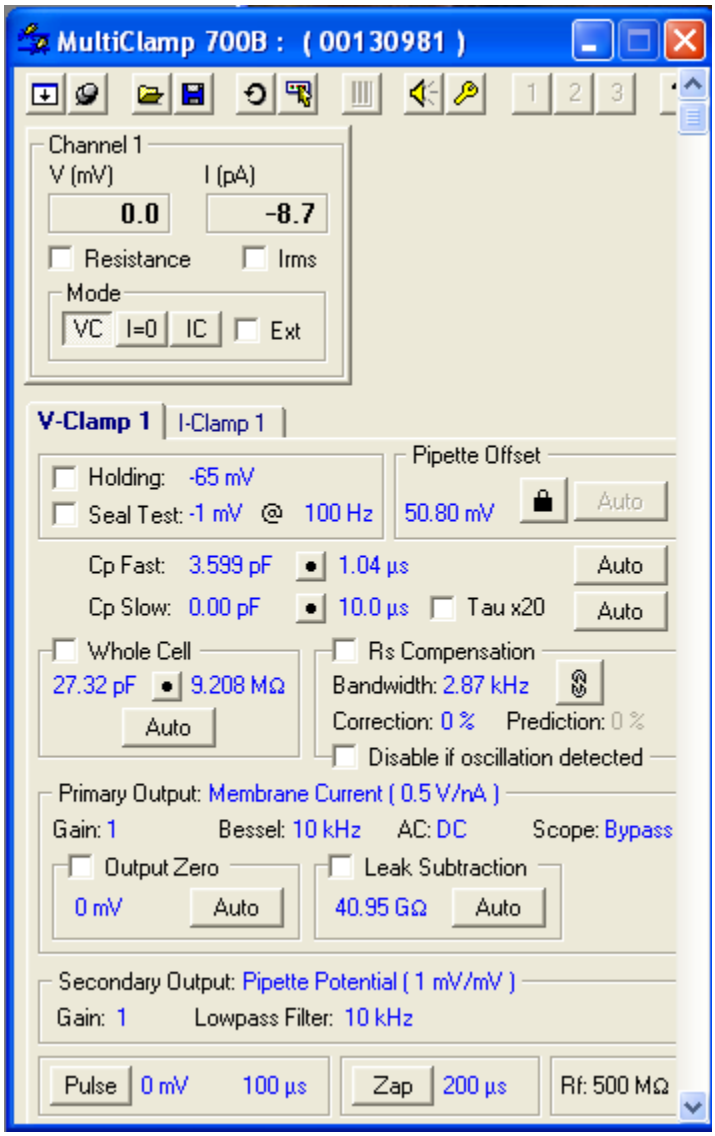


**Figure A.3:** Settings in the Multiclamp commander before Autopatcher program is executed

4. Open and run “Command_switch.vi”. Run this continuously during entire experiment. At any time the command input going to the Multiclamp 700B can be switched between NIDAQ USB 6259 (for autopatching) and Digidata 1440B (for post patch recording) using software controls.

**A. 5. Running the Autopatcher Program**

Select the control panel tab and run the Autopatcher_ver0.1 program in labview making sure all the setting in the tabs are specified as described in Section 2.2. The program is executed as described in **Chapter 2 (Section 2.12).**

1) The Autopatcher measures and displays the pipette resistance Racsf outside the brain.
2) The pipette is then lowered to the specified depth Zu under high positive pressure.
3) The pressure is lowered to low positive pressure and the pipette resistance Rzu is measured to check for blockage.
4) If the pipette is blocked, “Pipette blocked, install new pipette” message is displayed under Pipette Tip Status (See Fig. 2.2.1). It is then retracted back and the program stops. Install a new pipette, and performs the manual tasks described in section 3 before restarting the Autopatcher.

5) If the pipette is not blocked, “Pipette not blocked” message is displayed under Pipette Tip Status, and the Autopatcher initiates Neuron Hunt. Switch to the ‘Nueron Hunt’ tab.
6) The Autopatcher now moves the pipette in steps specifed by the user (e.g., 2 micrometers) and measures the pipette resistance at each step. Autopatcher either stops pipette actuation when a neuron is encountered or when it has scanned through to depth Zl without encountering a neuron. In the latter case the program stops. If a neuron is encountered, the Autopatcher initiates Seal formation protocol. Switch to ‘Seal formation’ tab.
7) The pipette resistance can be monitored over time in the Rseal graph indicator. Release of positive pressure and application of suction, as well as ramp down of holding potential takes places as described in **Chapter 2**. Typically in a successful attempt, a gigaseal is formed and holding voltage is ramped down to –65mV in 80 seconds. At the end of 80 seconds, if seal resistance less than a gigaohm, stop program. Retract pipette using the manual xyz positioner. A new trial can be started by installing a new pipette as described in Section 3.
8) If a break-in occurs spontaneously, stop program and go to Step 11.
9) If break-in does not occur spontaneously, switch to the Break-in tab. If attempting to break-in using suction pulses, restore the suction pressure in the suction port. Then press ‘Attempt break-in’. The Autopatcher will apply suction pressure for 100 ms, if successful typical membrane current

transients can be seen in the graph indicator. A similar procedure is followed for break-in using the zap function. If unsuccessful, press stop break-in attempt after 5 seconds, and retry until successful break-in occurs. Alternately, break-in can be achieved by using the manual overide of suction pressure option in the gigaseal formation tab and applying the requisite voltage zap using the 'Zap' button in the Multiclamp commander. If using this option, make sure the manual overide is switched off after break-in, else the cell contents may be dialized into the pipette.

10) Once a whole cell recording is established, stop program.
11) Set the amplifier to I=0 mode using the Multiclamp commander software and select clampex in the front panel of the "Command_switch.vi" program that was initiated in Step 4. This will automatically enable the command input to the amplifier to be sent by the Digidata 1440B. Whole cell recordings in Voltage clamp or current clamp can be carried out in using Pclamp software (Molecular Devices).

**Biocytin Filling Experiments**

After a neuron has been recorded in whole cell mode for a sufficiently long period of time to fill it with biocytin (~10 minutes), the "Retract_pipette.vi" program can be run to attempt to form an outside out patch. The program has two user set distances.

1) Specify the distance you want to retract the pipette at a slow speed (e.g., 3 mm/s). We typically set it at 100-150 mm to get an outside out patch.

2) Specify the distance you want the pipette to be rapidly retracted, typically set to the depth of the recording, as noted while running the “Autopatcher_ver1.0.vi”.
3) Run the program. The program will first retract the pipette at steps of 3 mm every second for the distance specified by the user. Once that distance is reached, the program rapidly retracts the pipette by the distance specified in Step 2.

# APPENDIX B

# MULTIPATCHER USER MANUAL

**Parts list for the multipatcher setup**

1. Patch clamp amplifiers: Multiclamp 700B (Molecular Devices)
2. Patch clamp headstages: CV-7B (Molecular Devices)
3. Primary computer interface board: Digidata 1440B (Molecular Devices)
4. Secondary computer interface board: NI cDAQ 9263 (National Instruments)
5. 3 axes linear actuators for manual positioning: MPC 285 (Sutter)
6. Programmable linear actuators: PZC200-KT (Newport)
7. Central switch box for addressing individual motors: PZC200-SB (Newport)
8. Linear stages: MX460A-X (Newport)
9. Electronic 2-way solenoid valves: LDA0533215H-A (Lee company)
10. BNC relay switches: (CX230, Tohtsu)

## B.1 Hardware Setup

### B.1.1. Installing programmable motor in standard in vivo electrophysiology setup

This will depend on the configuration of an existing setup. To install a programmable linear motor in our in vivo electrophysiology rig, we machined a custom dovetail groove mounting plate to fix the CV 7B headstage to the Newport linear stage that is controlled using the piezo-motor (**Fig. A.1.1**). Unlike the autopatcher setup where this was mounted onto a Siskiyou manipulator, we mounted this programmable linear stage to mount onto MPC-285 (Sutter Instruments Inc). This way we could control 4 MPC-285's using a single ROE 200 controller.

The motors was connected to a switch box (PZC-200SB) controller and interfacing with the computer was done as per the instructions in the NanoPZ system user manual provided by Newport Corporation:

1. ftp://download.newport.com/MotionControl/Current/MotionControllers/PZC200/Manual/NanoPZ.pdf

### B.1.2. Installing programmable pressure control valves

The circuit diagram for actuation of one set of solenoid valves solenoid valves used to set the pressure states in one of the pipettes is shown in **Fig. B.1.2**. Instructions to make pneumatic connections are shown in Fig. 4.1 and described below:

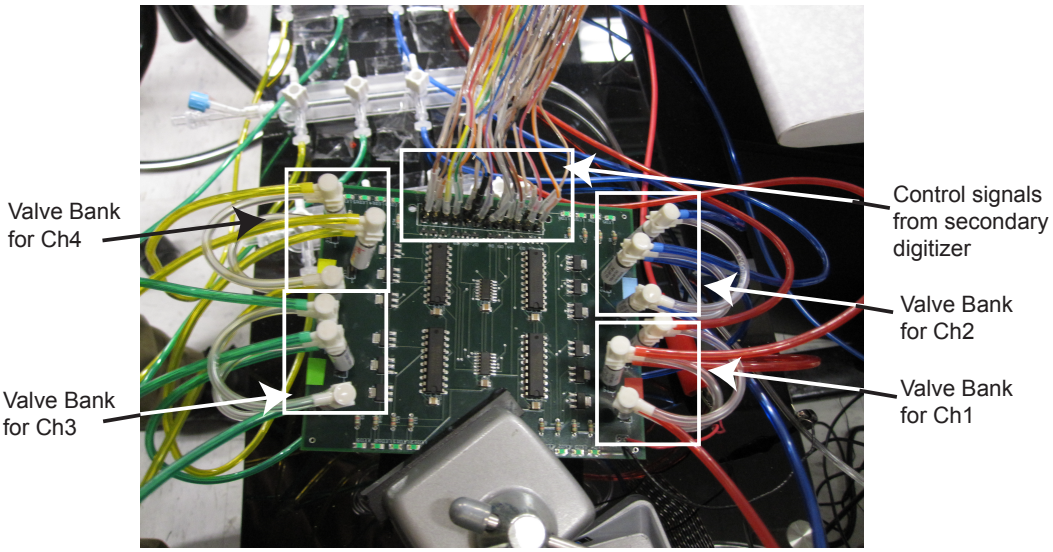


**Figure B.1.2:** Circuit for controlling solenoid valves for pressure modulation

1) Connect the Common port (output) of Valve 1 to pipette holder 1.

2) Connect the Common port (output) of Valve 2 to normally open (N.O.) input port of Valve 1.

3) Connect the Common port (output) of Valve 3 to normally closed (N.C.) input port of Valve 4.

This completes the valve tubing connections for pipette 1.

4) Connect the Common port (output) of Valve 4 to pipette holder 2.

5) Connect the Common port (output) of Valve 5 to normally open (N.O.) input port of Valve 4.

6) Connect the Common port (output) of Valve 6 to normally closed (N.C.) input port of Valve 4.

This completes the valve tubing connections for pipette 2.

7) Connect the Common port (output) of Valve 7 to pipette holder 3.

8) Connect the Common port (output) of Valve 8 to normally open (N.O.) input port of Valve 7.

6) Connect the Common port (output) of Valve 9 to normally closed (N.C.) input port of Valve 7.

This completes the valve tubing connections for pipette 3.

7) Connect the Common port (output) of Valve 10 to pipette holder 4.

8) Connect the Common port (output) of Valve 11 to normally open (N.O.) input port of Valve 10.

6) Connect the Common port (output) of Valve 12 to normally closed (N.C.) input port of Valve 10.

This completes the valve tubing connections for pipette 4.

To interface each of these four modules to the upstream pressure regulators, connect normally open (N.O.) input ports of Valve 2, 5, 8 and 11 to the high positive pressure source. Similarly, connect the normally closed (N.C.) input ports of Valve 2, 5, 8 and 11 to the low positive pressure source. Finally, connect the normally closed (N.C.) input ports of Valve 3, 6, 9 and 12 to the low positive pressure source.

For port locations, see the mechanical drawing of the soleniod valves:

http://www.theleeco.com/PDF.nsf/2355f3df133a527185256c9300562a42/e8bb4dc1b62a5f54852569a6006b64d8/$FILE/LHDA0030000BA.pdf

For computer control of the bank of valves,

1) Connect Analog Out 4 (AO4) of the cDAQ9263 to Gate of MOSFET1 to drive Valve 1.

2) Connect Analog Out 5 (AO5) of the cDAQ9263 to Gate of MOSFET2 to drive Valve 2.

3) Connect Analog Out 6 (AO6) of the cDAQ9263 to Gate of MOSFET3 to drive Valve 3.

4) Connect Analog Out 7 (AO7) of the cDAQ9263 to Gate of MOSFET4 to drive Valve 4.

5) Connect Analog Out 8 (AO8) of the cDAQ9263 to Gate of MOSFET5 to drive Valve 5.

6) Connect Analog Out 9 (AO9) of the cDAQ9263 to Gate of MOSFET6 to drive Valve 6.

7) Connect Analog Out 10 (AO10) of the cDAQ9263 to Gate of MOSFET7 to drive Valve 7.

8) Connect Analog Out 11 (AO11) of the cDAQ9263 to Gate of MOSFET2 to drive Valve 8.

9) Connect Analog Out 12 (AO12) of the cDAQ9263 to Gate of MOSFET3 to drive Valve 9.

10) Connect Analog Out 13(AO13) of the cDAQ9263 to Gate of MOSFET7 to drive Valve 10.

11) Connect Analog Out 14 (AO13) of the cDAQ9263 to Gate of MOSFET2 to drive Valve 11.

12) Connect Analog Out 15 (AO13) of the cDAQ9263 to Gate of MOSFET3 to drive Valve 12.

### B.1.3. Interfacing patch amplifiers to computer

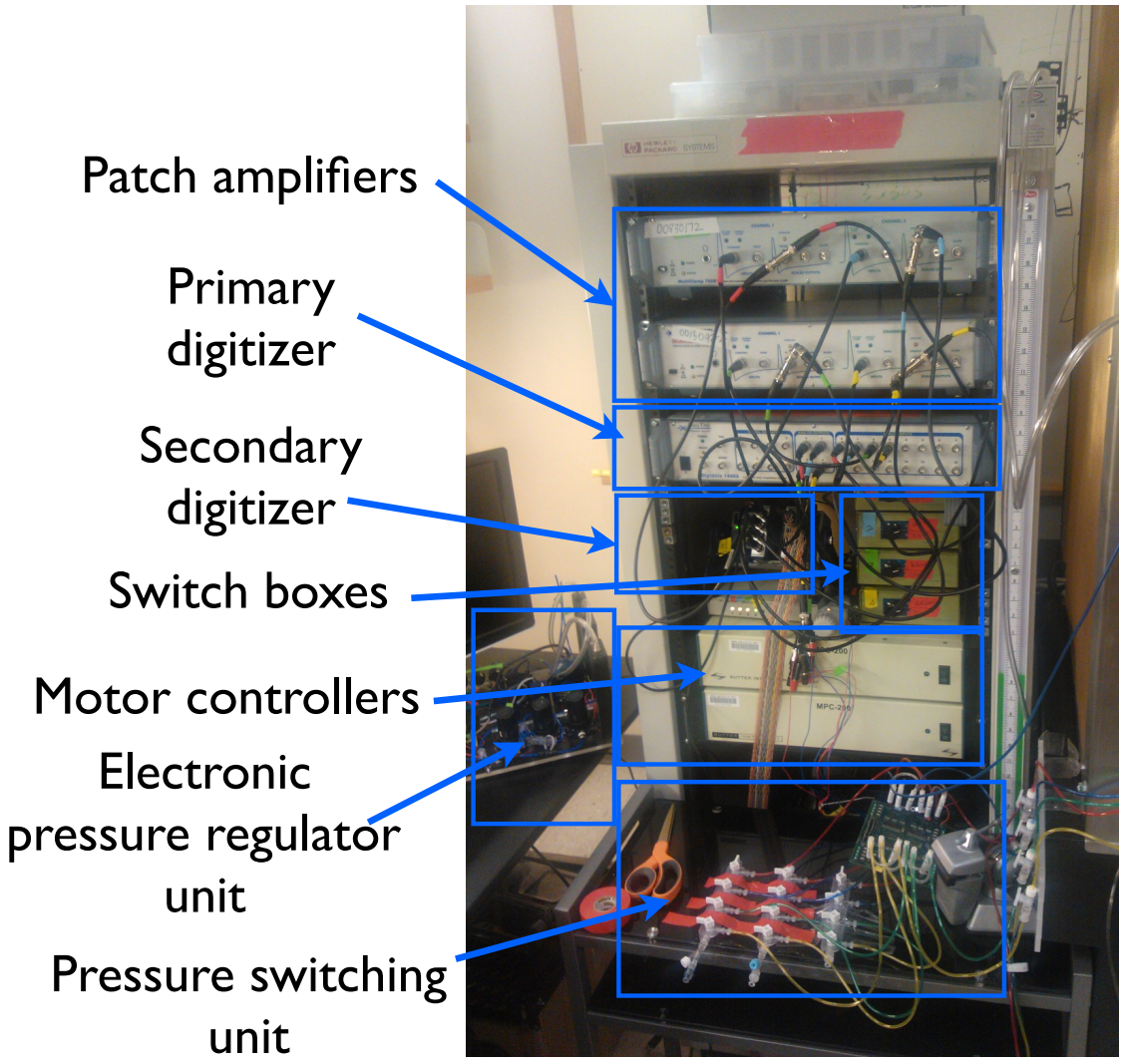

**Figure B.1.3: Illustration of the amplifier connections.** Also shown are the motor controllers and the pressure switching units.

The signals for the Multiclamp 700B amplifiers (Molecular Devices) are sent to and from two computer interface boards. The NI cDAQ 9204 (National instruments) board is used to send signals to the amplifier during multipatcher operation, and the Digidata 1440A is used for recording with commercial software Pclamp (Molecular Devices) once whole cell recordings are obtained. For this dual interface:

1) Connect Analog Out 0-3 (AO0, AO1, AO2 and AO3) of the NI cDAQ 9263 to the channels A of the 4 BNC relay switches.
2) Connect the Analog out 0-3 (AO0, AO1, AO2 and AO3) of the Digidata 1440B to channels B of the BNC relay switch.
3) Connect the outputs of the BNC relay switches 1-4 to the command inputs of the two Multiclamp 700B amplifiers. Each amplifier is equipped with 2 channels, thus making up 4 multipatcher channels.
4) Connect Analog Outs 13-16 of the cDAQ9263 board to the BNC relay inputs for switching the command inputs.
5) Connect the primary scaled output of Multiclamp 700B to Analog IN 1 (AI 1) of the NIDAQ USB-6259 and analog input 0 (AI0) of the Digidata 1440B.

In its default configuration, the input commands to the patch amplifier are sent from the cDAQ board for automated patch clamping. Once multipatching is completed, exiting the

program results in the BNC switches changing configurations so as to let the Digidata 1440B to send the command inputs during data acquisition.

**B.2. Initial Program Setup**

The Multipatcher program has been developed in Labview 2011 (National Instruments) programming environment running in a Windows 7 professional operating system. The mutlipatcher in its current form will thus require a version 2011 or higher version of Labview to run. All defaults values for the program user units are pre-saved in the program multipatcher_ver0.30.vi

Install the NiDAQmx driver for the USB-6259 data acquisition board. It can be downloaded from:

http://zone.ni.com/devzone/cda/tut/p/id/6913

For serial communication with the motor controller, ensure labview VISA is installed.

It can be downloaded from:

http://joule.ni.com/nidu/cds/view/p/id/2659/lang/en

Follow the instructions below for setting up the program for automated multicellular whole cell patch clamping *in vivo*.

**B.2.1. Establishing serial communication with motor controller**

1. Open multipather.llb in labview library manager window.

This contains all files that are called by the main program during multipatching. All files that need to be opened during the course of operation of the multipatcher can be accessed using this project manager.

2. Open “VisaInit.vi”

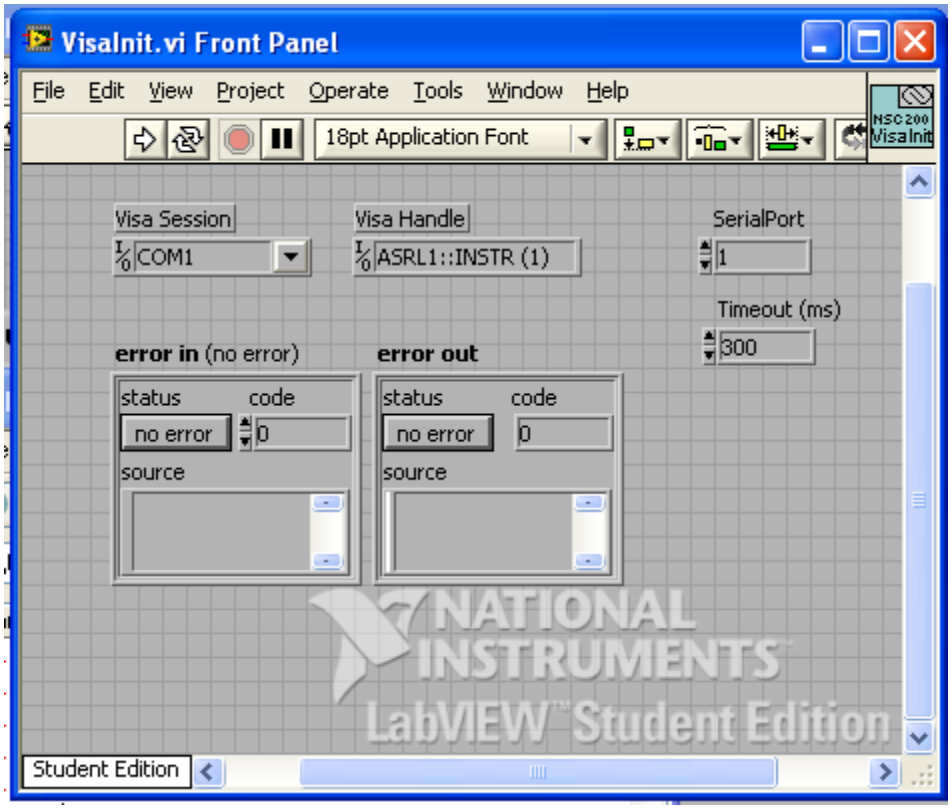


**Figure B.2.1:** Screen shot of the “Visainit.vi” program that needs to be run to initiate serial communication with motor controller

3. Specify the COM3 (for actual COM port assignment in your computer check device manager setting) port in the Visa Session and serial port number to which the motor controller is connected to in the computer, and run the program (Fig. 2.1).

NOTE: This needs to be done prior to the first multipatcher program operation after every computer bootup.

B. 2.2. User Settings in the “Multipatcher_ver.30.vi”

4. From the same library, open “Multipatcher_ver.30.vi”

The user interface for the Mutlipatcher program has 3 tabs: (a) Control panel, (b) Neuron hunt, and (c) Seal formation

**2.2.1. Control Panel Tab Settings (Fig. 2.2.1)**

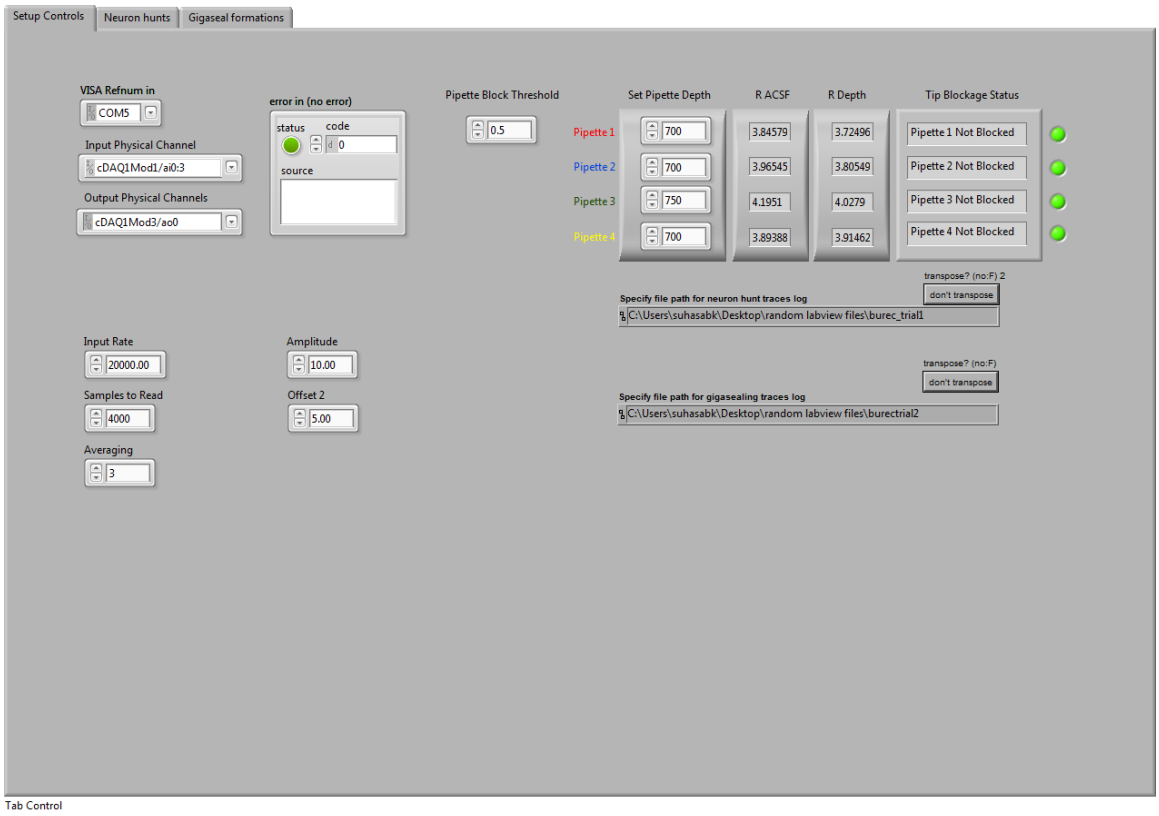


**Figure B.2.2.1:** Computer screen capture of the Control panel tab of the multipatcher program

1. Specify the COM port that was initialized in the "VisaInit.vi" program in the Visa Handle scroll down menu option.
2. Enter Controller number as 1.
3. Specify the upper depth (Zu in micrometers) for all the pipettes of the region you want to record from.
4. There are two file path dialog boxes to specify the location in which the plot of Pipette resistance as a funtion of depth (during neuron hunting) and pipette

resistance as a function of time (during attempted gigaseal formation) are stored. Specify these file paths as needed.

### B. 2.2.2. Neuron Hunt Tab Settings (Fig. A.2.2.2)

NOTE: This is a debug-oriented version of the Multipatcher software, allowing parameters to be changed; since we never changed the parameters in all of our autopatching experiments, these parameters in principle could be hardwired into the code.


**Figure B.2.2.2:** Computer screen capture of the Neuron Hunt tab in the multipatcher program

1. Specify the membrane test parameters in a manner similar to the Membrane test done in Pclamp. (e.g., Command frequency = 10 Hz, Holding = 0 mV, Pulse = 10 mV)
2. Set detection threshold between 0.2-0.3, as required.
3. Set pipette velocity at 2 micrometers/step.

NOTE: Status bar indicates the current state of the program execution. (i.e., 'Hunting for neurons at desired depth' or 'Neuron found') Two graphical charts are provided that plot the currents flowing through the pipette (Membrane test) and the pipette resistance as a function of position in the brain.

**B.2.2.3. Seal Formation Tab Settings (Fig. 2.2.3)**

NOTE: This is a debug-oriented version of the Mutlipatcher software, allowing parameters to be changed; since we never changed the parameters in all of our autopatching experiments, these parameters in principle could be hardwired into the code.

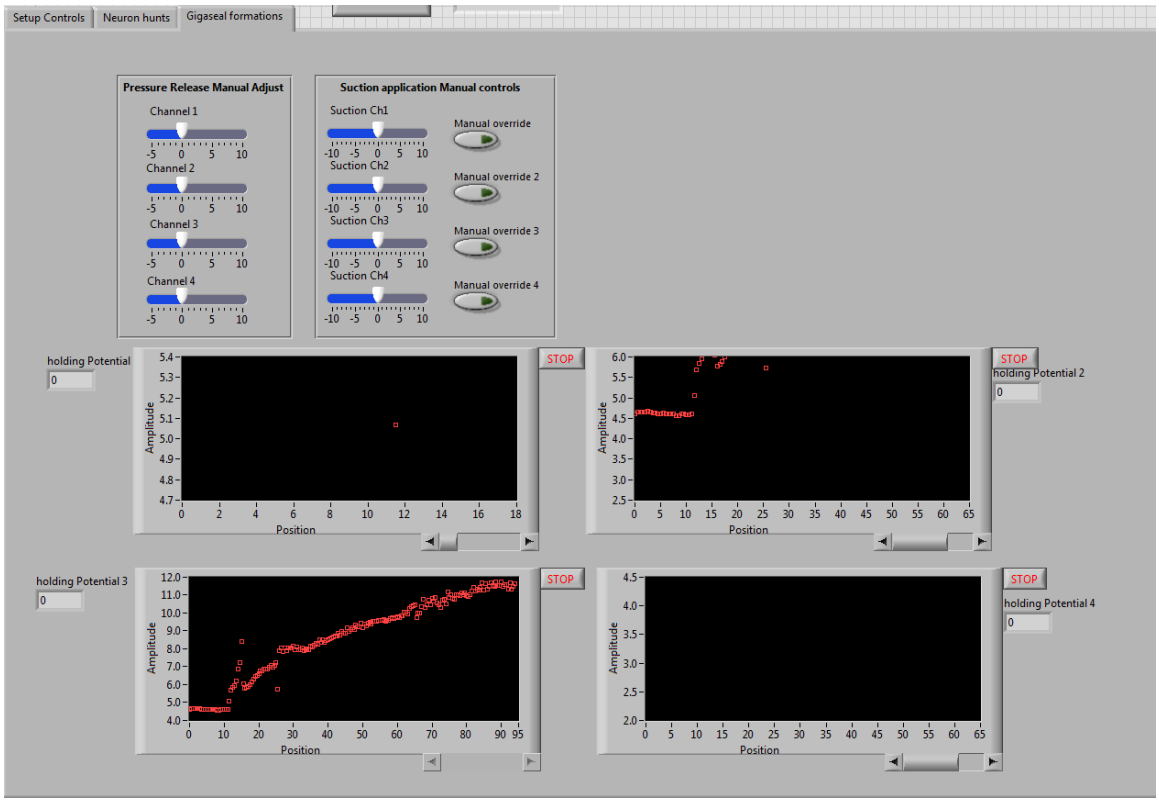


**Figure B.2.2.3:** Computer screen capture of Seal formation tab in Multipatcher program

1. The default value for releasing positive pressure during gigasealing was set at 10 seconds. The user can change these setting for the individual channels using the controls shown in the figure.
2. Similarly, by default, suction pressure during each gigasealing attempt was set so as to get activated between 15 to 25 seconds. This could be manually adjusted as well by the user. The user can chose to manually intervene in the suction pressure application as well using the manual override option.

NOTE: In this tab, there are four graphical charts that plot the pipette resistance during the gigasealing attempts.

## B.3. Manual Tasks before running the multipatcher program

1. Fill patch pipette with internal saline solution and install in pipettes in the four holders.
2. Open and run "Valves_reset.vi" to reset all valves to default configuration.
3. Ensure that the pressures from the analog pressure regulators are set at 800 mBar (high positive pressure), 25 mBar (low positive pressure), and -15 mBar (suction pressure).

In the default configuration, the valve system outputs high positive to all the pipettes to ensure that the tips do not get blocked accidently.

4. Position pipettes in the the craniotomy, 20-30 micrometers above the brain surface using a stereomicroscope for visualization. Ensure they are at the sufficient distance so as to not collide with each other during multipatcher operation.
5. Open two instances of Multiclamp 700B commander program. Assign the two multiclamp amplifiers to each of these commander windows. (**See Fig. B.3**)
6. Make sure all four channels of the patch amplifiers are in Voltage clamp mode by selecting VC mode button.
7. Ensure Holding currents are set at 0 mV.
8. Reset the pipette offsets by using the Auto pipette offset function.
9. Neutralize for pipette capacitances by Auto correcting for Cp Fast and Cp.

The multipatcher program can now be run for Automated whole cell patch clamping in vivo.

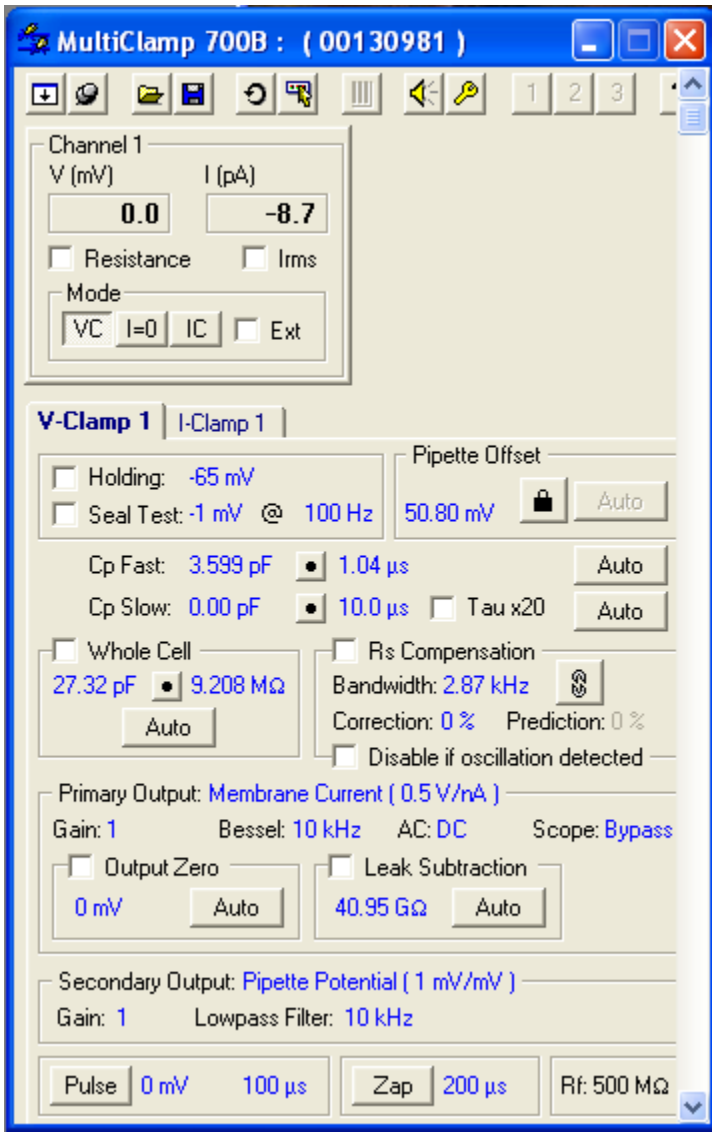


**Figure B.3.1:** Settings in the Multiclamp commander before multipatcher program is executed

10. Open and run “Command_switch.vi”. Run this continuously during entire experiment. At any time the command input going to the Multiclamp 700B can be switched between cDAQ (for multipatching) and Digidata 1440B (for post patch recording) using software controls.

Select the control panel tab and run the Multipatcher_ver0.30 program in labview making sure all the setting in the tabs are specified as described in Section 2.2. The program is executed as described in **Chapter 4 (Section 4.8).**

1) The multipatcher measures and displays the pipette resistances Racsf of all the pipettes outside the brain.
2) The pipettes are then lowered to the specified depths Zui under high positive pressure.
3) The pressures in the pipettes are lowered to low positive pressure and the pipette resistances Rzui are measured to check for blockage.
4) If any of the pipettes are blocked, they get deactivated, as indicated by the red Boolean displayed next to the depth settings.
5) For the unblocked pipettes, the multipatcher displays “Pipette not blocked” message is displayed under Pipette Tip Status, and the mulitpatcher initiates Neuron Hunt. Switch to the ‘Nueron Hunt’ tab.
6) The multipatcher now moves the each of the active pipettes in steps specifed by the user (e.g., 2 micrometers) and measures the pipette resistances at each step. When one of the channels encounters a neurons,

the mulitpatcher stops and shifts to gigasealing. Switch to 'Seal formation' tab.

7) The pipette resistance of the channel attempting to form gigaseals can be monitored over time in the Rseal graph indicator. Release of positive pressure and application of suction, as well as ramp down of holding potential takes places as described in **Chapter 2**. Typically in a successful attempt, a gigaseal is formed and holding voltage is ramped down to –65mV in 60 seconds. At the end of 80 seconds, the multipatcher deactivates the motor for the channel that just attemped gigasealing, and moves back to step 6. Steps 6 and 7 are repeated until all active pipettes attempt gigasealing.
8) The user can then use program "Breakin.vi" to select the channels that he/she wants to obtain whole cell recordings in and attempt break in as described in **Appendix A**.
9) Once whole cell recordings are obtained in all the necessary channels, the commandswitch.vi program is used to switch to digidata comman input.
10) Set the amplifier to I=0 mode for all channels, using the Multiclamp commander software and select clampex in the front panel of the. This will automatically enable the command input to the amplifier to be sent by the Digidata 1440B. Whole cell recordings in Voltage clamp or current clamp can be carried out in using Pclamp software (Molecular Devices).

## REFERENCES


1. Nowakowski, R.S. Stable neuron numbers from cradle to grave. *Proceedings of the National Academy of Sciences* **103**, 12219-12220 (2006).
2. Drachman, D.A. Do we have brain to spare? *Neurology* **64**, 2004-2005 (2005).
3. Markram, H. et al. Interneurons of the neocortical inhibitory system. *Nature reviews. Neuroscience* **5**, 793-807 (2004).
4. Hamill, O.P., Marty, A., Neher, E., Sakmann, B. & Sigworth, F.J. Improved patch-clamp techniques for high-resolution current recording from cells and cell-free membrane patches. *Pflugers Arch* **391**, 85-100 (1981).
5. Arthur, K. Patch-clamping in slices of mammalian CNS. *Trends Neurosci* **13**, 321-323 (1990).
6. Perin, R., Berger, T.K. & Markram, H. A synaptic organizing principle for cortical neuronal groups. *Proceedings of the National Academy of Sciences* **108**, 5419-5424 (2011).
7. Lefort, S., Tomm, C., Floyd Sarria, J.C. & Petersen, C.C.H. The Excitatory Neuronal Network of the C2 Barrel Column in Mouse Primary Somatosensory Cortex. *Neuron* **61**, 301-316 (2009).
8. Froemke, R.C., Tsay, I.A., Raad, M., Long, J.D. & Dan, Y. Contribution of individual spikes in burst-induced long-term synaptic modification. *J Neurophysiol* **95**, 1620-1629 (2006).
9. Froemke, R.C., Poo, M.M. & Dan, Y. Spike-timing-dependent synaptic plasticity depends on dendritic location. *Nature* **434**, 221-225 (2005).

10. Froemke, R.C., Debanne, D. & Bi, G.Q. Temporal modulation of spike-timing-dependent plasticity. *Front Synaptic Neurosci* **2**, 19 (2010).

11. Froemke, R.C. & Dan, Y. Spike-timing-dependent synaptic modification induced by natural spike trains. *Nature* **416**, 433-438 (2002).

12. Joshi, S. & Hawken, M.J. Loose-patch-juxtacellular recording in vivo--a method for functional characterization and labeling of neurons in macaque V1. *J Neurosci Methods* **156**, 37-49 (2006).

13. Wilson, C.J. & Sachdev, R.N. Intracellular and juxtacellular staining with biocytin. *Curr Protoc Neurosci* **Chapter 1**, Unit 1 12 (2004).

14. Eberwine, J. et al. Analysis of gene expression in single live neurons. *Proc Natl Acad Sci U S A* **89**, 3010-3014 (1992).

15. Morris, J., Singh, J.M. & Eberwine, J.H. Transcriptome Analysis of Single Cells. *J Vis Exp*, e2634 (2011).

16. Van Gelder, R.N. et al. Amplified RNA synthesized from limited quantities of heterogeneous cDNA. *Proc Natl Acad Sci U S A* **87**, 1663-1667 (1990).

17. Toledo-Rodriguez, M. et al. Correlation maps allow neuronal electrical properties to be predicted from single-cell gene expression profiles in rat neocortex. *Cerebral Cortex* **14**, 1310-1327 (2004).

18. Toledo-Rodriguez, M. & Markram, H. Single-cell RT-PCR, a technique to decipher the electrical, anatomical, and genetic determinants of neuronal diversity. *Methods Mol Biol* **403**, 123-139 (2007).

19. Margrie, T.W., Brecht, M. & Sakmann, B. In vivo, low-resistance, whole-cell recordings from neurons in the anaesthetized and awake mammalian brain. *Pflugers Arch* **444**, 491-498 (2002).

20. Wehr, M. & Zador, A.M. Balanced inhibition underlies tuning and sharpens spike timing in auditory cortex. *Nature* **426**, 442-446 (2003).

21. Wehr, M. & Zador, A.M. Synaptic Mechanisms of Forward Suppression in Rat Auditory Cortex. *Neuron* **47**, 437-445 (2005).

22. Zador, A.M., Yang, Y., DeWeese, M.R. & Otazu, G.H. Millisecond-scale differences in neural activity in auditory cortex can drive decisions. *Nat Neurosci* **11**, 1262-1263 (2008).

23. Par√©, D., Shink, E., Gaudreau, H.l.n., Destexhe, A. & Lang, E.J. Impact of Spontaneous Synaptic Activity on the Resting Properties of Cat Neocortical Pyramidal Neurons In Vivo. *J Neurophysiol* **79**, 1450-1460 (1998).

24. Margrie, T.W. et al. Targeted whole-cell recordings in the mammalian brain in vivo. *Neuron* **39**, 911-918 (2003).

25. Kitamura, K., Judkewitz, B., Kano, M., Denk, W. & Hausser, M. Targeted patch-clamp recordings and single-cell electroporation of unlabeled neurons in vivo. *Nat Meth* **5**, 61-67 (2008).

26. Chadderton, P., Margrie, T.W. & Hausser, M. Integration of quanta in cerebellar granule cells during sensory processing. *Nature* **428**, 856-860 (2004).

27. Poulet, J.F.A., Fernandez, L.M.J., Crochet, S. & Petersen, C.C.H. Thalamic control of cortical states. *Nat Neurosci* **15**, 370-372 (2012).

28. Gentet, L.J. et al. Unique functional properties of somatostatin-expressing GABAergic neurons in mouse barrel cortex. *Nat Neurosci* **15**, 607-612 (2012).

29. Gentet, L.J., Avermann, M., Matyas, F., Staiger, J.F. & Petersen, C.C. Membrane potential dynamics of GABAergic neurons in the barrel cortex of behaving mice. *Neuron* **65**, 422-435 (2010).

30. Crochet, S., Poulet, J.F., Kremer, Y. & Petersen, C.C. Synaptic mechanisms underlying sparse coding of active touch. *Neuron* **69**, 1160-1175 (2011).

31. Crochet, S. & Petersen, C.C.H. Correlating whisker behavior with membrane potential in barrel cortex of awake mice. *Nat Neurosci* **9**, 608-610 (2006).

32. Duguid, I., Branco, T., London, M., Chadderton, P. & H√ § usser, M. Tonic Inhibition Enhances Fidelity of Sensory Information Transmission in the Cerebellar Cortex. *The Journal of Neuroscience* **32**, 11132-11143 (2012).

33. Dombeck, D.A., Harvey, C.D., Tian, L., Looger, L.L. & Tank, D.W. Functional imaging of hippocampal place cells at cellular resolution during virtual navigation. *Nat Neurosci* **13**, 1433-1440 (2010).

34. Long, M.A., Jin, D.Z. & Fee, M.S. Support for a synaptic chain model of neuronal sequence generation. *Nature* **468**, 394-399 (2010).

35. Lee, D., Lin, B.-J. & Lee, A.K. Hippocampal Place Fields Emerge upon Single-Cell Manipulation of Excitability During Behavior. *Science* **337**, 849-853 (2012).

36. Lee, A.K., Manns, I.D., Sakmann, B. & Brecht, M. Whole-cell recordings in freely moving rats. *Neuron* **51**, 399-407 (2006).

37. Lee, A.K., Epsztein, J. & Brecht, M. Head-anchored whole-cell recordings in freely moving rats. *Nat. Protocols* **4**, 385-392 (2009).

38. Gray, C.M., Maldonado, P.E., Wilson, M. & McNaughton, B. Tetrodes markedly improve the reliability and yield of multiple single-unit isolation from multi-unit recordings in cat striate cortex. *J Neurosci Methods* **63**, 43-54 (1995).

39. Lakatos, P., Karmos, G., Mehta, A.D., Ulbert, I. & Schroeder, C.E. Entrainment of neuronal oscillations as a mechanism of attentional selection. *Science* **320**, 110-113 (2008).

40. Lubenov, E.V. & Siapas, A.G. Hippocampal theta oscillations are travelling waves. *Nature* (2009).

41. Hochberg, L.R. et al. Neuronal ensemble control of prosthetic devices by a human with tetraplegia. *Nature* **442**, 164-171 (2006).

42. Campbell, P.K., Jones, K.E., Huber, R.J., Horch, K.W. & Normann, R.A. A silicon-based, three-dimensional neural interface: manufacturing processes for an intracortical electrode array. *IEEE transactions on bio-medical engineering* **38**, 758-768 (1991).

43. Wilson, M.A. & McNaughton, B.L. Dynamics of the hippocampal ensemble code for space. *Science* **261**, 1055-1058 (1993).

44. O'Keefe, J. & Recce, M.L. Phase relationship between hippocampal place units and the EEG theta rhythm. *Hippocampus* **3**, 317-330 (1993).

45. Hoogerwerf, A.C. & Wise, K.D. A three-dimensional microelectrode array for chronic neural recording. *IEEE transactions on bio-medical engineering* **41**, 1136-1146 (1994).

46. Song, S., Sjostrom, P.J., Reigl, M., Nelson, S. & Chklovskii, D.B. Highly nonrandom features of synaptic connectivity in local cortical circuits. *PLoS Biol* **3**, e68 (2005).

47. Yoshimura, Y., Dantzker, J.L. & Callaway, E.M. Excitatory cortical neurons form fine-scale functional networks. *Nature* **433**, 868-873 (2005).

48. Dantzker, J.L. & Callaway, E.M. Laminar sources of synaptic input to cortical inhibitory interneurons and pyramidal neurons. *Nat Neurosci* **3**, 701-707 (2000).

49. Dunlop, J., Bowlby, M., Peri, R., Vasilyev, D. & Arias, R. High-throughput electrophysiology: an emerging paradigm for ion-channel screening and physiology. *Nat Rev Drug Discov* **7**, 358-368 (2008).

50. Wood, C., Williams, C. & Waldron, G.J. Patch clamping by numbers. *Drug Discovery Today* **9**, 434-441 (2004).

51. Fertig, N., Blick, R.H. & Behrends, J.C. Whole cell patch clamp recording performed on a planar glass chip. *Biophys J* **82**, 3056-3062 (2002).

52. Chen, C. & Folch, A. A high-performance elastomeric patch clamp chip. *Lab Chip* **6**, 1338-1345 (2006).

53. Stuart, G.J., Dodt, H.U. & Sakmann, B. Patch-clamp recordings from the soma and dendrites of neurons in brain slices using infrared video microscopy. *Pflugers Arch* **423**, 511-518 (1993).

54. Edwards, F.A., Konnerth, A., Sakmann, B. & Takahashi, T. A thin slice preparation for patch clamp recordings from neurones of the mammalian central nervous system. *Pflugers Arch* **414**, 600-612 (1989).

55. Blanton, M.G., Lo Turco, J.J. & Kriegstein, A.R. Whole cell recording from neurons in slices of reptilian and mammalian cerebral cortex. *J Neurosci Methods* **30**, 203-210 (1989).

56. Stuart, G.J. & Sakmann, B. Active propagation of somatic action potentials into neocortical pyramidal cell dendrites. *Nature* **367**, 69-72 (1994).

57. Borst, J.G., Helmchen, F. & Sakmann, B. Pre- and postsynaptic whole-cell recordings in the medial nucleus of the trapezoid body of the rat. *J Physiol* **489 ( Pt 3)**, 825-840 (1995).

58. Covey, E., Kauer, J.A. & Casseday, J.H. Whole-cell patch-clamp recording reveals subthreshold sound-evoked postsynaptic currents in the inferior colliculus of awake bats. *J Neurosci* **16**, 3009-3018 (1996).

59. Ferster, D. & Jagadeesh, B. EPSP-IPSP interactions in cat visual cortex studied with in vivo whole-cell patch recording. *J Neurosci* **12**, 1262-1274 (1992).

60. Margrie, T.W., Brecht, M. & Sakmann, B. In vivo, low-resistance, whole-cell recordings from neurons in the anaesthetized and awake mammalian brain. *Pflugers Arch* **444**, 491-498 (2002).

61. Harvey, C.D., Collman, F., Dombeck, D.A. & Tank, D.W. Intracellular dynamics of hippocampal place cells during virtual navigation. *Nature* **461**, 941-946 (2009).

62. Brecht, M., Schneider, M., Sakmann, B. & Margrie, T.W. Whisker movements evoked by stimulation of single pyramidal cells in rat motor cortex. *Nature* **427**, 704-710 (2004).

63. Sucher, N.J. & Deitcher, D.L. PCR and patch-clamp analysis of single neurons. *Neuron* **14**, 1095-1100 (1995).

64. Zador, A.M., Hromadka, T. & DeWeese, M.R. Sparse representation of sounds in the unanesthetized auditory cortex. *Plos Biol* **6**, 124-137 (2008).

65. Loewenstein, Y. et al. Bistability of cerebellar Purkinje cells modulated by sensory stimulation. *Nat Neurosci* **8**, 202-211 (2005).

66. DeWeese, M.R. Whole-cell recording in vivo. *Curr Protoc Neurosci* **Chapter 6**, Unit 6 22 (2007).

67. Cang, J. & Isaacson, J.S. In Vivo Whole-Cell Recording of Odor-Evoked Synaptic Transmission in the Rat Olfactory Bulb. *The Journal of Neuroscience* **23**, 4108-4116 (2003).

68. Arenz, A., Silver, R.A., Schaefer, A.T. & Margrie, T.W. The Contribution of Single Synapses to Sensory Representation in Vivo. *Science* **321**, 977-980 (2008).

69. DeWeese, M.R. & Zador, A.M. Non-Gaussian membrane potential dynamics imply sparse, synchronous activity in auditory cortex. *J Neurosci* **26**, 12206-12218 (2006).

70. Degenetais, E., Thierry, A.-M., Glowinski, J. & Gioanni, Y. Electrophysiological Properties of Pyramidal Neurons in the Rat Prefrontal Cortex: An In Vivo Intracellular Recording Study. *Cerebral Cortex* **12**, 1-16 (2002).

71. Petilla terminology: nomenclature of features of GABAergic interneurons of the cerebral cortex. *Nat Rev Neurosci* **9**, 557-568 (2008).

72. Rancz, E.A. et al. Transfection via whole-cell recording in vivo: bridging single-cell physiology, genetics and connectomics. *Nat Neurosci* **14**, 527-532 (2011).

73. Boyden, E.S. & Raymond, J.L. Active reversal of motor memories reveals rules governing memory encoding. *Neuron* **39**, 1031-1042 (2003).

74. Chow, B.Y. et al. High-performance genetically targetable optical neural silencing by light-driven proton pumps. *Nature* **463**, 98-102 (2010).

75. Olesen, S.P., Clapham, D.E. & Davies, P.F. Haemodynamic shear stress activates a K+ current in vascular endothelial cells. *Nature* **331**, 168-170 (1988).

76. Olsen, S.R. & Wilson, R.I. Lateral presynaptic inhibition mediates gain control in an olfactory circuit. *Nature* **452**, 956-960 (2008).

77. Dunlop, J., Bowlby, M., Peri, R., Vasilyev, D. & Arias, R. High-throughput electrophysiology: an emerging paradigm for ion-channel screening and physiology. *Nat Rev Drug Discov* **7**, 358-368 (2008).

78. Bruggemann, A. et al. Planar patch clamp: advances in electrophysiology. *Methods Mol Biol* **491**, 165-176 (2008).

79. Chen, C.Y., Tu, T.Y., Chen, C.H., Jong, D.S. & Wo, A.M. Patch clamping on plane glass-fabrication of hourglass aperture and high-yield ion channel recording. *Lab Chip* **9**, 2370-2380 (2009).

80. Milligan, C.J. et al. Robotic multiwell planar patch-clamp for native and primary mammalian cells. *Nat Protoc* **4**, 244-255 (2009).

81. Lima, S.Q., Hromadka, T., Znamenskiy, P. & Zador, A.M. PINP: a new method of tagging neuronal populations for identification during in vivo electrophysiological recording. *PLoS One* **4**, e6099 (2009).

82. Boyden, E.S., Zhang, F., Bamberg, E., Nagel, G. & Deisseroth, K. Millisecond-timescale, genetically targeted optical control of neural activity. *Nat Neurosci* **8**, 1263-1268 (2005).

83. Han, X. & Boyden, E.S. Multiple-color optical activation, silencing, and desynchronization of neural activity, with single-spike temporal resolution. *PLoS One* **2**, e299 (2007).

84. Boyden, E.S. A history of optogenetics: the development of tools for controlling brain circuits with light. *F1000 Biology Reports* **3** (2011).

85. Cohen, D. et al. Chemical cytometry: fluorescence-based single-cell analysis. *Annu Rev Anal Chem (Palo Alto Calif)* **1**, 165-190 (2008).

86. Mellors, J.S., Jorabchi, K., Smith, L.M. & Ramsey, J.M. Integrated Microfluidic Device for Automated Single Cell Analysis Using Electrophoretic Separation and Electrospray Ionization Mass Spectrometry. *Anal Chem* **82**, 967-973 (2010).

87. Pak, N., Dergance, M.J., Emerick, M.T., Gagnon, E.B. & Forest, C.R. An Instrument for Controlled, Automated Production of Micrometer Scale Fused Silica Pipettes. *Journal of Mechanical Design* **133**, 061006 (2011).

88. Boyden, E.S., Zhang, F., Bamberg, E., Nagel, G. & Deisseroth, K. Millisecond-timescale, genetically targeted optical control of neural activity. *Nat Neurosci* **8**, 1263-1268 (2005).

89. Han, X. et al. Millisecond-timescale optical control of neural dynamics in the nonhuman primate brain. *Neuron* **62**, 191-198 (2009).

90. Kodandaramaiah, S.B., Franzesi, G.T., Chow, B.Y., Boyden, E.S. & Forest, C.R. Automated whole-cell patch-clamp electrophysiology of neurons in vivo. *Nat Meth* **9**, 585-587 (2012).

91. Wang, H. et al. High-speed mapping of synaptic connectivity using photostimulation in Channelrhodopsin-2 transgenic mice. *Proceedings of the National Academy of Sciences* **104**, 8143-8148 (2007).

92. Hamill, O.P., Marty, A., Neher, E., Sakmann, B. & Sigworth, F.J. Improved patch-clamp techniques for high-resolution current recording from cells and cell-free membrane patches. *Pflugers Arch* **391**, 85-100 (1981).

93. Epsztein, J., Brecht, M. & Lee, A.K. Intracellular Determinants of Hippocampal CA1 Place and Silent Cell Activity in a Novel Environment. *Neuron* **70**, 109-120 (2011).

94. Hromadka, T., DeWeese, M.R. & Zador, A.M. Sparse representation of sounds in the unanesthetized auditory cortex. *Plos Biol* **6**, 124-137 (2008).

95. Rancz, E.A. et al. Transfection via whole-cell recording in vivo: bridging single-cell physiology, genetics and connectomics. *Nat Neurosci* **14**, 527-532 (2011).

96. Schjetnan, A.G. & Luczak, A. Recording large-scale neuronal ensembles with silicon probes in the anesthetized rat. *Journal of visualized experiments : JoVE* (2011).

97. Buzsaki, G. Large-scale recording of neuronal ensembles. *Nat Neurosci* **7**, 446-451 (2004).

98. Han, X. et al. A high-light sensitivity optical neural silencer: development and application to optogenetic control of non-human primate cortex. *Front Syst Neurosci* **5**, 18 (2011).

99. Chow, B.Y., Han, X. & Boyden, E.S. Genetically encoded molecular tools for light-driven silencing of targeted neurons. *Prog Brain Res* **196**, 49-61 (2012).

100. Suhasa B Kodandaramaiah, M.K., Jamison Go, Saifullah Malik, Jitendra P Khatait, Edward S Boyden, Ronald G.K.M. Aarts, Dannis M Brouwer and Craing R Forest in American Society for Precision Engineering Annual meetingDenver, Colorado, USA; 2011).

101. Steinmeyer, J.D. & Yanik, M.F. High-Throughput Single-Cell Manipulation in Brain Tissue. *PLoS One* **7**, e35603 (2012).

102. Weerakoon, P. et al. Patch-clamp amplifiers on a chip. *J Neurosci Methods* **192**, 187-192 (2010).